Vadose zone flow patterns and their implications for sodium transport and aquifer recharge in a reclaimed fen watershed in the Athabasca Oil Sands Region, Alberta, Canada

by

Gabriel William Yvan Dubé

A thesis

presented to the University of Waterloo

in fulfilment of the

thesis requirement for the degree of

Master of Science

in

Geography

Waterloo, Ontario, Canada, 2021

Author's declaration

I hereby declare that I am the sole author of this thesis. This is a true copy of the thesis, including any required final revisions, as accepted by my examiners.

I understand that my thesis may be made electronically available to the public.

Abstract

The reclaimed Nikanotee Fen watershed consists of an upland tailings sand aquifer, capped with a finer soil cover (LFH-mineral mix, or LFH) to support vegetation, that supplies groundwater to a low-lying fen peatland. Maintaining high water levels in the fen is crucial to the success of the reclamation project. To this end, furrows were tilled in the LFH to retain overland flow and increase aquifer recharge. LFH was also completely scoured in certain areas to allow direct infiltration into bare tailings sand "basins". Elevated concentrations of leachable Na^+ in unsaturated tailings sand is a long-term source of Na^+ into the groundwater, which poses a risk to the health of downstream fen vegetation and constitutes an additional challenge to peatland reclamation. The rate of Na^+ flushing from sand is dependent on wetting patterns of percolating water in the unsaturated zone, which is itself affected by microtopography (e.g., furrows) and preferential flow. In particular, preferential finger flow has been hypothesized to occur in tailings sand, but to date, percolation patterns in the reclaimed upland have not been studied in detail. The purpose of this study was to characterize unsaturated flow patterns under the influence of microtopography and investigate their impacts on groundwater recharge and Na^+ flushing.

A dye tracer study showed that large amounts of dye runoff collected and infiltrated in furrows. Finger-like flow was observed in sand, having a maximum width of 20.7 cm and a maximum depth of 65.9 cm below LFH under one furrow. Similar wetting patterns were observed in a dye test within a bare tailings sand basin. Combined with macropore flow, finger-like flow was shown to promote deep penetration and limited lateral spreading of dye, indicating that furrows are responsible for a large proportion of recharge and Na^+ flushing. Despite this, split spoon samples collected at several locations between 2013 and 2019 suggest that Na^+ concentrations in unsaturated tailings sand decreased by ~90% across the entire upland, including under a sampled ridge. Large wetting events and lateral spreading of water from sand under furrows into sand under ridges are believed to be responsible for the site-wide decrease of Na^+ concentrations in sand.

Flow tank experiments using repacked soils also showed that furrows collected large amounts of runoff (>22%) and were responsible for the majority of flow in sand under moderate rainfall, although finger-like flow could not be reproduced under lab conditions. Under heavy rainfall, the LFH moisture content increased sufficiently to transmit water across the entire LFH-sand interface. Modelling predicted that, when the fraction of runoff from ridges into furrows was low (<25%), furrows spaced 83 cm (as-built design) would provide less recharge than a flat surface under 0% runoff. However, this was deemed to be an underestimate of furrow recharge contributions, as runoff losses (for a runoff fraction >0%) in the flat case would reduce recharge. Increasing furrow spacing to 150 cm improved recharge compared to the 83 cm case, but had a higher risk of flooding and should be accompanied by larger landforms such as recharge basins.

Furrows are expected to be most important for recharge soon after reclamation, when runoff and LFH water retention are highest. They are particularly important for capturing runoff during high-volume wetting events, such as a large rainfall event or snowmelt. As weathering of the LFH progresses, more water would be able to enter the sand under ridges, thus decreasing the relative recharge improvements from furrows. Sedimentation and concentrated root water uptake from preferential establishment of vegetation in later years may also decrease the recharge contributions of furrows.

Acknowledgements

My time as a graduate student has been something of a rollercoaster, with a mixture of stress, fun times at the field house, failed experiments, exciting discoveries, and a pandemic to finish it off. In the end, it has been a positive experience. I would like to thank my supervisor Jon Price for mentoring me and continuously supporting my investigations throughout my Master's degree; Owen Sutton, James Sherwood, and Eric Kessel for their mentorship and aid on projects ranging from field work, to lab experiments, to modelling; Jacob Whitehouse for literally hauling ~1000 lbs of water on a sled across the Nikanotee upland; and all others who helped me throughout my thesis.

Thank you to the Suncor Field Services and Reclamation teams for facilitating my field work and to the research sponsors – the Natural Sciences and Engineering Research Council of Canada, the Northern Scientific Training Program, Suncor Energy Inc., Imperial Oil Resources Ltd., and Teck Resources Ltd. – who made all this possible with their funding contributions.

Finally, I would like to thank my parents, siblings, grandparents, friends, and fiancée for their love and support over the course of my studies. You guys are awesome, and you made the hard times so much easier.

Dedication

To my wonderful fiancée, Nicole Davy

Nicole, you brighten my day, and having you with me has, ironically, made 2020 and 2021 the best years of my life – so far. You are the best fiancé(e), and I cannot wait to marry you and spend the rest of my life with you.

Table of Contents

List of Figures

List of Tables

Did you ever hear the tragedy of Darth Plagueis the Wise? I thought not. It's not a story the Jedi would tell you. It's a Sith legend. Darth Plagueis was a Dark Lord of the Sith, so powerful and so wise, he could use the Force to influence the midi-chlorians to create…life. He had such a knowledge of the dark side, he could even keep the ones he cared about from dying. The dark side of the Force is a pathway to many abilities some consider to be unnatural. He became so powerful, the only thing he was afraid of was losing his power, which eventually, of course, he did. Unfortunately, he taught his apprentice everything he knew, then his apprentice killed him in his sleep. It's ironic, he could save others from death, but not himself.

– Sheev Palpatine

Chapter 1: Introduction

As of 2016, surface mining had disturbed over 900 km^2 of the Alberta Oil Sands Region (AOSR) landscape by removing overburden to access underlying bitumen deposits (Alberta Environment and Parks, 2017). This has had a direct impact on peatlands, which comprise nearly one third of the landscape (Vitt *et al*., 1996), and has perturbed hydrological regimes both within and around the mined area (Elshorbagy *et al*., 2005). The Nikanotee Fen watershed is a pilot reclamation project completed in 2013 using mine waste and salvaged materials (Daly *et al*., 2012), designed to meet provincial requirements for re-establishing equivalent land capability – that is, the ability of reclaimed land to support land uses similar to those supported prior to disturbance (Government of Alberta, 2015) and to assess the feasibility of reclaiming fen peatlands. Understanding how construction materials and design choices affect the hydrology and redistribution of solutes in the system is essential to projecting how the watershed will evolve and improving future peatland reclamation designs.

The constructed watershed includes an upland coarse tailings sand aquifer that supplies groundwater to a low-lying fen. The sand is capped with a soil cover known as LFH-mineral mix (herein referred to as "LFH") that is commonly used for reclamation in the AOSR to support vegetation growth (Naeth, 2013; Daly, 2012). Tailings sand was used as a building material due to its abundance as a waste product from the bitumen extraction process, but its pore water contains elevated residual concentrations of Na^+ – among other contaminants such as naphthenic acids – that present a challenge to peatland reclamation (MacKinnon *et al*., 2001; Scott *et al*., 2005; Rezanezhad *et al*., 2012; Simhayov *et al*., 2017). As water percolates through the vadose zone, it flushes Na^+ down to the water table, which creates a continuous flux of Na^+ towards the fen. Elevated concentrations of Na^+ in fen groundwater pose a risk to plant health (Pouliot *et al*., 2012;

Rezanezhad *et al*., 2012) and could significantly impact the long-term success of both the present and future fen reclamation projects.

Na^+ migration has previously been studied in the saturated zone by Kessel *et al.* (2018), who suggested that unsaturated tailings sand will constitute a long-term source of groundwater Na^+ being transported to the fen. However, the flux of Na^+ transported down to the water table and the longevity of leachable Na^+ in the upland vadose zone are thought to be dependent on percolation patterns through the unsaturated tailings sand. In fact, preferential flow recurring along the same flow paths through the sand over a multitude of rainfall events could disproportionately flush some areas in the upland compared to others that receive less percolating water. It has previously been suggested that unstable flow (finger flow) occurs in the Nikanotee upland tailings sand, as indicated by high moisture "peaks" in tailings sand that could not be predicted by solving Richards' equation in Hydrus-1D (Sutton & Price, 2020). Finger flow is a type of preferential flow that occurs primarily in coarse soils. While macropore consist of rapid flow moving along large pores such as cracks, live or decayed roots, or worm burrows (Bouma & De Laat, 1981; Beven & Germann, 1982; Cey & Rudolph, 2009), finger flow can arise in near-homogenous porous media (Wang *et al*., 2003). Most investigations into finger flow have been conducted using initially dry, homogeneous sand since finger flow is dampened and thus less prominent under higher moisture conditions (Diment & Watson, 1983, 1985; Parlange & Hill, 1976) and in finer soils (Wang *et al*., 1998). It can be initiated by a number of factors, including water repellency (Hendrickx *et al*., 1993; Ritsema & Dekker, 1994; Wallach *et al*., 2013) and fine-over-coarse layering (Hill & Parlange, 1972; Hillel & Baker, 1988; Baker & Hillel, 1990). Water may also infiltrate as a uniform front but subsequently become unstable during redistribution (Wang *et al*., 2003; Jury *et al*., 2003; Wallach & Jortzick, 2008). Although finger flow can occur in near-perfect homogeneous media

(Wang *et al*., 2003), the initiation of fingers relies on some variation in soil structure or initial moisture content at the pore scale (Philip, 1975; Hill & Parlange, 1972) or larger inconsistencies, such as perturbations at a textural interface or heterogenous moisture distributions (Hill & Parlange, 1972; Glass *et al*., 1988). In addition, fingers are more likely to form and re-occur in areas of lower potential water repellency (Dekker & Ritsema, 1994; Ritsema & Dekker, 1994; Ritsema et al., 1998). In homogeneous media, finger flow pathways have been shown to persist over long periods of time, recurring along the same paths up to 28 days following the previous rainfall event due to hysteresis, which causes higher residual moisture content and therefore higher hydraulic conductivity to exist along previous finger flow pathways at equilibrium (Glass *et al*., 1988; Wang *et al*., 2003; Glass *et al*., 1989c). However, flow paths can be "erased" by complete wetting or drying of the sand in homogeneous media (Glass *et al*., 1988; Selker *et al*., 1996), and as such, finger flow paths can vary throughout the year when there are very wet or extended dry periods (Wessolek *et al*., 2009).

Another challenge facing the success of fen reclamation is the need to ensure that high water tables are maintained in the fen (Price *et al*., 2010). This relies on sufficient groundwater fluxes from the upland aquifer, which is dependant on adequate infiltration into the LFH cap and drainage through the underlying tailings sand. The LFH cover retains much of the infiltrated water, allowing vegetation to establish and draw water from it. Furthermore, water retention in the LFH is significantly higher than in the coarse tailings sand, which creates a capillary barrier above the textural interface that restricts drainage of water into the sand and reduces recharge (Naeth, 2011; Sutton & Price, 2020). In order to help increase infiltration and aquifer recharge by detaining runoff, several depressional features, including tilled furrows oriented perpendicular to the upland slope direction, were incorporated in the final design of the upland (Ketcheson *et al*., 2017).

Furrow tillage is a "rain harvesting" strategy that is commonly applied to sloped agricultural fields to provide more water to crops in arid regions and reduce erosion (Yang *et al*., 1996; Gammoh, 2011). It is frequently used for similar reasons in other mine reclamation projects (Saynor *et al*., 2018), but while furrows have been observed to become ponded in the Nikanotee upland by capturing rainfall as intended (Irvine, 2018), it is not clear whether incorporating these features is truly necessary for fen reclamation in the AOSR. Freeze-thaw weathering of the LFH has greatly increased recharge into the aquifer (Sutton & Price, 2020), yet furrows may still play an important role in ensuring adequate aquifer recharge, especially within the first few years post-construction when much of the LFH remains unweathered.

Currently, neither the role of furrows in water partitioning nor their impact on Na^+ flushing from tailings sand have been examined in detail. The accumulation of runoff in furrows is hypothesized to concentrate flow through the LFH directly beneath the furrows, which could increase the likelihood of finger flow in sand at these locations. It has been shown that fingers tend to originate beneath depressions that collect runoff and focus infiltration, and that fingers penetrate deeper and faster beneath them due to the concentration of infiltrated water in these areas (Arbel *et al*., 2005; Sililo & Tellam, 2000; Larson *et al*., 1999). However, more research on this interaction is needed, as the interaction between depressions and finger flow has only been marginally addressed in the literature (de Rooij, 2000); instead, many studies have purposefully created flat surfaces to understand finger flow processes without the interaction of microtopography (e.g. Öhrström *et al*., 2004; Ghodrati & Jury, 1990; Sheng *et al*., 2009).

Establishing the role of furrows in ensuring adequate recharge to reclaimed peatland systems, particularly during the early post-construction period, is key to deciding whether furrows are necessary or whether they can be omitted on the basis of cost-saving. If these features do indeed

constitute areas of high recharge, they could affect solute movement, for example by causing uneven flushing of Na^+ from the vadose zone, which would affect the flux of Na^+ down to the water table and transported downgradient to the fen. An uneven distribution of flow in the vadose zone would also affect the persistence of Na^+ in the unsaturated tailings sand, and thus, the duration that Na^+ seeps into groundwater. Consequently, studying the fate of Na^+ in the unsaturated tailings sand will help improve predictions concerning fen evolution and success, and it will allow recommendations to be made for future fen designs. Several approaches can be taken to examine the interactions between microtopography, LFH, and tailings sand in the Nikanotee upland vadose zone, each with their own strengths and weaknesses. Laboratory experiments studying finger flow often make use of thin, transparent flow tanks filled with re-packed soil and are designed to examine 2-D flow patterns under a variety of controlled conditions (Saffman & Taylor, 1958; Hill & Parlange, 1972; Glass *et al*., 1988; Baker & Hillel, 1990; Wang *et al*., 2018). Field experiments often consist of dye tracer tests where dye is applied over a plot area to simulate rainfall, followed by incremental excavation of the soil under the plot to expose a series of cross sections showing dye-stained percolation (Glass *et al*., 1988; Kung, 1990; Flury *et al*., 1994). Other tracers, such as bromide, chloride, and iodide, may also be used (Wessolek *et al*., 2009; Sheng *et al*., 2009). Field tracer tests have the advantage of showing flow patterns in undisturbed soil and capturing plot-scale heterogeneity, but they are much more labour intensive than lab experiments and only provide a snapshot in time of the percolation patterns due to the destructive nature of the excavation step. Other field activities required to determine in-situ concentrations of Na^+, for example sampling tailings sand cores at depth, face the same challenges. Lastly, modelling allows rapid, detailed simulation of flow distribution under a variety of scenarios, but relies on measured inputs, assumptions, and finite element discretization that may not adequately replicate flow under field

conditions. Moreover, modelling unsaturated flow with programs such as Hydrus-2D compute moisture redistribution by solving Richards' equation, which cannot simulate finger flow because it cannot simulate localized near-saturation at the wetting front that is necessary to initiate and perpetuate flow fingers (Eliassi & Glass, 2003). Apparent successes in modifying Richards' equation to produce finger flow (e.g. Nieber, 1996; Ritsema *et al*., 1998; Nguyen *et al*., 1999) are inadequate because they are not supported by physical mechanics (Eliassi & Glass, 2001). The research conducted in the present paper uses a combination of field experiments, lab experiments, and modelling to undertake a comprehensive investigation into water and solute transport within the Nikanotee Fen upland vadose zone, with the following objectives:

1) Evaluate percolation patterns in the vadose zone in the field, and assess how these patterns change under a variety of initial moisture, rainfall, and microtopography scenarios using laboratory and modelling techniques; and
2) Evaluate the impacts of furrows on groundwater recharge and Na^+ flushing from sand in space and time, and make recommendations concerning the incorporation of depressional landforms in future upland reclamation designs.

Chapter 2: Field-based methods for exploring preferential flow patterns and the evolution of residual sodium concentrations in the vadose zone of a reclaimed fen upland

2.1 Introduction

As of 2016, surface mining within the Athabasca Oil Sands Region (AOSR) had disturbed over 900 km^2 of the landscape by removing overburden to access underlying bitumen deposits (Alberta Environment and Parks, 2017). This has profoundly changed the landscape, close to one third of which is composed of peatlands (Vitt *et al*., 1996), and has disrupted hydrological regimes both within and around the mined area (Elshorbagy *et al*., 2005). To meet reclamation requirements for re-establishing equivalent land capability (Government of Alberta, 2015) and assess the feasibility of reclaiming fen peatlands, the Nikanotee Fen watershed was constructed from mine waste and salvaged materials (Daly *et al*., 2012) in January 2013. Studying how design choices and the materials used to construct the system influence the hydrology and redistribution of solutes is essential to projecting how the watershed will evolve, and to improving future peatland reclamation designs.

The upland aquifer that supplies groundwater to the fen was built using coarse tailings sand capped with a soil cover known as LFH-mineral mix (herein referred to as "LFH") that is commonly used for reclamation in the AOSR to support vegetation growth (Naeth, 2013; Daly, 2012). The LFH cover retains a large portion of infiltrated water, allowing vegetation to establish and draw water from it. Higher soil water retention in the LFH compared to the underlying tailings sand creates a capillary barrier at the interface between the two soils, which restricts drainage of water into the sand and reduces recharge (Naeth, 2011; Sutton & Price, 2020). Sufficient infiltration in the upland is crucial for maintaining adequate water levels in the upland (Price *et al*., 2010). To this end, several depressional features, including tilled furrows oriented

perpendicular to the upland slope direction, were incorporated in the final upland design to retain runoff, thereby increasing infiltration and limiting erosion (Ketcheson, 2015). Creating furrows in sloped fields is a strategy commonly used in agriculture for "rain harvesting" to provide more water to crops in arid regions and reduce erosion (Yang *et al*., 1996; Gammoh, 2011), and it is frequently used for similar reasons in mine reclamation projects (Saynor *et al*., 2018). In the Nikanotee upland, the furrows were observed to become ponded during rainfall events (Irvine, 2018), further suggesting that they are important features for capturing runoff and increasing infiltration, but no formal attempts have been made to identify their impacts on system hydrology.

A major challenge facing peatland reclamation in the AOSR is the presence of elevated residual concentrations of sodium (Na^+) – among other contaminants such as naphthenic acids – in the tailings sand pore water (MacKinnon *et al*., 2001; Scott *et al*., 2005; Rezanezhad *et al*., 2012; Simhayov *et al*., 2017). Percolating water through the sand in the vadose zone is responsible for a continuous flux of Na^+ down to the saturated zone, where it is transported to the fen. Elevated Na^+ concentrations in fen groundwater pose a risk to plant health (Pouliot *et al*., 2012; Rezanezhad *et al*., 2012) and have the potential to significantly impact the long-term success of the pioneering fen project. As such, it is important to monitor and understand Na^+ migration in the watershed and its impacts on plant health, so as to better predict its future level of success and propose Na^+ mitigations strategies for future reclamation projects. Migration of Na^+ in the saturated zone of the upland and through the peat has previously been studied by Kessel *et al.* (2018), who highlighted that the tailings sand in the vadose zone will constitute a long-term source of groundwater Na^+ being transported to the fen. The longevity of this source and the flux of Na^+ down to the water table is expected to be dependent on percolation patterns through the unsaturated tailings sand. In fact, preferential flow through sand recurring along the same flow paths over a multitude of rainfall

events could disproportionately flush some areas in the upland compared to others that receive less percolating water.

Unstable flow (finger flow) is a type of preferential flow that occurs in coarse soils and that could affect Na^+ flushing by only wetting a small portion of the tailings sand. Unlike macropore flow, which consists of rapid flow moving along large pores such as cracks, live or decayed roots, or worm burrows (Bouma & De Laat, 1981; Beven & Germann, 1982; Cey & Rudolph, 2009), finger flow within porous media is not strictly a result of heterogeneous permeability or soil properties (Wang *et al*., 2003). Most investigations into unstable flow have been conducted using initially dry, homogeneous sand since finger flow is dampened and thus, less prominent in finer soils (Wang *et al*., 1998) and when soil moisture is increased (Diment & Watson, 1983, 1985; Parlange & Hill, 1976). Conditions instigating finger flow are numerous; research has shown that it can be occur due to water repellency (Hendrickx *et al*., 1993; Ritsema & Dekker, 1994; Wallach *et al*., 2013) and fine-over-coarse layering (Hill & Parlange, 1972; Hillel & Baker, 1988; Baker & Hillel, 1990). Water may also infiltrate as a uniform front but subsequently become unstable during redistribution (Wang *et al*., 2003; Jury *et al*., 2003; Wallach & Jortzick, 2008). Although finger flow can occur in near-perfect homogeneous media (Wang *et al*., 2003), the initiation of individual fingers relies on some variation in soil structure or initial moisture content at the pore scale (Philip, 1975; Hill & Parlange, 1972) or larger inconsistencies (Hill & Parlange, 1972; Glass *et al*., 1988). In addition, heterogeneous distributions of potential water repellency can cause fingers to preferentially form and re-occur is areas that are less water repellent (Dekker & Ritsema, 1994; Ritsema & Dekker, 1994; Ritsema *et al.*, 1998). It has been shown that finger flow pathways can persist in homogeneous media over long periods of time, with water being observed to flow along the same paths up to 28 days after the previous rainfall event due to hysteresis (Glass *et al*., 1988;

Wang *et al*., 2003; Glass *et al*., 1989c). However, complete wetting or drying of the sand can "erase" flow paths (Glass *et al*., 1988; Selker *et al*., 1996), and as such, finger flow paths can vary throughout the year when there are very wet or extended dry periods (Wessolek *et al*., 2009).

The occurrence of finger flow in the Nikanotee upland tailings sand has been suggested by Sutton & Price (2020), as indicated by high moisture "peaks" in tailings sand that could not be predicted by solving Richards' equation in Hydrus-1D, but they did not study finger flow in detail or describe its implications for recharge and Na^+ flushing. Considering that furrows capture runoff and increase infiltration, there is presumably higher flow through LFH and possibly a greater chance of finger flow initiation directly beneath the furrows. However, the interaction between depressions and finger flow has only been marginally addressed in the literature; on the contrary, many studies on finger flow purposefully created flat surfaces to understand finger flow processes without the effects of microtopography (e.g. Öhrström *et al*., 2004; Ghodrati & Jury, 1990; Sheng *et al*., 2009). It has been observed that flow fingers tend to originate beneath depressions that collect runoff and focus infiltration, and that fingers penetrate deeper and faster beneath them due to a higher supply of water (Arbel *et al*., 2005; Sililo & Tellam, 2000; Larson *et al*., 1999), but more research on this interaction is necessary (de Rooij, 2000).

Many studies have made use of dye tracers to visualize flow patterns in the vadose zone in field settings (Glass *et al*., 1988; Kung, 1990; Flury *et al*., 1994), though other tracers such as bromide, chloride, and iodide have also been used (Wessolek *et al*., 2009; Sheng *et al*., 2009). Until now, water flow patterns in the vadose zone of a capped tailings sand aquifer have not been adequately examined at the small scale to capture the effects of topographical variations of a few centimetres. The existence of localized high infiltration areas such as furrows could lead to uneven flushing of Na^+, which would affect the persistence of Na^+ in the unsaturated tailings sand, as well

as the flux of Na^+ down to the water table and transportation downgradient to the fen. As such, studying the fate of Na^+ in the unsaturated tailings sand will help improve predictions concerning fen evolution and success. Therefore, this chapter has the following objectives: 1) determine the impact of microtopography on percolation patterns through the vadose zone, using a field dye tracer study; and 2) assess the impacts of flow patterns on Na^+ flushing, based on residual Na^+ concentrations in sand samples collected from the upland.

2.2 Site description

The reclaimed Nikanotee Fen watershed is located on an oil sands mining lease, approximately 25 km north of Fort McMurray, Alberta (56°55'59" N, 111°25'00" W). It consists of a 7.7 ha upland and a 2.9 ha fen, which are bounded by a natural slope to the south (2.8 ha) and slopes reclaimed in 2007 to the east (8.1 ha) and in 2011 to the southeast (8.2 ha) and west (2.4 ha). These were in addition to a berm to the north (Figure 2.1), yielding a total watershed area of 32.1 ha, with a high upland-to-fen area ratio (2.7:1), selected to ensure sufficient groundwater supply to the fen by the upland (Price *et al*., 2010).

Moderately decomposed peat was salvaged and directly placed from a nearby donor fen on the mine lease (Nwaishi *et al*., 2015; Daly *et al*., 2012). The peat was placed in a 2 m thick layer in the reclaimed fen, overtop of a petroleum coke underdrain layer that supplies an upward flux of water originating from the upland. The petroleum coke underdrain extends ~100 m into the upland aquifer (transition zone), which consists of a ~2-3 m-thick coarse tailings sand layer capped with approximately 30 cm of LFH. Tailings sand samples collected by Ketcheson (2015) were classified as either sand or sandy loam, with an average composition of 88% sand, 11% silt, and <1% clay.

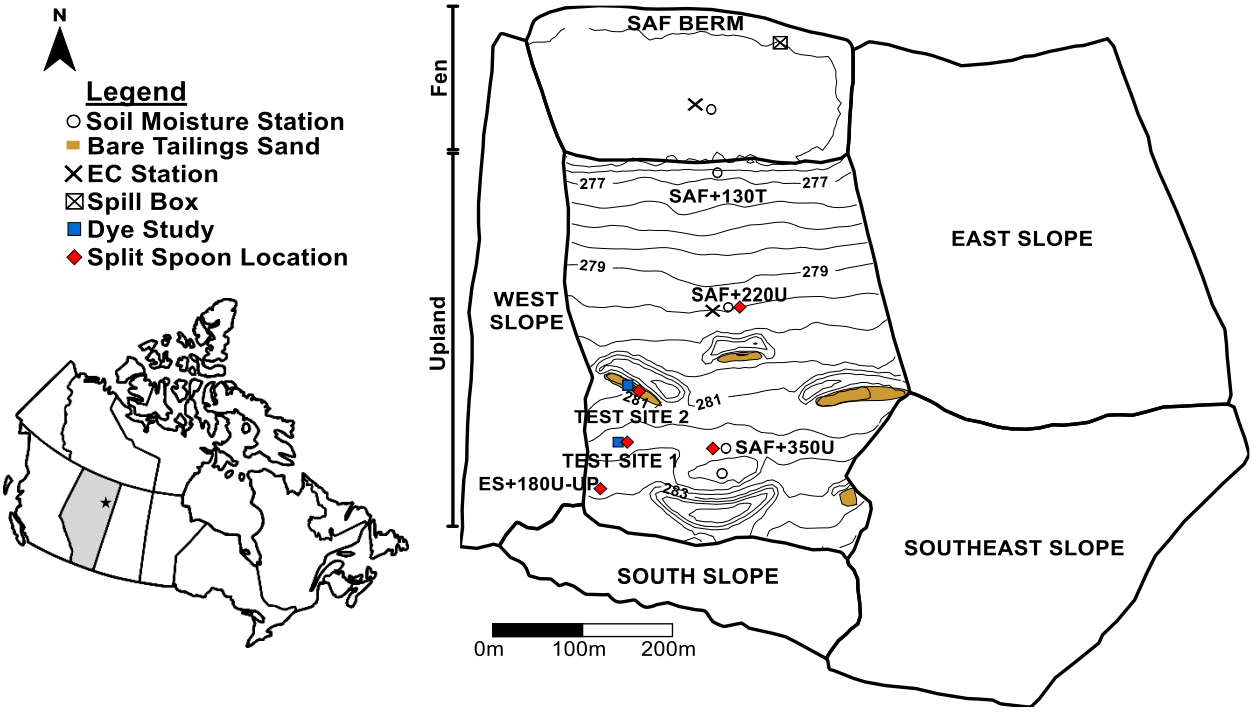

Figure 2.1: Location and plan view of the Nikanotee fen watershed showing topography in the constructed fen and upland, monitoring stations, bare sand basins, dye study locations, and split spoon sampling locations.

The average classification of the LFH material was sandy loam, composed of 52% sand, 42% silt, and 6% clay (Ketcheson, 2015). A geosynthetic clay liner was placed at the base of the constructed fen and upland to limit seepage into the underlying material and ensure that sufficient amounts of water were supplied to the fen. The upland was sloped towards the fen with a ~2% grade at the surface and a ~3% grade at the basal liner. An outlet at the north-east corner of the fen allowed outflow from the system into a retention pond.

To increase recharge of the upland aquifer and ensure a sufficient groundwater supply to the fen, two types of landscape features were incorporated into the final design of the upland. First, in response to large amounts of runoff that were observed during snowmelt in spring of 2013, furrows were tilled perpendicular to the upland slope in August of 2013 to retain runoff (WorleyParsons,

2014), using a ripper shank pulled by a bulldozer. The average furrow width, depth, and spacing were 24 cm, 10 cm, and 83 cm, respectively (Ketcheson, 2015). Second, LFH was raised in four areas to create "hummocks" behind which LFH was stripped, thereby creating bare tailings sand depressions ("recharge basins") capable of detaining runoff and having a high infiltration capacity (Ketcheson, 2015). The furrows initially had an average infiltration capacity of 128 mm/hr that was nearly double the average infiltration capacity of 68 mm/hr in the ridges between the furrows, though the difference was not statically significant (Ketcheson, 2015). However, the infiltration capacity of the ridges and furrows became more similar, and no significant difference was observed between them in 2014 and in 2016 (Asten, unpublished data). The furrows nonetheless continued to retain runoff and increase infiltration in the upland.

Precipitation was measured in 30-min intervals at a meteorological station installed in the upland (Figure 2.1) that was configured with a TR-525M tippling bucket rain gauge (Texas Instruments Canada Ltd.). Three soil moisture stations (SAF+130T, SAF+220U, and SAF+350U) were installed near the north-south centreline of the upland and logged data on an hourly basis. The nomenclature of these stations was derived from their distance, in metres, from the berm at the northern fen boundary. Each station had coaxial impedance dielectric reflectometry soil water sensors (Stevens Hydra Probe II) installed nominally at 5, 10, 15, and 30 cm bgs in LFH and 40, 60, 100, and 150 cm bgs in tailings sand. The actual depths of the probes placed in LFH vary from their nominal depths (data not shown), as reported by Sutton & Price (2020), which was accounted for when assessing measurements from these stations.

2.3 Methods

Dye experiments

To investigate flow patterns in the tailings sand, two dye tracer experiments were undertaken. These experiments consisted of applying dye over a typical LFH-sand plot on June 19, 2019 (Dye Test 1, Figure 2.2a) and over bare sand in the West recharge basin on July 17 (Dye Test 2, Figure 2.2b). For both tests, 7 g/L of a Brilliant Blue FCF dye solution was applied in 30 min intervals over a 4 hr period using watering cans, such that a total of 20 mm of dye solution was applied over 4 hrs. Dye and water were applied at a rate of 4 mm/hr from 0-0.5 hrs, 12 mm/hr from 0.5-1.0 hrs, and 4 mm/hr from 1.0-4.0 hrs; the higher rate applied over the 0.5-1.0 hr interval was included to simulate a hyetograph peak. Aluminum edging was placed around the dye plot area and was sealed with expanding foam to detain dye runoff. However, the edging was not placed into the ground, because a preliminary dye test showed that disturbing the ground was responsible for a significant amount of edge flow. Dye was applied within a 2.6 m x 1.6 m area in Test 1 and a 1.6 m x 1.6 m area in Test 2. These plots were designed to be large enough to accommodate a 30 cm "buffer zone" that could be discarded to remove most edge flow. Test 1 had a greater width so that it would span two furrows and capture runoff from adjacent ridges, whereas Test 2 was not designed to capture depressions and so did not require a large width. In both tests, water was simultaneously applied around the edges of the dye plots at the same rate so as to better mimic a rainfall event and limit lateral flow of the percolating dye. This methodology was based on the double ring infiltrometer method, although the outside edge of the watered area was not confined by a barrier. Antecedent moisture data preceding Test 1 was retrieved from the SAF+350U soil moisture station, which was the closest station and was located ~65 m away from the dye test. For Test 2, two sets of moisture measurements were taken at identical depths with a soil water sensor (Stevens

Figure 2.2: Photographs taken of the dye test setup for: a) Test 1, after dye application, facing east, with red dashed lines showing the approximate locations of furrow centrelines; and b) Test 2, prior to application, facing east. The pink strings shown in a) were used as guides for incrementally excavating the plot area.

Hydra Probe II) in a trench within the West recharge basin, immediately prior to the start of the experiment.

The day following application, excavation of the dye plot was commenced to expose vertical cross-sections at 10 cm intervals. Each vertical section was photographed using a DSLR camera, with a leveled vertical measuring stick and a horizontally-placed measuring tape included for scale. The excavation timeline and overnight rainfall volumes are shown in Table 2.1. Ideally, the

excavation process would have been conducted over a single day for each test to minimize differences in drainage time and rainfall volume between soil section photographs. However, this was not possible due to the considerable amount physical labour needed to remove the soil, combined with interruptions from wildlife and inclement weather.

Table 2.1: Vertical cross-section excavation schedule and cumulative prior rainfall (relative to beginning of test)

Test	Date	Cross-sections (cm from west edge of plot)	Cum. prior rainfall (mm)
1	Jun 20, 2019	0	1.6
1	Jun 21, 2019	20 to 80	2.3
1	Jun 22, 2019	80 to 130	13.5
2	Jul 18, 2019	-70 to -20	0
2	Jul 19, 2019	0 to 160	3.8

Next, images were processed to obtain numerical data for the observed dye distribution in sand. A custom MATLAB software application with a graphical user interface was developed to carry out image analysis of the cross-section photographs and to provide an easy-to-use tool for other users seeking to undertake similar analyses. This set of custom algorithms was necessary to isolate dye in sand under an uneven LFH-sand boundary and quantitatively analyse the distribution of blue (dyed) pixels in sand, which cannot be achieved with commonly available image processing tools. The software package and the program manual are included as supplementary material. The MATLAB application requires a region of interest (ROI) to be interactively selected within each cross-sectional image, corresponding to a rectangular real-world area. It is recommended that a rectangular frame of known dimensions be placed around the ROI when photographing the soil cross-sections so that the ROI can be easily identified during the analysis phase. The program uses this ROI and its associated real-world dimensions to apply a projective transformation that removes image tilt with respect to the cross-sectional area. This results in a scaled image that

contains only the ROI, which is then further cropped to provide a consistent image width for all cross-section photographs. If image tilt persists, it may be corrected through an optional tilt correction step. The top boundary of the analysis area, such as the soil surface or the boundary between two soil layers, must also be traced by the software user; the region above this boundary is excluded from the analysis. Dye colour thresholds, based on the pixel values of the hue and/or saturation channels, must be defined to allow for dyed pixels to be isolated from non-dyed regions. Finally, noise removal thresholds must be set to improve the accuracy of the dye isolation algorithm; additional steps also allow for manual noise manipulation if this automated noise removal tool is insufficient. Following these steps, the dye coverage within each image ROI can be accurately analysed to provide dye coverage data for the individual images, which can then be compiled to provide a summary of dye distribution within the entire plot. Due to the difficulty of isolating dyed areas in multiple soil layers that contain heterogeneities, and because Na^+ flushing patterns in tailings sand were of greatest interest, emphasis was placed on the accuracy of dyed pixel selection in the sand rather than in the overlying LFH.

Collection and analysis of sand samples

Continuous tailings sand split spoon samples were collected from several locations in the upland using a Pionjar hammer drill between 2013 and 2019. The sampling strategy was designed to monitor Na^+ concentration changes over time and at various depths, while capturing Na^+ distributions at various locations. A decline in residual Na^+ concentrations over time, as well as similarities in Na^+ content between sampling locations within a given year, would indicate that Na^+ flushing was occurring site-wide, regardless of preferential flow; otherwise, the persistence of high concentrations in some areas would suggest that preferential flow was responsible for flushing

more Na^+ from certain parts of the upland than others. Split spoon locations are recorded in Table 2.2, along with approximate LFH thickness and years sampled; the approximate sampling locations are also shown in Figure 2.1. Split spoon cores were taken near the same wells in 2013, 2014, and 2015. Cores were also taken in the three bare tailings sand basins in 2015. Microtopography was not noted while taking cores between 2013 and 2015. In 2019, two pairs of cores were collected to sample sand under depressions and adjacent high points. The first pair was taken over LFH in the southern portion of the upland, near Dye Test 1: one sample was taken in a 4 cm deep furrow, and the other was taken in an adjacent ridge. The second pair was taken over bare tailings sand within the West recharge basin: one sample was in a depression where water was observed to pool during a rainfall event; the other sample was collected 1 m upslope of the first.

The split spoon cores were subdivided into 10 cm increments, then every other subsample was analysed for total leachable Na^+ mass. Stones and debris were removed, and the remaining sand was ground with a mortar and pestle to remove clumps. Approximately 500 mL of ultrapure water was added to ~200 g of the sand sample (2.5:1 water-soil mass ratio) and the mixture was manually shaken for 60 s to ensure that the entire sand sample was impregnated with water. For the 2013 and 2014 samples, the 2.5:1 water-soil mass ratio was only used for odd number samples, while a 5:1 ratio was used for even number samples to evaluate the impact of increasing the water-soil mass ratio on Na^+ extraction. The mixture was then placed on a shaker table for 24 hrs, after which it was passed through 3 coffee filters to retain the soil, then passed through a 0.45 μm syringe filter. The final filtrate was analysed for aqueous Na^+ concentration using an ion chromatograph (DIONEX ICS 3000 for 2013-2015 samples; DIONEX ICS 6000 for 2019 samples), while the

sand residue was dried at 105°C for 24 hrs and weighed to allow for the mass of leachable Na^+ per mass of dry sand to be calculated.

Table 2.2: Split spoon sampling location, date, and recorded LFH thickness

Location	Year	Date	Recorded LFH thickness
SAF+350U	2013	Oct 19	25 cm
	2014	Aug 18	35 cm
	2015	Oct 4	~35 cm
	Average depth		~31.7 cm
SAF+220U	2013	Oct 19	48 cm
	2014	Aug 15	~50 cm
	2015	Oct 4	~45 cm
	Average depth		~47.7 cm
ES+180U-UP	2013	Not recorded	Not recorded
	2014	Aug 18	50 cm
	2015	Oct 4	~30 cm
	Average depth		~40 cm
East basin	2015	Not recorded	NA
Mid basin	2015	June 3	NA
West basin	2015	June 4	NA
West basin, near dye Test 2	2019	Aug 15	NA
Near dye Test 1	2019	Aug 19	Furrow: 27.5 cm Ridge: 31.5 cm

2.4 Results

Dye tests

Antecedent moisture conditions prior to the dye tests are shown in Figure 2.3. The sand had a relatively low, uniform volumetric water content (θ) prior to both tests, ranging between 0.094 to 0.123. The LFH was also relatively dry prior to Test 1, with θ increasing from 0.098 at the surface to 0.150 at the capillary barrier between the LFH and sand.

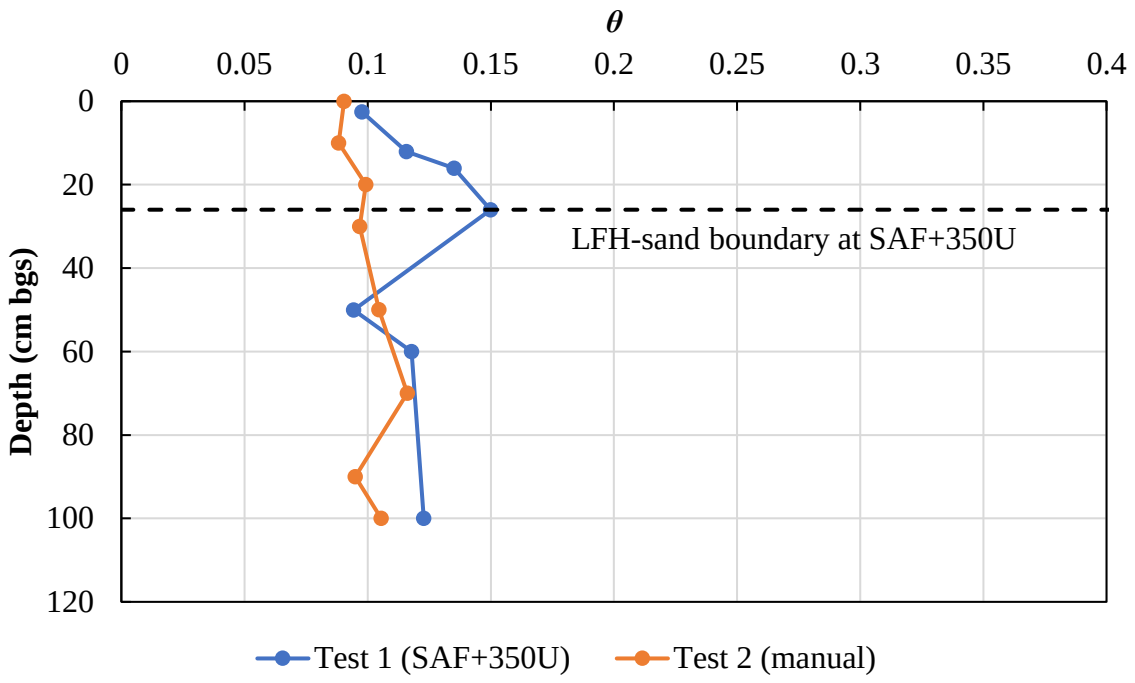

Figure 2.3: Antecedent moisture prior to the dye tests. Test 1 moisture was retrieved from the SAF+350U station and Test 2 moisture was manually measured with a portable probe.

In Dye Test 1, finger-like flow was observed under the north furrow, though little flow was observed in sand under the south furrow. The north furrow and south furrow had average depths of 8.0 cm and 4.0 cm, respectively, and it is likely that the greater depth of the north furrow was responsible for more dye accumulation. Considering that flow through sand was of greatest interest for the dye experiment, it was decided that only the north furrow (Figure 2.4) would be analysed in detail. Each vertical cross-section photograph was analysed over an area that was 1 m in width to capture the entire north furrow and approximately half of the ridge area on each side of the furrow; the processed images for each cross-section are shown in Figure A.1 (Appendix A). Cross-sections are referred to by their distance from the west edge; for example, the 40 cm cross-section was excavated 40 cm from the west edge of the plot.

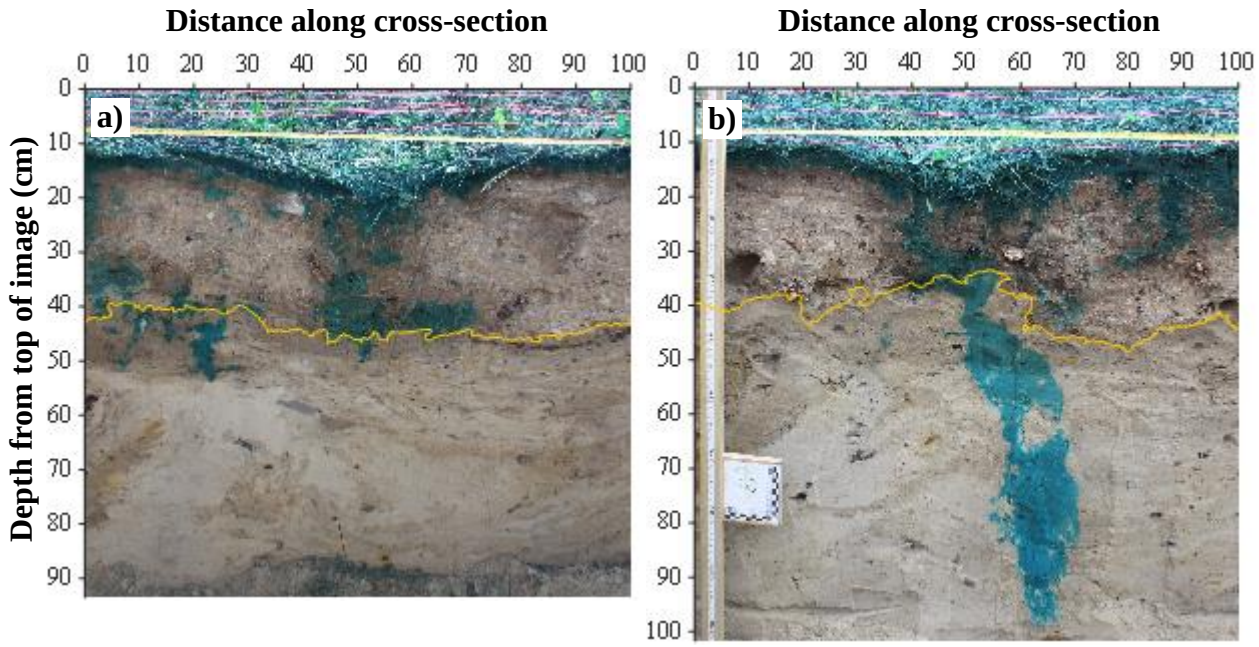

Figure 2.4: Perspective-corrected images of the north furrow taken during Test 1 at a) the 40 cm cross-section and b) the 90 cm cross-section. The furrow centreline is located at the 50 cm mark in the horizontal direction in each image, with ridges on each side of the furrow. The interface between LFH and sand was traced in yellow.

The dye distribution data from all cross-sections was compiled and plotted to show horizontal distribution and average wetted fraction with depth (Figure 2.5). Wetted fraction is defined as the number of dyed pixels at a given depth below LFH divided by the number of pixels along the 1 m width of the cross-section. The centre of mass of the dyed sand in the horizontal direction was calculated to be 9.9 cm to the right of the furrow centreline. Further analysis showed that 93.2% of the dye passing through sand was located within 20 cm of the horizontal centre of mass, as the furrow accumulated runoff from the adjacent ridges, producing large amounts of flow under the furrow. Average wetted fraction did not surpass 6.3% below the top 1 cm of sand and generally decreased with depth. The most significant dye coverage in sand was observed at the vertical cross-sections that were 90 cm, 100 cm, 110 cm, and 130 cm from the west edge of the plot (Figure A.1). All of these dyed areas belonged to flow fingers originating beneath the furrow. The dye patterns

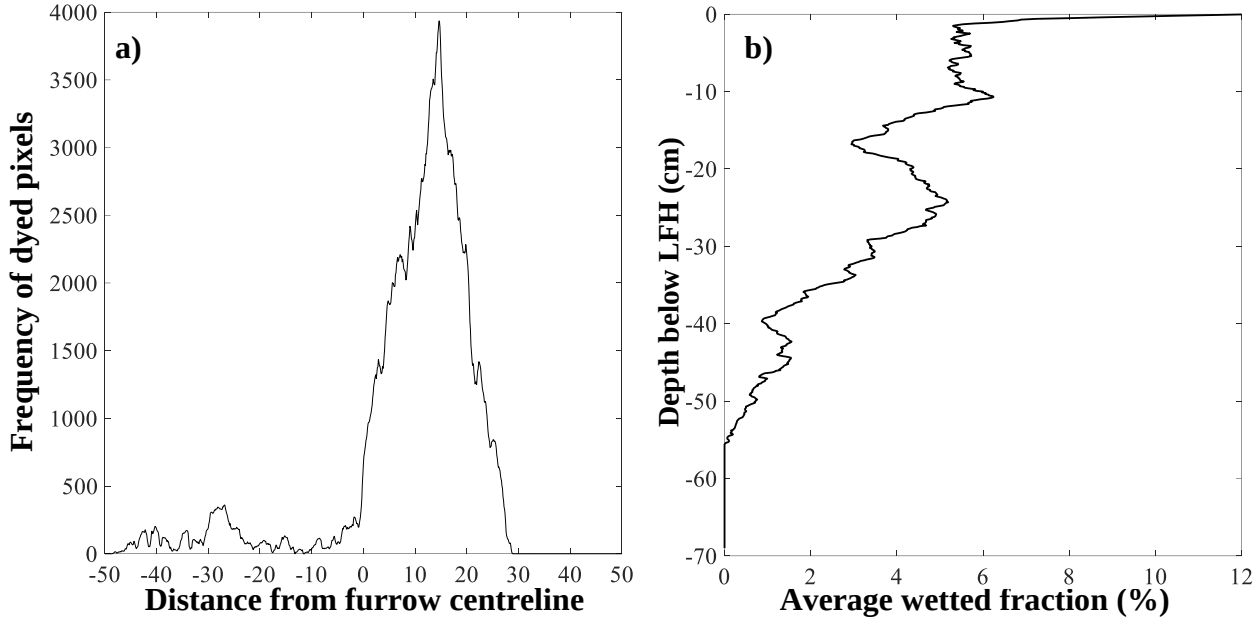

Figure 2.5: Results for all cross-sections combined, showing a) horizontal dye distribution and b) average wetted fraction

in sand from the 90 cm to 110 cm cross-sections appeared to belong to a single finger, while dye staining in the 130 cm cross-section appeared to be part of a separate finger. Further analysis of the fingers observed at these locations were conducted to determine the width and length of the finger along the plumes' trajectories, which were estimated by fitting a line of least squares through the plumes. Vertical penetration distance of the dye beneath the LFH was also calculated with respect to cartesian coordinates. Analysis of the finger occurring from the 90 cm to 110 cm cross-sections showed that the plume's maximum width, length, and vertical penetration below the LFH-sand interface were 20.7 cm, 67.2 cm, and 65.9 cm, respectively. For the finger observed below the furrow at the 130 cm cross-section, these dimensions were 18.1 cm, 39.0 cm, and 38.9 cm, respectively.

Some dye originating from the ridge surface also penetrated into the sand and formed fingers. The most significant breakthrough beneath a ridge occurred at the 40 cm cross-section, where the

maximum plume width, plume length, and vertical penetration were 8.4 cm, 13.7 cm, and 13.7 cm, respectively.

Breakthrough into sand occurred at discrete points that often coincided with macropores near the LFH-sand interface, such as voids surrounding roots and stones (Figure 2.6). Root channels appeared to act as conduits where dye was able to rapidly traverse the LFH, which encourages breakthrough into sand under the root systems (Figure 2.6a).

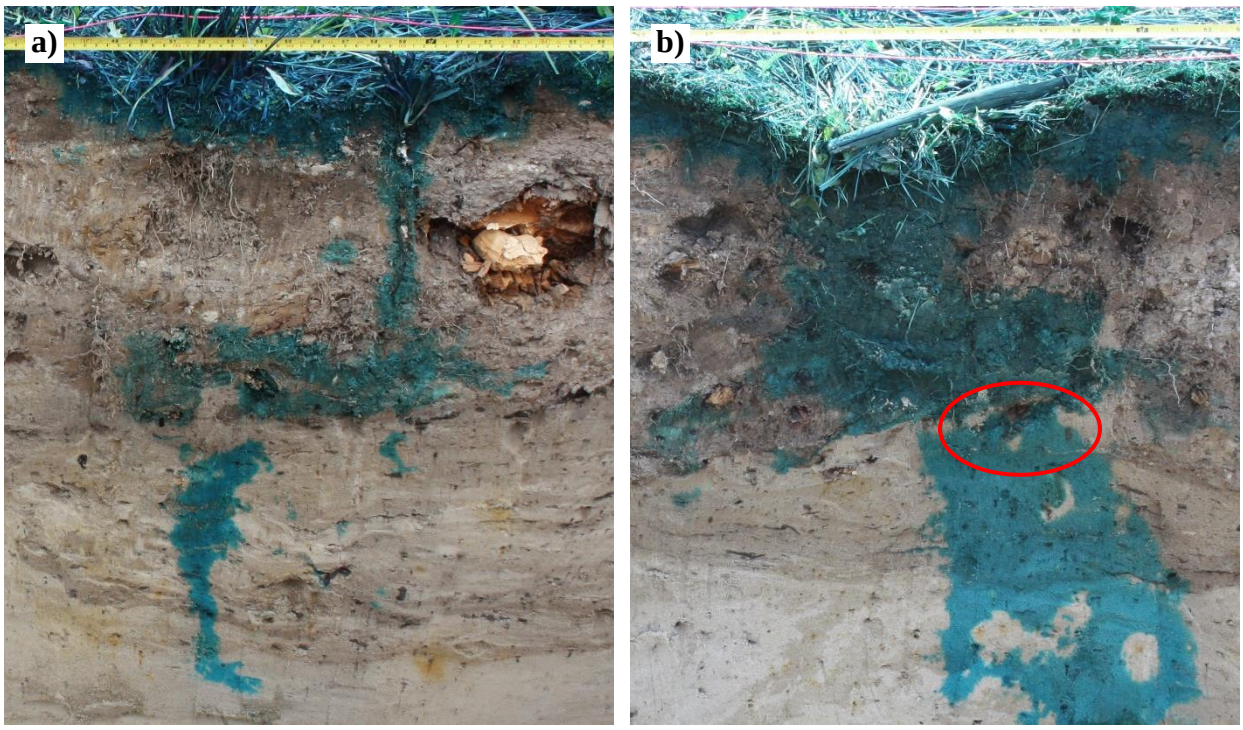

Figure 2.6: Dye flow along macropores created by: a) a root channel throughout the vertical LFH profile, under the north furrow at the 20 cm cross-section; and b) a cavity surrounding a stone at the LFH-sand interface (circled in red), at the 100 cm cross-section.

In Dye Test 2, the majority of applied dye became runoff and was temporarily retained by the aluminum edging along the perimeter of the plot, before exiting the plot area and accumulating in an elongated depression running east-west along the hummock. A ~0.5 cm-thick hydrophobic crust

noted at the soil surface is thought to have been responsible for the low infiltration rate in the sand and, consequently, the high amount of runoff. The tailings sand had previously been shown by Ketcheson & Price (2016) to be slightly hydrophobic at low θ (~0.09), and it was anecdotally observed to be highly water repellent when sand was completely dry (oven dried at 80°C until

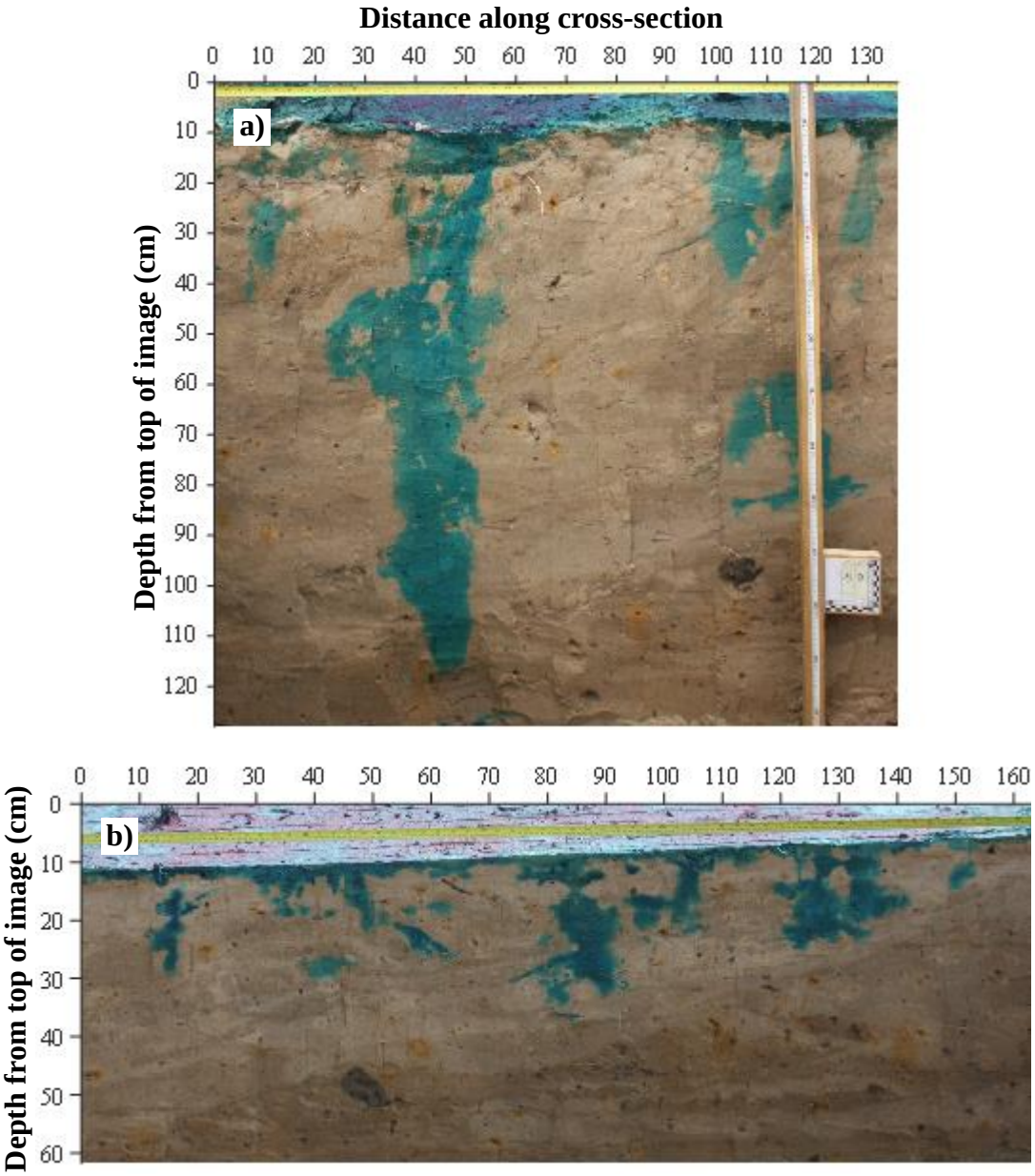

Figure 2.7: Perspective-corrected photographs taken of the trench face within the West recharge basin during Test 2 at a) the 60 cm cross-section and b) the -40 cm cross-section (outside the application area). Both photographs were taken facing east.

moisture content no longer decreased). Vertical cross-sections exposing dye infiltration patterns within the plot (Figure 2.7) showed that discretized breakthrough occurred through the crust into the underlying sand. Flow patterns inside the plot were finger-like and reached a maximum depth of about 38 cm, with variable widths. Below the depression where dye accumulated outside the plot, maximum finger depth and width were approximately 120 cm and 35 cm, respectively. Runoff into depressions within the West basin was also observed during an 8.1 mm natural rainfall event that occurred on August 5th, 2019 (Figure 2.8). Dye flow patterns in Test 2 were not analysed in greater detail, because the majority of flow exited the dye plot area and because the tailings sand basins are not representative of the upland area, most of which is capped with LFH.

Figure 2.8: Accumulation of runoff into a local depression within the West basin during an 8.1 mm rainfall event in 2019

Split spoon Na^+ analysis

At sampling sites where sand was capped with LFH, residual Na^+ concentrations in sand were relatively similar between 2013 and 2014 but were much lower in 2015 (Figure 2.9a-c). At the SAF+350U and ES+180U-UP locations, Na^+ concentrations increased with depth for all years. At SAF+350U (Figure 2.9a), values in 2013 and 2014 ranged from ~20 mg Na^+/kg sand at 25 cm below LFH to ~90 mg/kg at depths greater than 150 cm below LFH. At ES+180U-UP, concentrations ranged from ~30 mg/kg at 25 cm below LFH to 125 mg/kg at 175 cm below LFH in 2013 and 2014. In 2015, the concentrations at SAF+350U ranged from 3 mg/kg at 25 cm depth to 17 mg/kg at 125 cm depth; at ES+180U-UP, concentrations varied from 12 mg/kg at 25 cm depth to 33 mg/kg at 175 cm depth.

In contrast, no consistent trend with depth was observed in any sampling year at SAF+220U, and a high degree of variability in concentrations existed between samples collected in 2013 and 2014 (Figure 2.9b). The average concentrations at SAF+220U in 2013, 2014, and 2015 – calculated from trapezoid-approximated integration divided by the depth interval – were 49.0 mg/kg, 80.4 mg/kg, and 25.7 mg/kg, respectfully.

By 2019, the concentrations of Na^+ in samples taken from a furrow and an adjacent ridge near Test 1 were consistently lower than in previous years and did not exceed 13 mg/kg (Figure 2.9a-c). The biggest differences between the samples taken under the furrow and ridge occurred between 5 and 65 cm below LFH, where the furrow had 4.8 mg/kg less Na^+ compared to the ridge, on average. Below 65 cm, no consistent difference existed between the furrow and ridge.

Na^+ concentrations in most of the samples collected from the bare tailings sand basins were very low by 2015 (Figure 2.9d). Some samples did, however, contain moderately elevated

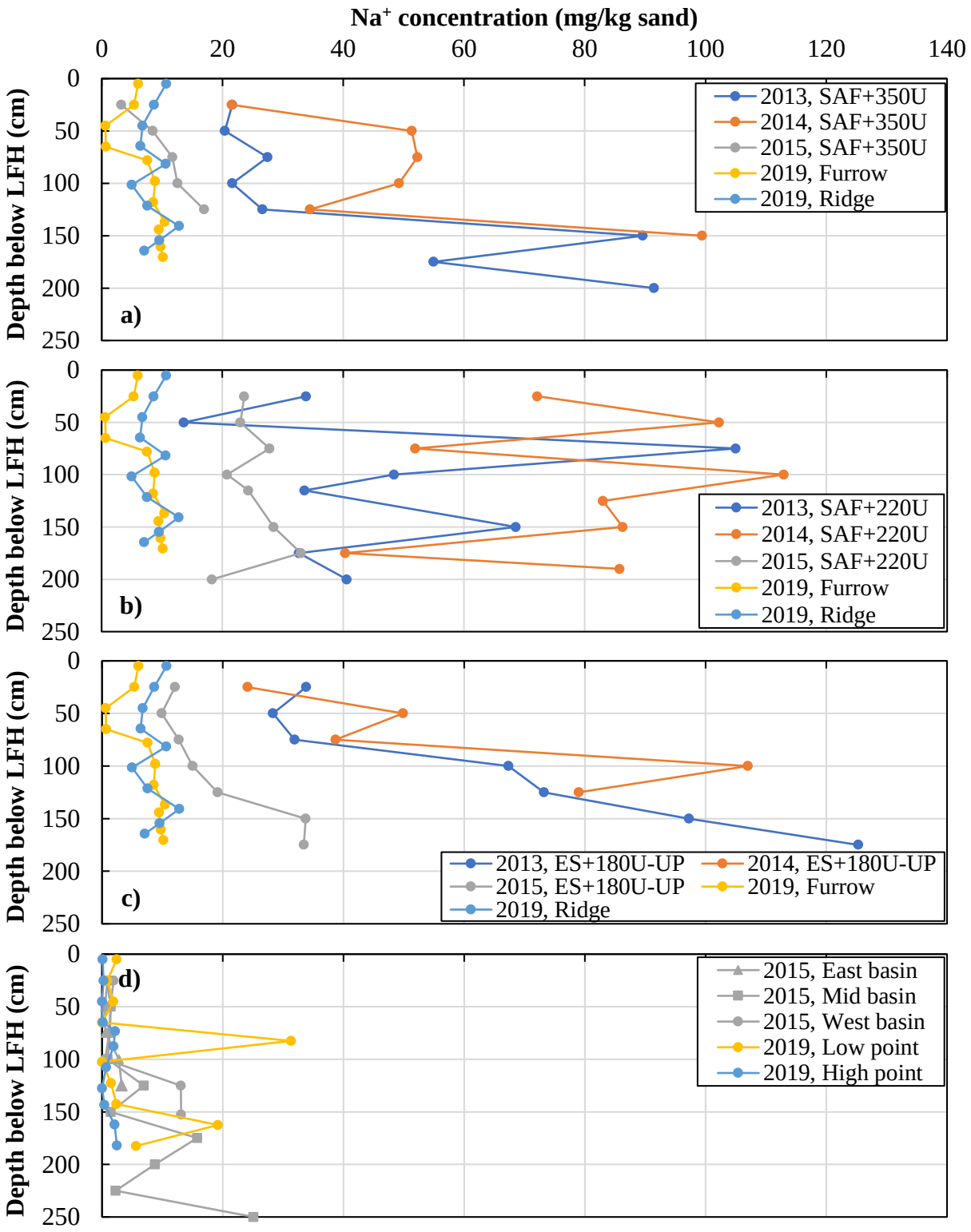

Figure 2.9: Leachable Na^+ concentrations in tailings sand at a) SAF+350U, b) SAF+220U, c) ES+180U-UP, and d) bare tailings sand basins. Results for cores collected east of the Test 1 dye plot in 2019 are included in plots a), b) and c), and results for cores collected east of the Test 2 dye plot in 2019 are included in plot d).

concentrations, up to 31.3 mg/kg in a sample taken from the West basin low point in 2019. Table 2.3 shows the average residual Na^+ at the four locations sampled in 2019 and the fraction that had been flushed, assuming an initial, uniformly distributed Na^+ concentration of 72 mg/L equal to the average leachable concentration reported by Simhayov *et al*. (2017) in stockpiled tailings sand prior to placement. Average residual Na^+ concentration was highest under the ridge, where 88% of Na^+ was estimated to have been flushed.

Table 2.3: Average residual Na^+ concentration and estimated average fraction of flushed Na^+ in 2019 split spoon samples

Location	Average Na^+ conc. (mg/kg)	Average fraction of flushed Na^+ (%)
Furrow	6.55	90.9
Ridge	8.36	88.4
Basin low point	6.67	90.7
Basin high point	0.85	98.8

2.5 Discussion

Finger flow in tailings sand

The first indication of finger flow occurrence in tailings sand was noted by Sutton and Price (2020), who found that moisture station probes measured sporadic moisture "peaks" that could not be predicted by Hydrus-1D, where θ rapidly increased to values that were near saturation, then rapidly decreased. The seemingly random occurrence of these moisture peaks suggested that flow patterns were finger-like in nature and bypassed much of the tailings sand soil matrix, inconsistently intersecting the sensing volume of the soil moisture probes. Finger flow was hypothesized to occur in sand because of lower saturated hydraulic conductivity in unweathered

LFH compared to the unsaturated hydraulic conductivity in sand at the estimated water entry pressure of -0.11 m (Sutton & Price, 2020), which would cause a uniform wetting front to constrict at the LFH-sand interface and split into flow fingers (Hillel & Baker, 1988; Baker & Hillel, 1990).

Although not directly discussed by Sutton and Price (2020), the peaks in moisture content are indicative of saturation overshoot, a percolation pattern characterized by a near-saturated finger tip and a draining "tail" directly behind the wetting front tip (Glass et al., 1989c; Liu et al., 1994). The decreasing moisture content behind the wetting front is associated with a decreasing pressure gradient (Selker *et al*., 1992), which is a prerequisite to finger flow (Raats, 1973; Philip, 1975). Richards' equation lacks the physical mechanics to simulate the build-up of moisture at finger tips, and consequently, it cannot simulate finger flow (Eliassi & Glass, 2001, 2003). The occurrence of finger flow would therefore help explain why Hydrus-1D could not predict the moisture peaks observed in tailings sand (Sutton & Price, 2020).

In the present study, dye experiments showed that deep percolation occurred under furrows (Figure 2.4) and in the depression in the recharge basin (Figure 2.7a), with little lateral spreading of percolating water and a low wetted fraction (Figure 2.5), all of which are characteristic of finger flow (Jury *et al*., 2003). It is difficult, however, to ascertain whether flow through the upland tailings sand can truly be defined as finger flow. Moisture content within the LFH profile (Figure 2.3) indicates that the textural interface between the finer LFH and the coarser underlying sand created a capillary barrier (Sutton & Price, 2020), only allowing discrete breakthrough of flow into the sand (Figures 2.4 and 2.6), which is often a precursor to finger flow in two-layered systems (Hill & Parlange, 1972; Glass *et al*., 1988; Hillel & Baker, 1988; Baker & Hillel, 1990). Macropores or disturbances at the textural interface were observed to direct flow into sand at discrete points in the present study (Figure 2.6) and have been observed to induce finger flow in

other studies (Hill & Parlange, 1972; Glass *et al*., 1988). Similarly, the crust in the bare tailings sand basin functioned as a thin, low permeability soil that only allowed infiltration to proceed at discrete locations, analogous to a fine-over-coarse layered system (Raats, 1973; Philip, 1975). In addition, there was limited lateral spreading of percolating dye, which was especially noticeable under depressions where high flow volumes and percolation depths occurred. The slight hydrophobicity of tailings sand at low moisture contents (Ketcheson & Price, 2016) may also have contributed to flow fingering (Hendrickx *et al*., 1993; Ritsema & Dekker, 1994).

Test 2, however, showed that areas upslope of the depression, where flux through the sand is lower, often experienced higher lateral spreading at depth, creating bulbous flow patterns in deeper areas that resembled stable flow and occasionally merge (Figure 2.7b, right side). This could signify one of two things: either finger flow is indeed occurring and that higher moisture at depth is causing the fingers to widen, as has been shown to occur in previous studies (Diment & Watson, 1983, 1985; Parlange & Hill, 1976); or, that the apparent finger flow is actually a stable wetting front resembling finger flow as a result of high pressures from point sources at the top of sand, such as below a furrow. This condition can drive large volumes of water downward, with lateral spreading by capillary action becoming more apparent at lower flux rates (Philip, 1968). Given the uncertainty as to whether observed dye patterns in tailings sand can be characterized as finger flow, these patterns are herein referred to as "finger-like" flow.

Current and future hydrological role of furrows

It was clear from Test 1 that large volumes of runoff accumulate and infiltrate in furrows, reaching depths of up to 66 cm below the LFH, with little lateral spreading. Ponding was observed

during a large rainfall event in 2016 (Irvine, 2018), further highlighting the importance of furrows in capturing runoff from ridges. The ability of furrows to not only reduce water losses from runoff, but also transmit water deep into the sand where losses to ET are small (Sutton & Price, 2020), indicates that incorporating furrows into upland designs increases aquifer recharge. Furrows are expected to have the greatest impact on recharge in earlier years when substantial weathering is still ongoing. During this period, furrows would help overcome the strong capillary barrier at the LFH-sand interface (Sutton & Price, 2020) by capturing runoff and promoting localized high moisture contents that are needed to overcome the pressure at which water can cross the capillary barrier. In addition, runoff would be highest in early years due to low infiltration capacity of the LFH, such that large amounts of runoff would be captured by furrows and allowed to infiltrate.

Furrows also accelerated the establishment of vegetation. In fact, plant cover measurements taken in 2016 – three years after watershed construction was complete – showed that ridges had a mean cover fraction of 16% that was significantly different than the mean furrow cover of 55% (Asten, unpublished data). In 2019, cover was visually noted to be higher in furrows than in ridges, though no quantitative vegetation cover data was collected. Higher cover in furrows is thought to be a result of higher moisture content in the furrows that provided more water for root uptake. Hence, root networks are likely denser under furrows, which would increase macropore flow under furrows and promote deep percolation of water, potentially increasing recharge. High amounts of runoff, and especially ponding, would also create high pressures in soil under furrows, which is known to increase macropore flow (Cey & Rudolph, 2009).

In later years, the degree of weathering of LFH may increase, thereby increasing the infiltration capacity of LFH and reducing runoff. This, in turn, would increase moisture in the ridges, and could promote a more uniform distribution of vegetation and roots across the upland. At the same

time, furrows are expected to become progressively filled with sediment (Saynor *et al*., 2018) and will not be able to capture as much runoff. Therefore, potential increases in recharge and Na^+ flushing from furrows will decrease over time, giving way to more uniform flow through sand. The net effect of greater vegetation establishment on the amount of flow into sand and on recharge in later years is uncertain. More developed root networks would promote rapid macropore flow through the LFH, promoting flow into the underlying sand, and increased litter cover would limit evaporation. However, increased interception from higher amount of litter and leaf cover would reduce infiltration, and increased root water uptake could create dryer conditions at depth.

Na^+ flushing from unsaturated tailings sand

Na^+ concentrations in 2013 and 2014, especially near the water table, were near or above the average leachable Na^+ concentration of 72 mg/kg sand reported by Simhayov *et al*. (2017) for tailings sand prior to watershed construction. At SAF+350U and ES+180U-UP, Na^+ appeared to have been flushed from the upper layers of the sand and possibly accumulated in the lower layers where concentrations were well above 72 mg/kg (Figure 2.9). Approximately 5000 m^3 of water – equivalent to 65 mm over the entire 7.7 ha upland area – was sprayed over the tailings sand in 2012 during the fen construction to help raise the water table. Along with percolation from rainfall, water application would have flushed Na^+ from the upper layers of sand. However, Na^+ concentration was not observed to increase with depth at SAF+220U, which may have arisen from uneven water application during sand placement and/or from thicker LFH at the SAF+220U sampling locations (~47.7 cm on average) that would have decreased the amount of percolation in sand compared to the other locations (Sutton & Price, 2020).

Na^+ concentrations were generally similar between 2013 and 2014, though some differences (especially at SAF+220U) existed, which is likely due to heterogeneous distribution of Na^+ during sand placement. The similarity in Na^+ concentrations between these two years may have been from very high LFH retention in the first two years post-construction that severely restricted passage of water from the LFH into the underlying sand (Naeth, 2011; Sutton & Price, 2020). In the years following 2014, a sharp decrease in residual Na^+ concentrations occurred, which is likely related to LFH weathering that allowed greater amounts of percolation into sand.

The concentration of flow under furrows with minor lateral spreading, as exemplified in the Test 1 dye experiment was expected to disproportionately flush Na^+ in unsaturated sand under furrows, leaving higher residual concentrations under ridges. Surprisingly, Na^+ concentrations were observed to decline at all sites in 2015, and both the furrow and ridge had low concentrations (<13 mg/kg) in 2019. At SAF+350U and ES+180U-UP, concentrations declined with depth, indicating that percolating water had flushed Na^+ into deeper layers and into the saturated zone at the two locations. As such, despite high volumes of finger-like flow in sand located beneath furrows, some Na^+ may be flushed by downward percolating water under ridges in sand during large rainfall events or during snowmelt, when LFH in ridges becomes wet enough to transmit water into sand due to increased infiltration in ridges and spreading of water from furrows into ridges above the capillary barrier.

Nonetheless, there is evidence that more Na^+ is flushed from the upper layers of sand under furrows. In fact, the top ~65 cm of sand under the furrow sampled in 2019 had lower Na^+ concentrations than adjacent samples collected under the ridge (Figure 2.9). This suggests that furrows and preferential flow are responsible for a larger proportion of Na^+ flushing during most wetting events. Na^+ under ridges may still be flushed by water that initially percolates downward

through sand under furrows as finger-like flow, but subsequently migrates laterally into the ridges by capillary action (Glass *et al*., 1988, 1989c), with some of the water that migrated under ridges eventually draining to the water table. This could create a more even flushing of Na^+ with depth, compared to the top-down flushing of Na^+ observed in the furrow and at SAF+350U and ES+180U-UP (Figure 2.9), since more drainage from lateral spreading would be expected in deeper portions of sand, where drying via ET would be reduced. This flushing mechanism in low recharge areas may have been especially important for Na^+ removal at SAF+220U, where there was little evidence of downward Na^+ flushing from upper layers in any of the years of sampling.

In the bare tailings sand basins, the absence of an overlying LFH layer allowed vast amounts of water to percolate down through the sand, flushing nearly all Na^+ by 2015. The higher Na^+ concentrations (~25-30 mg/kg) encountered in some samples taken from under the low point of the West basin in 2019 may have arisen because of heterogeneity in the tailings sand. Finer soil particles could decrease hydraulic conductivity, increase adsorption of Na^+ (Simhayov *et al*., 2017), or contribute to finger-like flow around these sampling points. In fact, Ketcheson (2015) found that silt content can vary considerably between samples, with the silt fraction having a mean value of 10.5% and a standard deviation of 5.4%.

Error and limitations

During the field dye experiments, pulses of dye were applied over ~5-10 min intervals every 30 mins, rather than at a consistent rate over the entirety of the experiments. This would have simulated intermittent periods of very high intensity rainfall, which would have created more runoff into furrows than would have occurred during a natural rainfall event. In addition, the dye

plots were excavated over several days, during which a total 13.5 mm of natural rainfall occurred in Test 1 and 3.8 mm of rainfall occurred in Test 2 (Table 2.1). Rainfall and drainage time likely influenced wetted area and dye finger geometry, but this was not accounted for in the analyses on the dye plot cross-sections because their effects could not be easily distinguished. It is believed that higher amounts of flow observed in sand between the 90 cm and 130 cm cross-sections were a result of higher drainage time and cumulative rainfall since the beginning of the experiment, compared to the 30-80 cm cross-sections that were excavated earlier in time.

Error also exists with regards to the mobility of the dye compound itself, as Brilliant Blue FCF has been shown to be retarded compared to pure water. For example, Flury & Flühler (1995) found a retardation factor of 1.2 compared to a conservative iodide tracer, while Öhrström *et al*. (2004) found a factor of 1.5 compared to bromide. Brilliant Blue FCF adsorbs predominantly to clay (Ketelsen & Meyer-Windel, 1999) and would therefore be expected to be adsorbed much more strongly in LFH (6% clay content on average) than in sand (<1% clay content on average; Ketcheson, 2015). It should be noted, however, that adsorption of the dye in the sand could be increased by the presence of high concentrations of leachable ions such as Na^+, Ca^{2+}, Mg^{2+}, and SO_4^{2-} (Simhayov *et al*., 2017), since high ionic strength has been found to increase adsorption of Brilliant Blue FCF (Germán-Heins & Flury, 2000). Consequently, the movement of dye in sand may have been slightly retarded, but the shape of the flow patterns in sand were probably not seriously impacted.

Na^+ was extracted from tailings sand using either a 5:1 water-sand mass ratio (even numbers for samples in 2013 and 2014) or a 2.5:1 ratio (all other samples), which constitutes a source of error and would account for some variability between samples in 2013 and 2014. In fact, data presented by O'Kane Consulting (2011) showed that, compared to a 2:1 water-soil mass ratio (9.6

pore volumes), average extractable Na^+ in sand was 3.3% higher for a 5:1 ratio (24 pore volumes) and 6.5% higher for a 10:1 ratio (48 pore volumes). As such, the values presented in Figure 2.9 underestimate actual Na^+ concentrations. This source of error would extend to the leachable Na^+ values presented by Simhayov *et al*. (2017), who used a similar water-sand mass ratio of 2:1. According to adsorption theory, total solute mass is proportional to the mass of solute that remains adsorbed at equilibrium. Hence, the mass of Na^+ that was not accounted for in the leaching experiments conducted by Simhayov *et al*. (2017) would be higher that the mass that was not accounted for when processing the 2019 samples, which had relatively low residual Na^+ concentrations. It follows that the fractions of flushed Na^+ presented in Table 2.3 are likely lower than the true fractions of flushed Na^+.

2.6 Conclusions

Dye tracer studies showed that local depressions, either in the form of tilled furrows or low points within recharge basins, retain large volumes of runoff and promote infiltration of precipitation. The concentration of infiltration in depressions was accompanied by finger-like flow that produced deep percolation of dye with little lateral spreading, wetting only a small fraction of the sand in the excavated cross-sections. In furrows, deep percolation was enhanced by macropore flow along root networks that allowed dye to bypass much of the LFH soil matrix, which is expected to be a more prominent process in furrows than in ridges, given the higher density of vegetation in furrows. Other macropores at the LFH-sand interface, such as cavities surrounding stones, also encouraged the passage of percolating water across the capillary barrier at the base of the LFH.

The low wetted fraction associated with finger-like flow under furrows was expected to primarily flush Na^+ under furrows, leaving high concentrations of Na^+ in sand under ridges. Although the top of the sand profile under the furrow sampled in 2019 had slightly lower Na^+ concentrations than under the adjacent ridge, differences in concentration were small, and a site-wide decline in Na^+ concentrations between 2013 and 2019 was observed at all sampled locations. By 2019, it was estimated that at least 88% of Na^+ had been flushed from the tailings sand under the sampled ridge. As such, it is hypothesized that the majority of Na^+ is directly flushed by vertical flow occurring under furrows, but that large wetting events induced flushing under ridges, driving built-up Na^+ under ridges downward via drainage. During events that primarily produce breakthrough across the capillary barrier under furrows, lateral migration of water from fingers in sand under furrows into adjacent ridges may also drive Na^+ under ridges down to the water table. It would be beneficial to collect and analyse more split spoon samples so as to capture Na^+ distribution heterogeneity across the upland, as well as monitor the decline in Na^+ concentrations in later years.

Furrows were shown to not only increase infiltration by detaining runoff, but also potentially reduce losses of infiltrated water to ET by promoting deep percolation. As such, furrows are believed to be responsible for providing additional groundwater recharge. Recharge contributions from furrows would be expected to be highest during the first few years post-reclamation when only a portion of the LFH profile is weathered. During these early years, runoff captured by furrows would be highest because of the low infiltration capacity of the LFH. In addition, the high volumes of water retained by the furrows would create localized increases in total head, thereby promoting the passage of water across the capillary barrier, which retains the most water in earlier years but allows progressively more water to pass into sand due to successive freeze-thaw cycles

(Sutton & Price, 2020). Further research is needed to confirm these hypotheses and quantify recharge contributions from furrows. It should be noted that the suction head at which breakthrough of moisture into sand occurs would not be affected by the changing soil hydraulic properties of the LFH (Stormont & Anderson, 1999). Instead, weathering increases the hydraulic conductivity of the LFH (Sutton & Price, 2020), thereby allowing more water to reach the interface of the LFH-sand layer, which in turn increases the pressure at the interface and allows more water to break through into the sand. Furthermore, weathering would decrease the moisture content in the LFH corresponding to the breakthrough pressure head, thus reducing the difference in moisture content across the LFH-sand interface.

Chapter 3: Characterizing the effects of furrows on vadose zone flow patterns and aquifer recharge in the upland of a reclaimed fen watershed, using flow tank experiments and modelling

3.1 Introduction

As of 2016, over 900 km^2 of the Athabasca Oil Sands Region (AOSR) had been disturbed by surface mining (Alberta Environment and Parks, 2017). Peatlands comprise nearly one third of the regional landscape (Vitt *et al*., 1996) and have been directly impacted by the removal of overburden in the area, which is necessary to access underlying bitumen deposits. Hydrological regimes have also been disturbed, both within and around mined areas (Elshorbagy *et al*., 2005). In order to meet provincial requirements for re-establishing equivalent land capability of the mined landscape (Government of Alberta, 2015) and to study the feasibility of fen peatland reclamation, a pilot reclaimed peatland system – known as the Nikanotee Fen watershed – was designed, incorporating primarily mine waste and salvaged materials (Daly *et al*., 2012). Construction of the watershed commenced in 2012 and was completed in 2013. Understanding the implications of design choices and materials used to construct the system on the hydrology and migration of solutes is essential to projecting the trajectory of the constructed system, and to improving future designs.

A major challenge facing peatland reclamation is the need to maintain high fen water tables by ensuring that sufficient groundwater fluxes are supplied by the tailings sand aquifer (Price *et al*., 2010), which is itself reliant on adequate infiltration and drainage in the upland. For this reason, several depressional features, including tilled furrows oriented perpendicular to the upland slope direction, were incorporated into the final design of the upland to retain runoff, thus increasing infiltration and reducing erosion (Ketcheson, 2015). Furrows have previously been incorporated in other mine reclamation projects for similar reasons (Saynor *et al*., 2018), as well as in

agriculture, particularly in arid regions where furrow "rain harvesting" provides additional water to crops on sloped fields (Yang *et al*., 1996; Gammoh, 2011). In the Nikanotee Fen upland, ponding in furrows has been observed during rainfall events (Irvine, 2018), suggesting that they function as intended by increasing infiltration and recharge. To date, however, the recharge contributions provided by furrows in the upland have not been quantified, and it is not clear whether incorporating furrows is truly necessary for fen reclamation in the AOSR. Another challenge facing peatland reclamation in the AOSR is the presence of elevated pore water concentrations of sodium (Na^+) in tailings sand, among other contaminants such as naphthenic acids (MacKinnon *et al*., 2001; Scott *et al*., 2005; Rezanezhad *et al*., 2012; Simhayov *et al*., 2017). Kessel *et al.* (2018) suggested that the flushing of residual concentrations of Na^+ in unsaturated tailings sand by percolating water will constitute a long-term source of Na^+ of in groundwater, which poses a risk to downstream fen vegetation (Pouliot *et al*., 2012; Rezanezhad *et al*., 2012). In Chapter 2, furrows were shown to accumulate large volumes of runoff from the adjacent ridges (i.e., the areas between furrows) and were responsible for almost all breakthrough of percolating water across the capillary barrier between the LFH and the underlying tailings sand, flushing more residual Na^+ from sand under furrows than under the ridges, at least in the early years after construction.

Much of the water that infiltrates in the upland following a precipitation event is retained in the LFH, allowing vegetation to establish and draw water from it. Higher soil water retention in the LFH compared to the underlying tailings sand creates a capillary barrier at the interface between the two soils, which restricts drainage of water into the sand and reduces recharge (Naeth, 2011; Sutton & Price, 2020). However, Sutton & Price (2020) analyzed data collected from three upland soil moisture stations over a three-year study period (2014, 2015, and 2017) and suggested

that weathering driven primarily by freeze-thaw cycling has increased drainage into the sand aquifer by profoundly altering soil hydraulic properties (Sutton & Price, 2020). The suggested that weathering began near the surface and progressively increased in depth with each freeze-thaw cycle, reaching 35 cm depth on average in 2017 after 4 seasonal freeze-thaw cycles since completion of the reclaimed watershed. Modelling indicated that weathering processes increased saturated hydraulic conductivity by ~1000%, decreased the absolute value of air entry pressure by ~75%, and decreased the van Genuchten *n* parameter by ~50%. This allowed more percolation into the underlying sand and ultimately increasing groundwater recharge by approximately 64% over the study period (Sutton and Price, 2020).

In Chapter 2, finger-like flow patterns were observed in the sand, penetrating up to 66 cm below the LFH but having limited lateral spreading, and only wetting a small fraction (<6.3%) of the sand at depths greater than 1 cm below LFH. The occurrence of finger flow in the Nikanotee upland had previously been suggested by Sutton & Price (2020), based on high moisture "peaks" measured in tailings sand that could not be predicted by solving Richards' equation in Hydrus-1D. Finger flow is a type of preferential flow that arises due to instability in the flow domain but isn't necessarily caused by a heterogeneous distribution of permeability or soil properties (Wang *et al*., 2003). It can be initiated by a number of factors, including water repellency (Hendrickx *et al*., 1993; Ritsema & Dekker, 1994; Wallach *et al*., 2013) and fine-over-coarse layering (Hill & Parlange, 1972; Hillel & Baker, 1988; Baker & Hillel, 1990). Although finger flow can occur in near-perfect homogeneous media (Wang *et al*., 2003), the initiation of fingers relies on some variation in soil structure or initial moisture content at the pore scale (Philip, 1975; Hill & Parlange, 1972) or larger inconsistencies (Hill & Parlange, 1972; Glass *et al*., 1988). Lab tests studying finger flow have generally been conducted in thin flow tanks (Hele-Shaw cells) with at least one

transparent face, such that percolation was confined to two-dimensional flow that could be visually observed (Saffman & Taylor, 1958; Hill & Parlange, 1972; Glass *et al*., 1988; Baker & Hillel, 1990; Wang *et al*., 2018; Sililo & Tellam, 2000). To help visualize flow patterns, dyes may be added to the infiltrating solution during lab experiments (Glass *et al*., 1988; White *et al*., 1976). Numerical models such as Hydrus-2D cannot be used reliably to simulate finger flow, since Richards' equation lacks the physical mechanics for solving flow instability (Elisassi & Glass, 2001). Nonetheless, Hydrus-2D is useful for studying steady unsaturated flow under various conditions and domain geometries that may generate finger flow. In the case of this reclaimed watershed, it can be used to investigate how different furrow configurations direct water through the LFH and the underlying sand, and how this can ultimately affect recharge, considering that the flow accumulation in furrows is accompanied by a decrease in flow under ridges due to runoff.

Although the findings by Sutton & Price (2020) were key to characterizing early soil evolution in a reclaimed landscape of this type, their flow modelling was carried out with Hydrus-1D and did not account for differential infiltration contributions between furrows and ridges. From the perspective of peatland reclamation, establishing the role of furrows in ensuring adequate recharge, particularly during early post-construction period, is crucial for deciding whether furrows are necessary or whether they can be omitted to save costs. This chapter therefore has the following objectives: 1) determine how furrows, rainfall intensity, and initial moisture conditions affect percolation patterns in sand, using a series of lab flow tank experiments and modelling simulations; 2) evaluate how changing the distance between furrows influences modelled aquifer recharge; and 3) make recommendations concerning the incorporation of furrows in future upland designs for peatland watersheds.

3.2 Site description

The Nikanotee Fen Watershed is a pilot reclamation project built on an oil sands mining lease roughly 25 km north of Fort McMurray, Alberta (56°55’59” N, 111°25’00” W). It was designed with a high upland-to-fen surface area ratio of 2.7:1, so as to ensure that sufficient recharge is provided to the fen by the upland aquifer (Price *et al*., 2010). The total watershed area is 32.1 ha and includes the upland (7.7 ha), the fen (2.9 ha), slopes reclaimed in 2011 to the west (2.4 ha) and to the southeast (8.2 ha), a slope reclaimed in 2007 to the east (8.1 ha), a natural slope to the south (2.8 ha), and an engineered berm to the north (Figure 3.1).

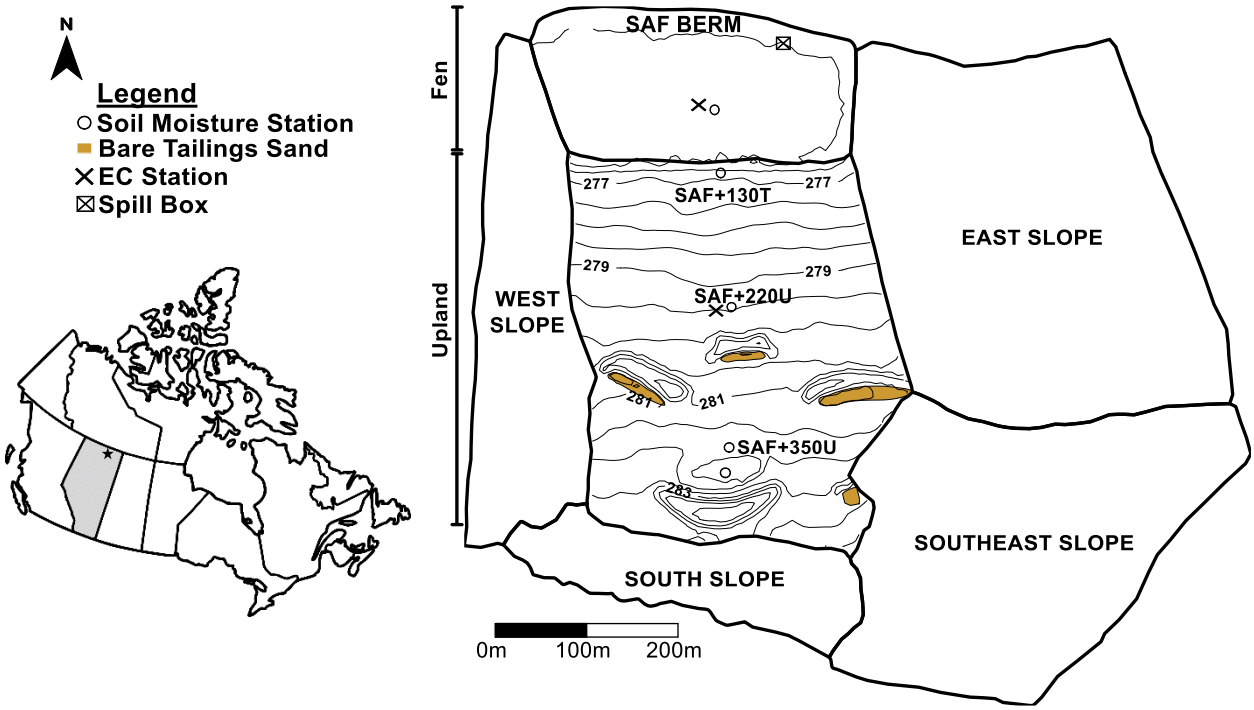

Figure 3.1: Location and plan view of the Nikanotee fen watershed showing topography in the constructed fen and upland, monitoring stations, and bare sand basins

The fen design includes a ~2 m thick layer of moderately decomposed peat, which was stripped from a rich fen to access underlying bitumen deposits within the mining lease area (Nwaishi *et al*.,

2015; Daly *et al.*, 2012). The upland aquifer consists of ~2-3 m of coarse tailings sand that was capped with ~30 cm of LFH to support vegetation growth. The average classification of the LFH material was sandy loam, composed of 52% sand, 42% silt, and 6% clay (Ketcheson, 2015). Tailings sand samples were classified as either sand or sandy loam, with an average composition of 88% sand, 11% silt, and <1% clay (Ketcheson, 2015). The upland surface was sloped towards the fen with a ~2% grade, while the basal liner was sloped at a ~3% grade. This incline, combined with a high-permeability petroleum coke underdrain extends from the northern ~100 m-wide margin of the upland (known as the "transition zone") into the fen, provides a flux of groundwater from the upland aquifer that passes upward through the fen peat. The upland and fen were underlain by an impermeable geosynthetic clay liner to promote high water table levels in the fen. Outflow from the system occurs at the north-east corner of the fen, where an outlet was installed to allow drainage into a retention pond.

The final design of the upland incorporated tilled furrows oriented perpendicular to the upland incline in order to capture runoff, thereby increasing aquifer recharge and reducing erosion of the LFH. Infiltration capacity in the furrows was initially found to be 68 mm/hr on average in 2013, which was nearly double the average infiltration capacity in ridges. However, this difference was not statistically significant, and the infiltration capacities of the ridges and furrows became similar in subsequent years (Asten, unpublished data). In addition to the furrows, LFH was stripped in 4 areas to create bare tailings sand depressions ("recharge basins") paired with LFH mounds ("hummocks") that were placed immediately downslope of the depressions. A function of these hummock-basin features was to increase recharge by retaining runoff from the upland and adjacent slopes, which could rapidly infiltrate through the sand in the absence of the lower-permeability LFH layer.

Hourly moisture data was retrieved from three stations (SAF+130T, SAF+220U, and SAF+350U) along the north-south centreline of the upland. Data from these stations were used for determining appropriate initial moisture conditions in the lab and modelling experiments described in Section 3.3 below. A meteorological station installed in the upland measured net radiation, wind speed and direction, relative humidity, air temperature, ground heat flux, and precipitation. Details concerning site instrumentation are provided in Chapter 2. From the meteorological data, hourly potential evapotranspiration (PET) was calculated using the Penman equation (Penman, 1948). Hourly rainfall and PET measurements were used in model simulations to evaluate flow under realistic atmospheric conditions.

3.3 Methods

Laboratory experiments

Flow tank experiments were performed in a thin acrylic tank with internal dimensions of 88.4 x 89.8 x 1.2 cm, allowing vertical flow patterns to be visually observed in 2D. Sturdy tank walls (1.2 cm thick) were chosen to reduce bowing under pressure of the packed soil. In addition, a 2.5 cm-wide square aluminum bar was placed horizontally at the front of the tank, along with a wooden beam at the back of the tank, to provide additional support to the acrylic wall and reduce bowing. The tank was held vertically with the use of 4 vertical wooden beams. The front wall was held to the sides with a series of clamps and was sealed with silicone gasket, to prevent leakage along the edges while also allowing for the front to be easily removed. Holes were drilled at the bottom of the tank every ~5 cm to allow air to escape freely. A gravity-driven rainfall simulation apparatus was placed along the top of the tank, consisting of a PVC half-pipe that was perforated every 2 cm

with 3 mm-wide holes along the bottom. Wicks were passed through the holes to help deliver a steady, uniform application rate across the length of the tank. During rainfall simulation, the PVC pipe was re-filled with 13 mL of water (equivalent to an application depth of 1.25 mm) every 15 mins to maintain an application rate of 5 mm/hr. The small amount of water within the apparatus helped maintain a low application rate, and frequent re-filling ensured a quasi-uniform rate over the application period.

Bulk disturbed LFH and tailings sand samples were collected within a 2x2 m area on May 29th and 30th, 2019 from the south end of the upland, and shipped to the University of Waterloo Wetlands Hydrology Lab, where the experiments were performed. Surface soil (<20cm) was removed prior to collection so that vegetation and large root networks were not incorporated in the LFH mix; then, LFH and the underlying sand were placed into separate containers. Large pieces of gravel, woody debris and/or bitumen were also manually removed or crushed since they would not have fit in the 1.5 cm-thick flow tank. The goal of the laboratory experiments was to study flow under conditions that reflected the field site as closely as possible. As such, the sand and LFH were neither ground nor graded with sieves.

The tank was filled with 30 cm of LFH overtop 53.5 cm of sand. During upland construction, tailings sand was placed in 0.5-1.0 m lifts with dozers (WorleyParsons, 2014), then compacted by passing over the lifts with dozers. LFH was placed in a 30 cm lift and compacted by the same means. For this experiment, in an attempt to achieve relatively uniform compaction throughout the tank and to avoid undue stress on the tank walls, the sand and LFH were added in 2.5 cm lifts, though larger lifts (<10cm) were sometimes used for the sand, for example at the bottom of the tank where packing was more difficult. The lifts were packed by tamping the soil to achieve a target bulk density of 1.45 g/cm^3 for tailings sand and 1.33 g/cm^3 for LFH, which correspond to

the average in-situ bulk density values of these materials as reported by Ketcheson (2015), and were estimated during tank packing based on added soil mass and internal tank dimensions. Repacking the LFH and sand was deemed a reasonable approach for emulating field conditions soon after reclamation (i.e., prior to weathering), since the soils were mechanically placed in a series of lifts during upland construction. The top 1.5 cm of sand was mixed in with 5.0 g of Brilliant Blue FCF dye (0.031 g dye/g sand) so that percolating water would mix with the dye, allowing for percolation patterns in the sand to be visualized.

Four experiments (Tests A, B, C, and D) were conducted in the tank to provide insight into how topography, rainfall depth, drainage time, and initial moisture content of sand affect percolation patterns. Table 3.1 summarizes the experimental setups and water application schedules of each test; here, "time since last event" indicates the time interval between the start of the two events. Two LFH topography scenarios were tested with the tank setup: a furrow that was 24 cm wide and 10 cm deep, placed in the middle of the tank, to represent as-built upland conditions (Tests A-C); and a flat surface, to represent scenarios where furrows were not incorporated into the upland design or when furrows were completely filled in by runoff sedimentation (Test D). In Test A, four separate 30 mm rainfall events were sequentially simulated, with variable amounts of time between each event. The tank was cleared and re-packed, and Test B was commenced, which consisted of simulating 3 sequential events that were each 3 days apart and had total volumes of 30 mm, 15 mm, and 15 mm, respectively. The procedure for Test B was then repeated for Tests C and D. Prior to packing the tank for each experiment, 3 samples of LFH and 3 samples of sand were dried at 105°C for 24 hrs to determine their respective volumetric water contents (θ). Tap water was then mixed with the soils to bring the θ in LFH to 15% and bring the θ in sand to either 8% or 5%. In the LFH, the moisture content was set at 15% since this was

representative of dry conditions in the upper portions of the LFH, based on probes installed at depths of -5, -10, and -15 cm bgs at the SAF+220U moisture station. Similarly, the 8% sand θ was chosen by calculating the average moisture content prior to significant probe responses to rainfall and at the end of the growing season between 2014 and 2018, measured at 50 cm bgs, immediately below the LFH-sand interface at the 220U moisture station. Meanwhile, the 5% sand θ used in Test C represents very dry conditions measured by the probe at 50 cm bgs in 2017 and 2018 at the 220U station. It should be noted that all the sand used in Test A was completely dried in the oven before wetting it to a θ of 8%, but this drying step was abandoned in subsequent experiments because it was not necessary to bring θ to the desired level. Tap water was used for all rainfall simulations except the fourth event of Test A, for which a 7 g/L solution of Brilliant Blue FCF dye was used. Although the 15% θ in LFH was representative of conditions in the upper portions of the LFH, it was drier than conditions encountered near the tailings sand (~25%), meaning that the repacked LFH initially had an a very high available water retention capacity that would strongly resist breakthrough into the underlying sand. To overcome this issue, the first rainfall simulation event (30 mm) was designed to raise the LFH moisture to a point that moisture would be released into the sand during subsequent events.

Prior to packing the soil in Test C, seven samples were randomly collected from the homogenized sand (5% moisture content), dried at 105°C for 24 hrs, gently crushed with mortar and pestle to break clumps, passed through a 2.83 mm sieve (U.S. sieve No. 7), split into triplicate subsamples, and analysed with a Horiba Partica LA-950V2 laser diffraction particle size distribution analyser. The results from the soil subsamples were divided into sand (0.05-2.0 mm), silt (0.002-0.05 mm), and clay (<0.002 mm) fractions, as specified by the Canadian System of Soil

Classification (Soil Classification Working Group, 1998). The triplicate soil fraction data were then averaged to yield a single set of soil fraction values for each of the seven samples.

Table 3.1: Setup and application depths used in the flow tank tests

	Test A	Test B	Test C	Test D
Topography	Furrow	Furrow	Furrow	Flat
θ in sand	8%	8%	5%	8%
Event 1				
Depth	30 mm	30 mm	30 mm	30 mm
Event 2				
Time since last event	3 d	3 d	3 d	3 d
Depth	30 mm	15 mm	15 mm	15 mm
Event 3				
Time since last event	1 d	3 d	3 d	3 d
Depth	30 mm	15 mm	15 mm	15 mm
Event 4				
Time since last event	8 d			
Depth	30 mm			

The front of the tank face was photographed in RAW format with a DSLR camera set with an ISO of 100, a shutter speed of 1/6 s, and an aperture of F11.0, as per the methodology employed by Belfort *et al*. (2017). An automated camera controller was used to take photographs continuously and avoid camera shake. Black cloth was placed around the photography area to minimize surface reflection. Images were processed in MATLAB (ver. 2019b) by first correcting image tilt using perspective transformation algorithms. The images were subsequently converted to the HSV (hue, saturation, value) colour domain, allowing for the hue channel to be used for isolating dyed areas, though the red and intensity channels were used in conjunction with the hue channel in the shadow of the aluminum support bar where hue was poorly represented. A custom algorithm processed each image autonomously to create black and white images using these channels, where white pixels corresponded to dyed regions. The algorithm then applied a mask to

remove the aluminum bar, remove noise, and crop the images. Cropping removed 3.8 cm from the left and right sides of the tank for Tests 1, 2, and 3 to remove the metal brace (1.3 cm) and impacts of edge flow (an additional 3 cm). For Test D, 5.3 cm was removed from the left side and 14.8 cm was removed from the right side due to high amounts of edge flow.

In order to determine whether the dye had a substantial impact on infiltration rate in the soils, constant head saturated hydraulic conductivity tests were performed on LFH and sand with tap water (n=10 for each soil) and a 7 g/L Brilliant Blue FCF dye solution (n=10 for each soil). The soil was packed into steel cylinders that had a diameter of 5.4 cm and a height of ~5 cm. Water was ponded over the cylinders and maintained at a constant level by adding water or dye as needed and recording added volumes. Saturated hydraulic conductivity, K_S (cm/hr), was calculated from Darcy's Law:

$$q = K_S \frac{dh}{dl} \quad (1)$$

where q (cm/hr) is flux through the soil, dh (cm) is total head, and dl (cm) is length of the cylinder packed with soil.

Numerical modelling

A series of modelling scenarios were created and run to evaluate the impacts of furrows on flow patterns through sand and on aquifer recharge. Modelling was performed using Hydrus-2D (ver. 2.05), which solves Richards' equation over a 2-dimensional finite element mesh to simulate vadose zone flow (Šejna *et al.*, 2014). Although Richards' equation cannot be used to simulate finger flow (Eliassi & Glass, 2001), these simulations were carried out to give insight into moisture

dynamics under ridges and furrows when water is diverted to furrows, and how these influence deep percolation through sand and affect recharge. In other words, modelling can help understand why recharge increases or decreases when water is removed from ridges – creating drier areas – but accumulates in furrows, where large amounts of infiltration occur. Three parameters were systematically varied: initial moisture conditions; furrow configuration (i.e., the presence of furrows and spacing between them); and the fraction of water diverted from ridges into furrows as a result of runoff. Seven initial conditions were evaluated (Table 3.2), representing a realistic range of dry to wet conditions that were derived from moisture patterns observed at the SAF+130T, SAF+220U, and SAF+350U moisture stations. Five furrow configurations were tested: furrows spaced 50 cm, 83 cm (the average as-built furrow spacing), 150 cm, and 200 cm apart, as well as the flat case (no furrows present). Rainfall diversion from ridges to furrows was varied between 0 and 100% in 5% increments, such that 21 fractions were evaluated for all scenarios where furrows were present. In total, 595 parameter combinations were evaluated.

Table 3.2: Initial conditions tested throughout the series of modelling scenarios

Initial condition	θ at top of LFH	θ at bottom of LFH	θ at top of sand	θ at bottom of sand
IC 1 (driest)	0.060	0.180	0.098	0.145
IC 2	0.090	0.210	0.108	0.145
IC 3	0.120	0.240	0.122	0.145
IC 4	0.150	0.270	0.141	0.145
IC 5	0.180	0.300	0.167	0.145
IC 6	0.210	0.330	0.206	0.145
IC 7 (wettest)	0.240	0.360	0.265	0.145

A single rainfall event was included in all modelling scenarios, representing the 25.8 mm of rainfall that occurred over 61 hrs between July 29th and 31st, 2014. This event was chosen because it produced a rapid increase in sand θ at the SAF+220U moisture station that nearly reached

saturation, followed by a rapid decrease, which is characteristic of finger flow (Glass *et al*., 1989c; Liu *et al*., 1994). The simulation period was extended to include 30 days where rainfall was set to 0, so as to observe prolonged drainage without additional precipitation. PET – calculated as described in Section 3.2 – was applied to the surface atmospheric boundary over the entirety of the modelling period.

Separate model domains were created for the various furrow configurations and for each initial condition, such that 35 different model domains were defined. The model domains – apart from the flat case – consisted of two furrows separated by a ridge, with half a ridge on the left and right extremities of the domain (example shown in Figure 3.2). The inclusion of two furrows was necessary to capture potential interactions between them during water redistribution, which could affect θ and flow under the central ridge. A series of observation nodes was assigned under both the centre ridge and the right furrow, with nodes placed at the same elevations, so that comparisons could be made between simulated θ under ridges and furrows. The nominal depths of these nodes (e.g. 50 cm bgs) were designated in terms of depth relative to ridge surface to facilitate comparisons between adjacent furrow and ridge nodes. The symmetrical domain design allowed for edge effects to be minimized near the observation nodes. Furrows were simplified as triangles with a depth of 10 cm and a width of 24 cm, which are the average as-built furrow depth and width (Ketcheson, 2015). In the case of flat LFH (no furrows), the same domain dimensions were applied as in the 83 cm furrow spacing domain, though without furrows.

Simulation domains incorporated 30 cm of LFH overtop of 120 cm of sand, with no-flow boundaries on the sides, a free drainage boundary on the bottom, and atmospheric boundaries at the top. As was demonstrated by Sutton and Price (2020), nearly the entire LFH profile was weathered by 2017, that is, 5 years after the upland was reclaimed. Hence, weathered LFH soil

hydraulic parameters derived by Sutton and Price (2020) were used in the model. Modelling conditions beyond the initial five-year period was of interest since it would help predict the long-term functioning of the watershed. This would also allow for comparisons to be made against flow

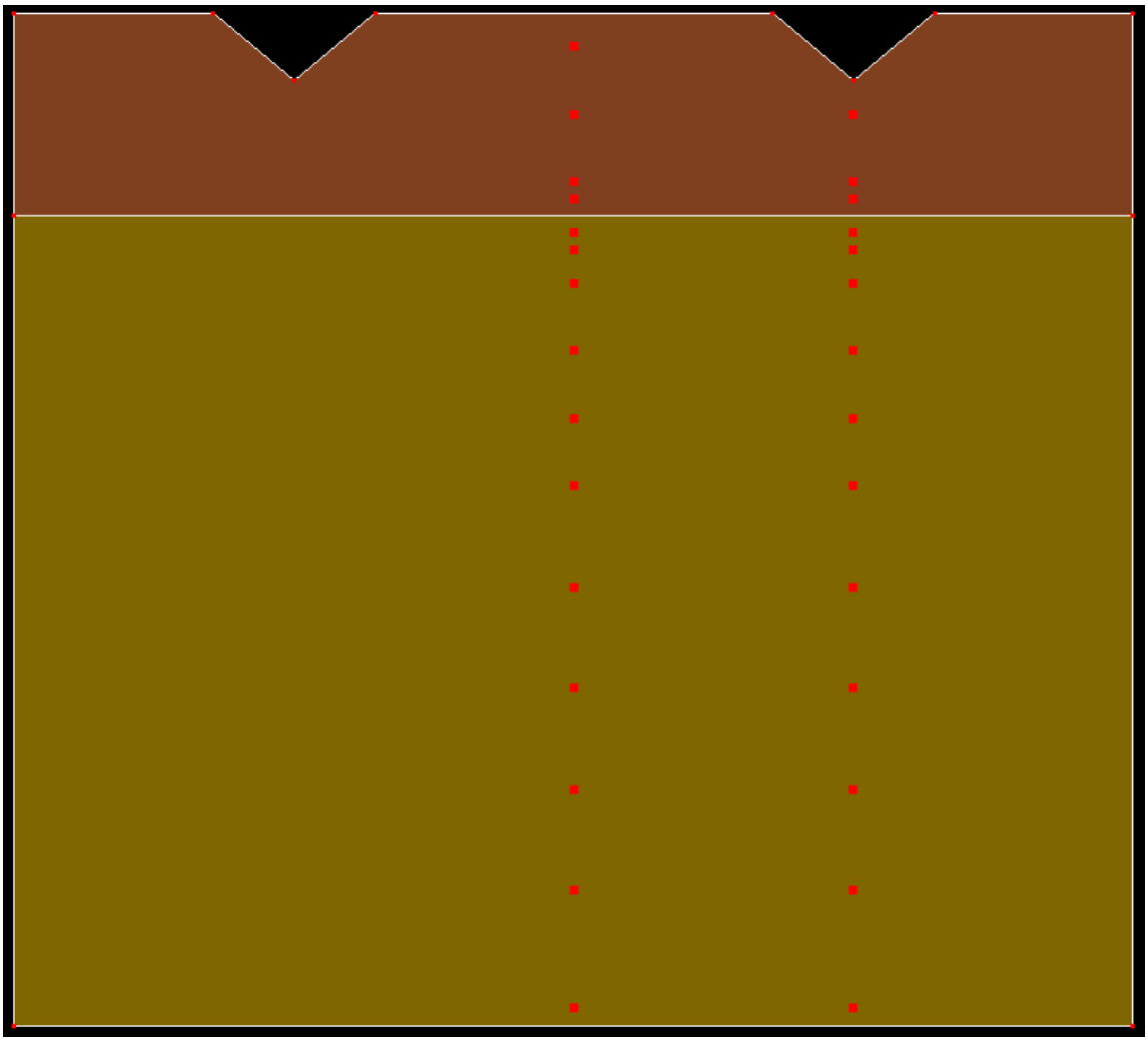

Figure 3.2: Model geometry and material distribution for the furrows spaced 83 cm apart (average as-built conditions). The top and bottom soil layers correspond to LFH and tailings sand, respectively. Red squares show the locations of observation nodes the under the ridge (left) and the furrow (right).

pattern data from the field dye tracer experiment conducted in 2019 (Chapter 2), when all of the LFH would likely have been weathered. The average calibrated soil hydraulic properties put forth

by Sutton & Price (2020) for tailings sand and weathered LFH, following an analysis of soil moisture data in 2014, 2015, and 2017, are shown in Table 3.3. The same set of soil hydraulic properties was used for the furrows and ridges since an analysis of single-ring infiltrometer tests conducted in 2016 showed no significant difference between furrow and ridge steady-state infiltration rates (Asten, unpublished data). These parameters are used in the van Genuchten-Mualem equation (van Genuchten, 1980) employed by Hydrus-2D to describe water retention:

$$\theta(\psi) = \begin{cases} \theta_r + \dfrac{\theta_s - \theta_r}{(1 + |\alpha\psi|^n)^m} & , \quad \psi < 0 \\ \theta_s & , \quad \psi \geq 0 \end{cases} \tag{2}$$

$$K(\psi) = \begin{cases} K_s \left(\dfrac{\theta(\psi) - \theta_r}{\theta_s - \theta_r}\right)^L \left(1 - \left(1 - \left(\dfrac{\theta(\psi) - \theta_r}{\theta_s - \theta_r}\right)^{\frac{1}{m}}\right)^m\right)^2 & , \quad \psi < 0 \\ K_s & , \quad \psi \geq 0 \end{cases} \tag{3}$$

where θ_r is residual volumetric moisture content, θ_s is saturated volumetric moisture content, K_s is saturated hydraulic conductivity, α is a parameter inversely related to air-entry pressure ψ_{ae}, n is a parameter related to pore size distribution, m is equal to 1-1/n, and L is a parameter related to tortuosity and pore connectivity. Sutton & Price (2020) found that the soil moisture dynamics were not sensitive to L, so an arbitrary value of 0.5 was used in the present study.

In order to account for the fraction of ridge rainfall that was diverted into furrows due to runoff, model precipitation inputs for the ridges and furrows were corrected as follows:

$$P_{adj,r}(t) = P_{real}(t) - R(t) = P_{real}(t)(1 - k) \tag{4}$$

$$P_{adj,f}(t) = P_{real}(t) + R(t)\frac{W_r}{W_f} = P_{real}(t)\left(1 + (1 - k)\frac{W_r}{W_f}\right) \tag{5}$$

where $P_{adj,r}(t)$ [mm/hr] and $P_{adj,f}(t)$ [mm/hr] are the adjusted model precipitation inputs at time t for the ridge and furrow, respectively, $P_{real}(t)$ [mm/hr] is real precipitation, $R(t)$ [mm/hr] is

runoff, W_r [cm] is ridge width, W_f [cm] is furrow width, and k [–] is runoff fraction. For each parameter set, a MATLAB script calculated the values of $P_{mod,r}(t)$ and $P_{mod,f}(t)$ over the simulation period and ran Hydrus-2D with the modified precipitation inputs (i.e., accounting for the ridge spacing and runoff fraction).

Table 3.3: Average soil hydraulic properties of upland materials (Sutton & Price, 2020)

Soil hydraulic property	Weathered LFH	Tailings sand
θ_r [m^3/m^3]	0.04	0.08
θ_s [m^3/m^3]	0.41	0.41
α [1/m]	5.8	12.1
n [–]	1.56	2.2
K_s [m/h]	0.02	0.167

Since different precipitation inputs from runoff were to be simulated in the furrows and the ridges, the "Atmospheric Boundary Condition" was applied to the surface of ridges (flat ground) and "Variable Flux 1" (time-variable flux) was applied to the surface of the furrows (ground sloped in "V" shape). Using boundary condition options provided in Hydrus-2D, the time-variable flux that was applied to the surface of the furrows was set to be treated as an atmospheric boundary condition, that is, with minimum pressure heads defined by the values of hCritA, which was set to 375 m of negative pressure head (equivalent to a volumetric moisture content of 4.5% in weathered LFH). The time-variable flux at the furrow surface was calculated by subtracting PET from precipitation, then correcting the resulting values to account for higher surface area associated with the sloped ground in the furrows, as follows:

$$q_{cor,f}(t) = \frac{q_{f,uncor}(t)}{2\sqrt{\left(h_f\right)^2 + \left(W_f/2\right)^2}} \tag{6}$$

where $q_{cor,f}(t)$ [mm/hr] is corrected furrow flux, $q_{f,uncor}(t)$ [mm/hr] is flux prior to correction, and h_f [cm] is furrow depth.

The maximum number of iterations for reaching convergence was set to 20, water content tolerance was set to 0.001, and pressure head tolerance was set to 10^{-5} m. The initial conditions (Table 3.2) were varied linearly throughout LFH and the sand and were set in terms of water contents, rather than pressure heads, to best represent the gradual change from very dry conditions near the top of the LFH to wet conditions and the base of the LFH. In order to preserve pressure continuity across the LFH-sand interface, the initial moisture content at the top of sand was defined based on the pressure head that corresponded to the moisture content at the base of the LFH. This pressure head, as well as the associated moisture content at the top of the sand, were manually calculated using Equations 2 and 3 and the soil hydraulic properties shown in Table 3.3.

3.4 Results

Laboratory experiments

From the constant head hydraulic conductivity tests, no statistically significant difference was found between the K_S of water ($\overline{K_{S,w}}$ = 23.3 cm/hr) and of a 7 mg/L Brilliant Blue dye solution ($\overline{K_{S,d}}$ = 27.0 cm/hr) in sand. A statistically significant difference of 0.6 cm/hr was found between the K_S of water ($\overline{K_{S,w}}$ = 2.9 cm/hr) and of dye ($\overline{K_{S,d}}$ = 2.3 cm/hr) in LFH, though this difference was deemed to be small and to have had little effect when dye solution was used instead of water in Event 4 of Test A. However, differences in intrinsic permeability between soils under different solutions (dye or tap water) were not determined because the viscosity (μ) and density (ρ) of the

dye solution were not measured. It is possible that the permeability of both soils under dye solution was lower than under tap water if the ratio of ρ/μ was lower for the dye solution than for the water; inversely, if the ratio of ρ/μ was higher for the dye solution, the permeability of both soils under dye solution could have been higher than under tap water.

Grain size distribution was very similar between the seven sand samples (Figure 3.3). The average sand, silt, and clay fractions were 95.6%, 4.4%, and 0.0% by weight, respectively; the respective standard deviations were 1.4%, 1.4%, and 0.0%.

Changes in sand wetted fraction (wetted area divided by total area of the rectangle enclosing the top of the sand and the deepest point of the wetting font) and protrusion length (difference

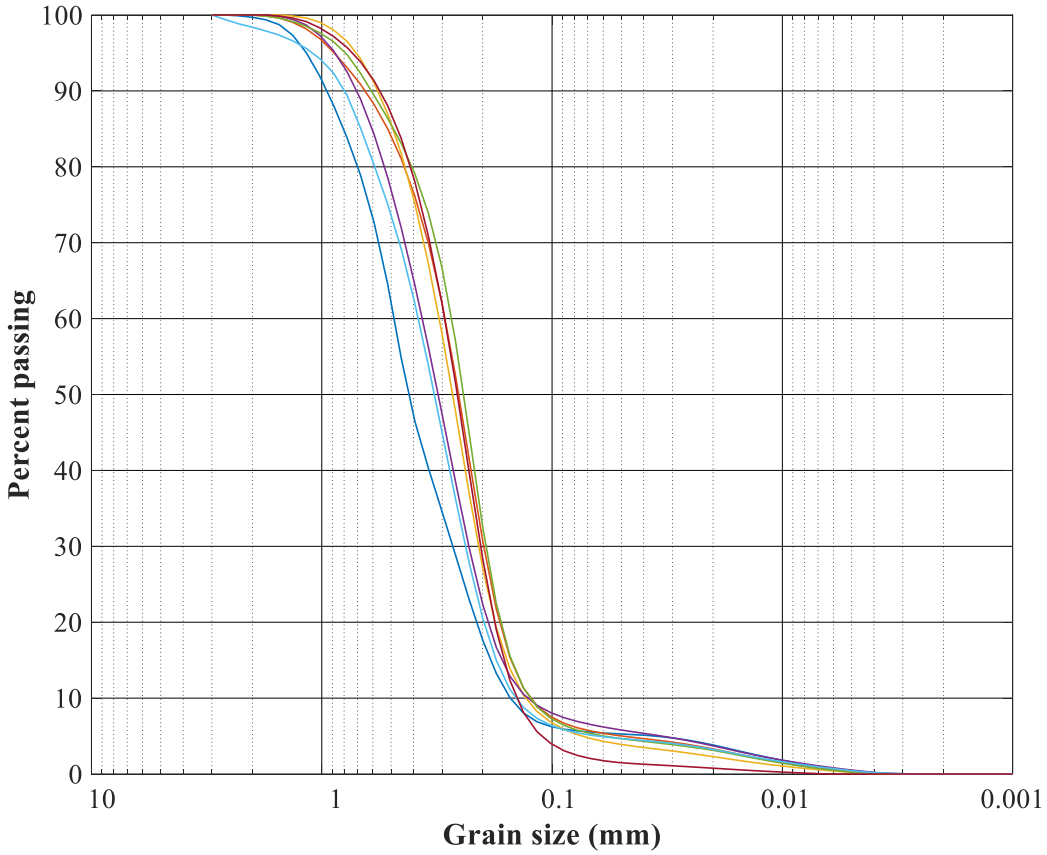

Figure 3.3: Grain size distribution graph of the seven sand samples collected prior to Test C.

between the deepest and shallowest points of the wetting front) throughout the four flow tank experiments are presented in Figure 3.4. Images taken throughout Tests A-D are shown in Figures B.1-B.4 (Appendix B), respectively. None of the experiments showed any evidence of breakthrough into sand after the first application event, which was intended as a preliminary step to sufficiently wet the LFH so that breakthrough would occur in subsequent events. The second event produced breakthrough in the first three experiments (Test A-C) that was concentrated primarily under the furrow, leading to a sharp decrease in wetted fraction (Figure 3.4A-C). Events 3 and 4 produced substantial amounts of uniform flow under the adjacent ridge areas in Test A, nearly reaching the same depth as the wetting front under the furrow after Event 4, as can be seen at the end of the experiment (Figure 3.6b). This led to a decrease in protrusion length to decrease over time, while wetted fraction reached unity (Figure 3.4A). In Tests B and C, only small amounts of flow were observed under the ridge areas throughout the experiments (Figure 3.5b-c).

In all experiments, the protrusion length was initially low (<1.3 cm), as the dye in the top 1.5 cm of sand had been placed as evenly as possible, but protrusion length increased after Event 2 in Tests A-C once infiltrated water percolated into sand (Figure 3.4). The increase in protrusion length was most pronounced in Test A (consisting of four 30 mm events), rising from 1.6 cm at the beginning of Event 2 to 23.4 cm over a 24 hr period leading up to Event 3; in Tests B and C, where only 15 mm were applied in Events 2 and 3, protrusion length increased from 1.0 to 12.7 cm and from 1.1 to 13.3 cm, respectively, over the 72 hr period between Events 2 and 3 (Figure 3.4). Wetted fraction was also affected, decreasing from 0.81 to 0.47 in Test A following Event 2, corresponding to an extension of the protrusion under the furrow. Conversely, in Test A, Event 3 led to a sharp rise in wetted fraction as more water percolated across the LFH-sand barrier under the ridge, reaching 0.71 over a 36 hr period, followed by a slow increase to 0.78 by the beginning

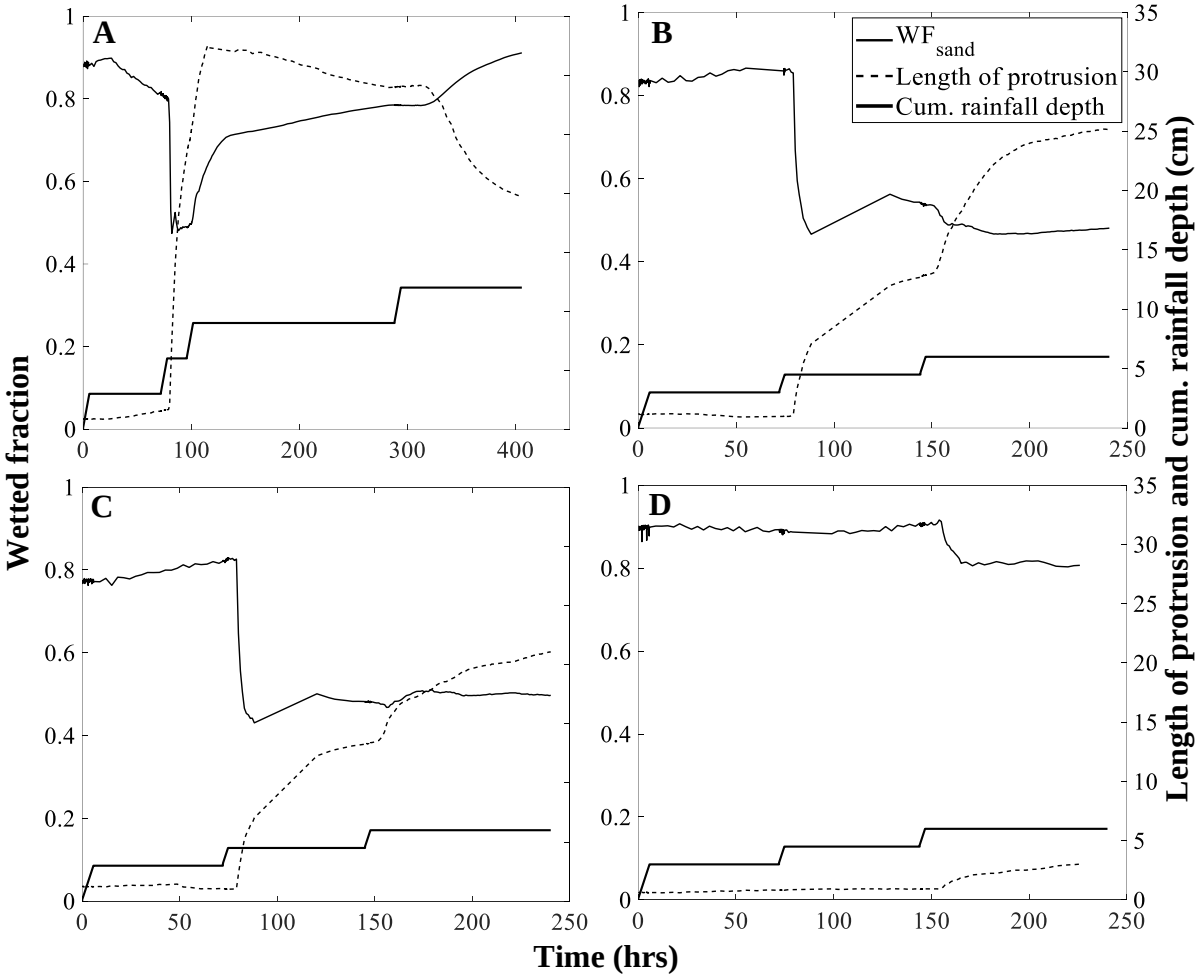

Figure 3.4: Evolution of wetted area and protrusion length over the course of each experiment for Tests A, B, C, and D.

of Event 4 (Figure 3.4). Event 4 further increased the wetted fraction to 0.91, at which point the experiment was ended. In Test B, wetted fraction decreased rapidly corresponding to protrusion development, from 0.78 to 0.46 following Event 2, with little variability occurring over the rest of the experiment. Similarly, wetted fraction decreased from 0.82 to a minimum of 0.43 after Event 2 in Test C, remaining relatively unchanged thereafter. The flow patterns that developed in Tests A, B, and C were generally stable, including under the furrow. Some lateral spreading in sand appeared to occur, especially after the second 30 mm event in Test A (Figure 3.6a) when large amounts of water flowed into the sand under the furrow. Moderate amounts of flow instability did

develop during redistribution after Event 3 in Tests A-C (Figure 3.5), though its effects on penetration depth and wetted area were limited.

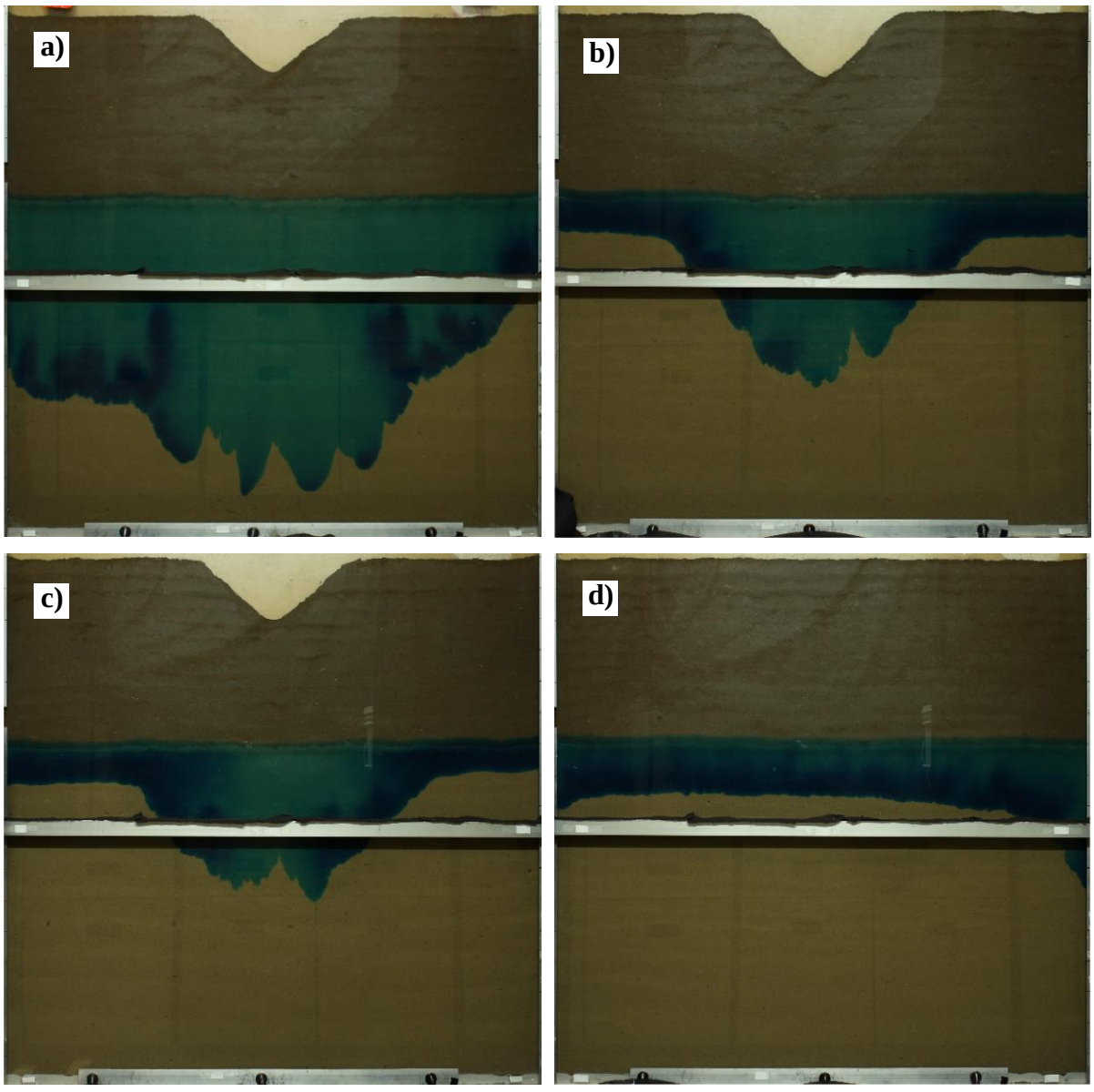

Figure 3.5: Photographs of the flow tank face in a) Test A at t=144.4 hrs, b) Test B at t=240.6 hrs, c) Test C at t=240.2 hrs, and d) Test D at t=240.1 hrs. Holes drilled at the bottom of the tank allowed passage of water and air.

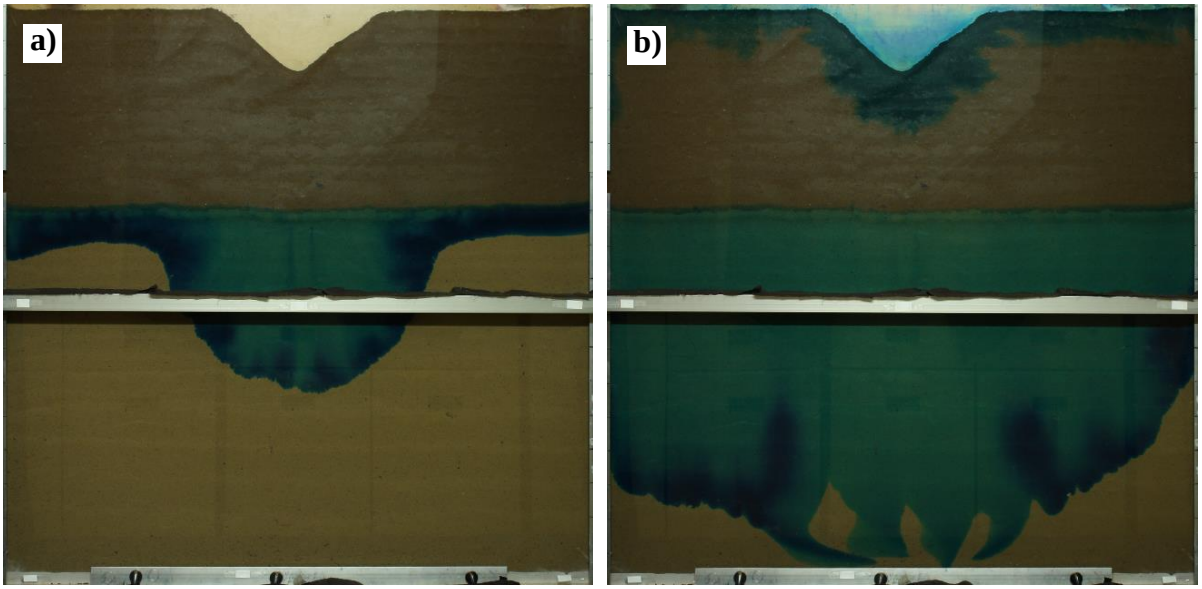

Figure 3.6: Bulbous wetting pattern showing evidence of lateral spreading during Test A in a) sand, 18 hrs after the end of the Event 2 (30 mm of applied water), and b) LFH, 56 hrs after the end of Event 4 (30 mm of applied dye).

In Test D (flat case), little movement of water was noted in the sand until after Event 3, which created a uniform wetting front, though more flow occurred along the left and right sides of the tank due to edge effects (Figure 3.5). This edge flow causing the wetted fraction to decrease slightly from 0.9 to 0.8 and the protrusion length to increase from 0.9 to 3.0 cm (Figure 3.4).

Ponding was noted in all experiments. Only small amounts of ponding occurred after Event 1, while subsequent events led to higher ponding depths, increasing with each event. In Test A, the furrow was nearly completely filled with water at the end of Events 2 and 3 and was completely filled with dye at the end of Event 4, leading to ponding over the ridge areas. In Tests B and C, ponding depth reached at least 5 cm in the furrow following Events 2 and 3. In Test D, ponding reached ~0.5 cm across the flat LFH surface after Events 2 and 3. The use of dye in Event 4 of Test A revealed that ponded water in the furrow infiltrated as a stable, bulbous wetting front, spreading downward and laterally through the LFH (Figure 3.6b). The maximum ponded depths

at the end of Event 2 for each experiment were recorded in Table 3.4, along with the fraction of water that was ponded compared to the total applied volume of water. The volume of ponded water ranged between 23.0% and 33.3% at the end of Event 2.

Table 3.4: Maximum ponded depth and ponded fraction of applied water at the end of Event 2 in each test

Test	Max. ponded depth (cm)	Event 2 application depth (cm)	Max. fraction ponded (%)
A	8.2	3.0	30.3
B	5.0	1.5	23.0
C	5.2	1.5	24.7
D	0.5	1.5	33.3

Numerical modelling

Figure 3.7 shows the maximum simulated θ occurring under the furrow and the maximum θ difference between adjacent furrow and ridge observation nodes, and how these maximum values change with depth (Figure 3.7a) and when model parameters (initial moisture conditions, runoff fraction, and furrow spacing) are independently varied (Figure 3.7c-d). In each plot, parameters that were not varied were set to mid-range values, which were: IC 4 (initial condition number 4 for initial moisture conditions; see Table 3.2), 83 cm furrow spacing (average as-built spacing), and 25% runoff fraction. Results in b), c) and d) were derived from data at 50 cm bgs. It was found that maximum furrow θ neared saturation in the LFH (depths <30 cm), but maximum θ in sand was otherwise approximately 0.15 at all depths when all other parameters were fixed. Higher initial moisture content was, naturally, associated with higher maximum furrow moisture, with rises in maximum furrow θ being approximately equal to the rises in initial moisture at 50 cm bgs (Figure

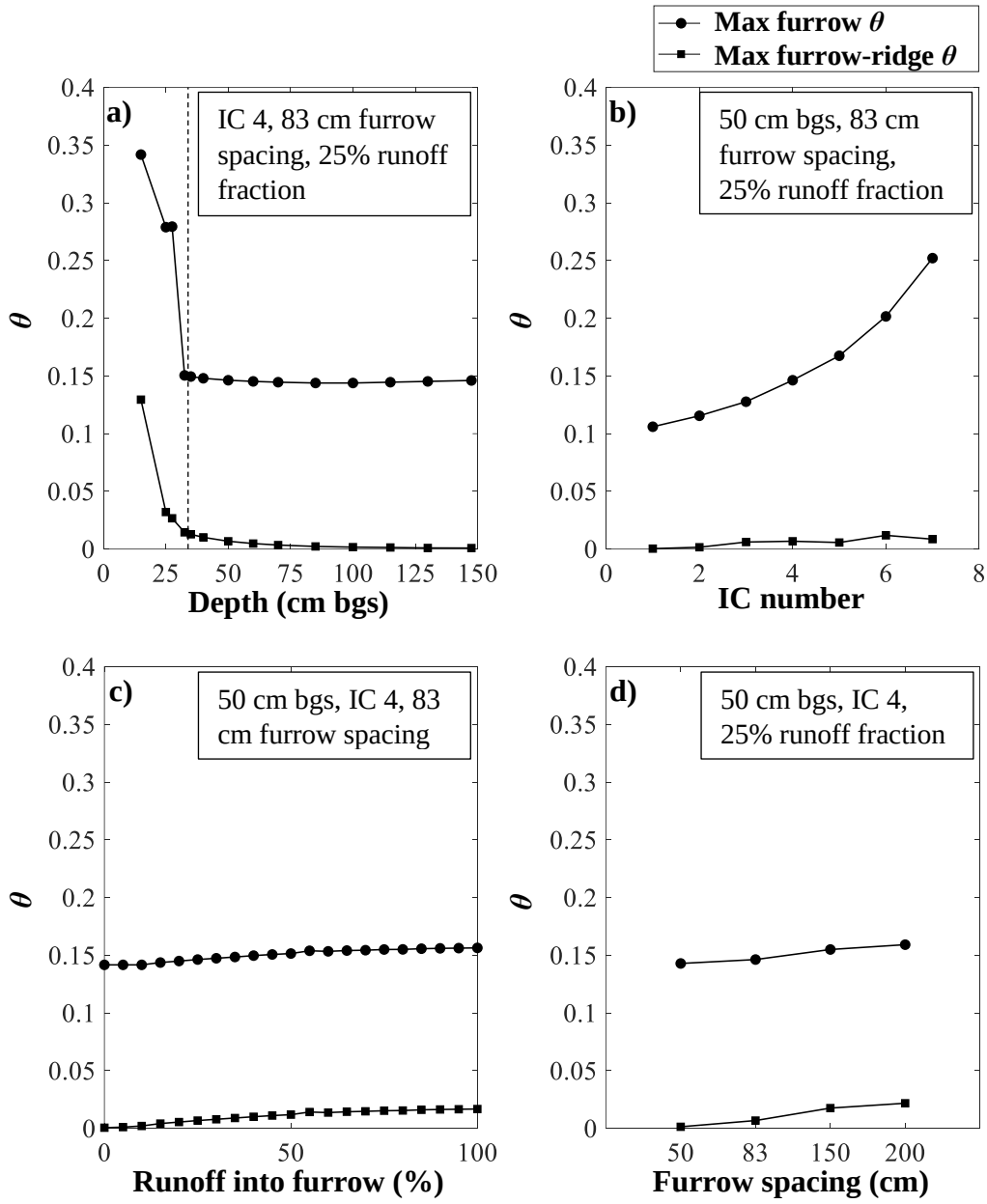

Figure 3.7: Maximum simulated furrow θ and maximum difference between furrow-ridge θ a) at different depths (dashed line shows the LFH-sand boundary), b) under various initial conditions, c) for different runoff fractions, and d) for different furrow spacings.

3.7b). Increasing runoff fraction and furrow spacing was found to slightly increase maximum furrow θ in sand, though it remained close to 0.15 in both cases (Figure 3.7c, d). The maximum difference between furrow and ridge sand θ followed the same trends as the maximum furrow θ in

sand (Figure 3.7a), decreasing with depth and increasing with IC number, runoff fraction, and furrow spacing. However, the impact of varying these parameters was small, and the maximum difference between furrow and ridge θ did not exceed 0.025 in sand.

The amount of additional recharge (i.e., the amount of water that exits the model domain by crossing the free drainage boundary at the bottom of the domain) from the simulated rainfall event was highly dependent on the fraction of runoff into furrows and on furrow spacing (Figure 3.8). Additional recharge was calculated by subtracting the amount of recharge in the flat domain without rainfall – attributed to deep drainage of excess water from initial conditions – from the

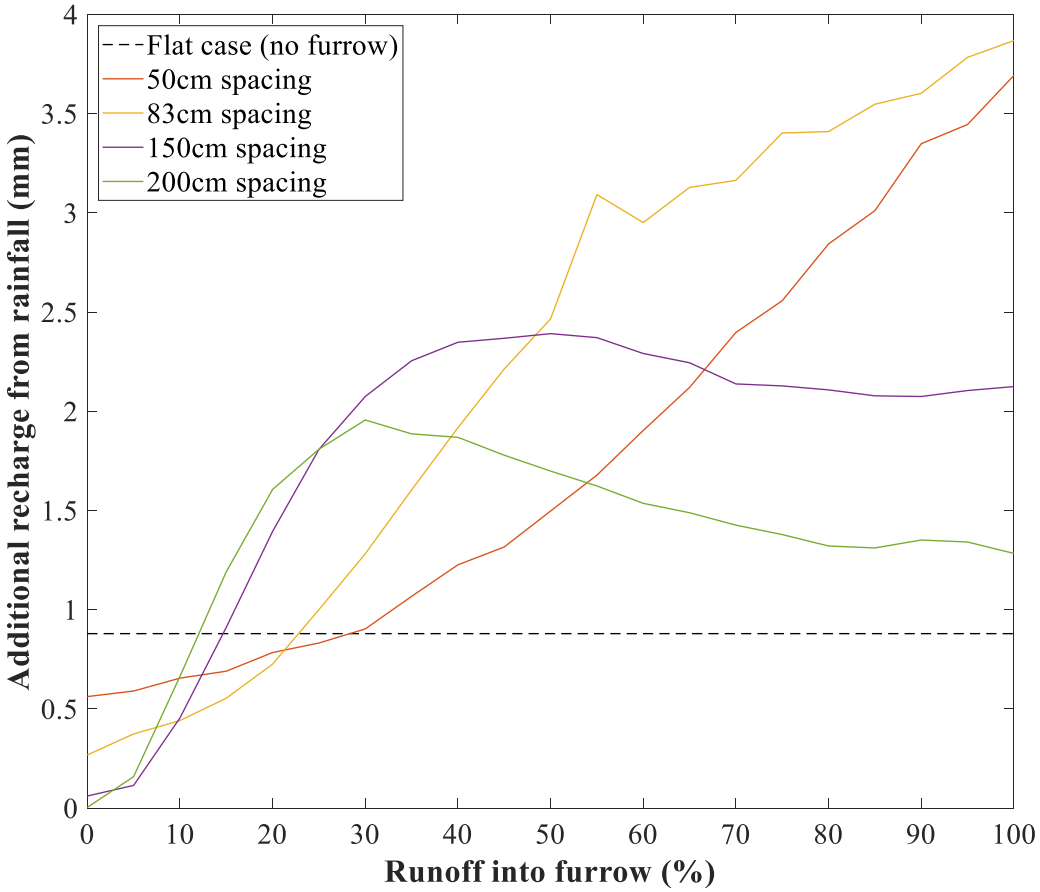

Figure 3.8: Additional recharge from simulated rainfall for different furrow configurations as a function of runoff fraction (for non-flat domains), with a moderate initial moisture condition (IC 4). The flat case assumes 0% runoff.

amount of recharge that occurs when rainfall is simulated. Under moderate initial moisture conditions (IC 4), additional recharge in domains with 150 cm and 200 cm furrow spacing initially increased rapidly with runoff fraction compared to the 50 cm and 83 cm cases. Beyond 30% runoff, recharge in the 200 cm spacing domain began to decrease; for 150 cm case, recharge leveled off at 40% runoff and then slightly decreased, ultimately having 0.75 mm more recharge than the 200 cm-spaced furrows. Additional recharge for both the 50 cm and 83 cm spacings followed a roughly linearly increasing trend with respect to runoff fraction, with the 83 cm case having more recharge than the 50 cm case for most runoff fractions. Recharge for the 50 cm and 83 cm cases surpassed the 150 cm case at runoffs greater than ~70% and ~50%, respectively, reaching close to 4 mm at 100% runoff. For the flat case, which considers a domain with no furrow and no runoff, additional recharge was estimated to be 0.88 mm, and was surpassed by all configurations at runoff fractions exceeding 30%.

Figure 3.9 shows that furrow spacing also affects moisture content under the ridge, as interactions between closely spaced furrows by lateral spreading raised moisture content under ridges. Ridge moisture was highest for furrows spaced 50 cm apart, surpassing θ observed in the flat case (no furrow) at 27.5 cm bgs (in the LFH) and at 50 cm bgs (in the sand). Moisture was also relatively high for 83 cm spacing, surpassing the flat case θ at 50 cm bgs but not at 27.5 cm bgs. For furrows spaced 150 cm and 200 cm apart, θ under the ridge was lower than the flat case, both in the LFH and in the sand. For all domains that incorporated furrows, the ridge moisture content eventually dropped below the moisture content of the flat case, converging towards values of 0.17 and 0.11 at depths of 27.5 cm bgs and 50 cm bgs, respectively.

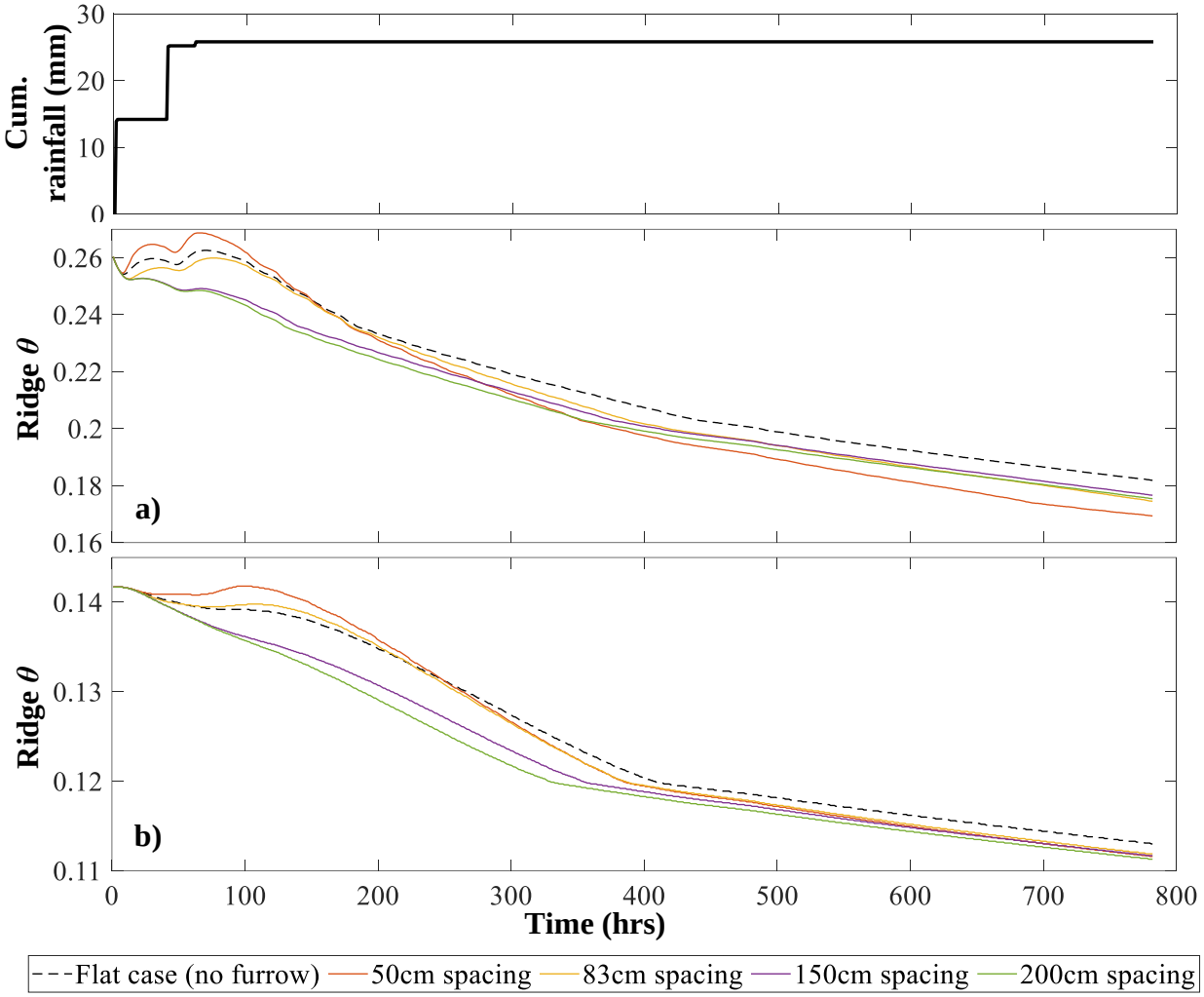

Figure 3.9: Change in ridge θ over time for the different model domain configurations at a) 27.5 cm bgs (LFH) and b) 50 cm bgs (sand). Results are shown for IC 4 and 25% diversion of rainfall into the furrow.

3.5 Discussion

Stability of flow in tank experiments

Water drop penetration tests have shown the sand to be slightly hydrophobic at the low initial moisture contents (≤8%) tested during the tank experiments (Ketcheson & Price, 2016). Because hydrophobicity is a driver of finger flow (Hendrickx *et al.*, 1993; Ritsema & Dekker, 1994) and

field dye experiments showed finger-like patterns consisting of deep penetration of dye under the furrows with little lateral spreading (Chapter 2), it was expected that flow fingering would be observed during the tank experiments. Instead, the lab tests showed gradual migration of water from the LFH into the sand, with the wetting front remaining relatively stable in the sand. In the field experiments, breakthrough into sand only occurred at discrete points at the LFH-sand interface, rather than as a continuous front, and these breakthrough points frequently coincided with root channels and stones located along the interface (Chapter 2). Many of these macropores and heterogeneities were removed during the collection and mixing of the soils used in the tank experiments. Although finger flow can arise in homogeneous systems (Wang *et al*., 2003), macropores, such as root systems, can direct large amounts of flow through the soil until the end of the macropore network, where water passes into the soil as a point source from which unstable finger flow (Glass & Nicholl, 1996; Glass *et al*., 1988) or stable finger-like flow can develop. Even without a network of macropores, perturbations created by heterogeneities at the interface between fine soil and underlying coarse soil can direct flow into fingers within the coarse layer (Hill & Parlange, 1972). Point sources have been shown to produce elongated flow patterns even without hydrophobicity (Wallach *et al*., 2013), though slight hydrophobicity can also enhance elongation (Wallach & Jortzick, 2008).

Similarly, homogenization of the sand prior to packing likely reduced variability in permeability within the sand. Evidence for this is supported by field samples collected by Ketcheson (2015) that had higher standard deviations of soil fractions, which were 5.8% for sand, 5.4% for silt, and 0.4% for clay. In comparison, the standard deviations for homogenized lab sand were 1.4% for sand, 1.4% for silt, and 0.0% for clay. The decrease in permeability variation within the sand would have favoured stable breakthrough of moisture across the LFH-sand interface.

Localized areas of higher permeability in a heterogenous sand layer could created point-source breakthrough into sand, which, as described in the previous paragraph, can instigate finger-like flow patterns.

It is also possible that the hydrophobicity of the tailings sand has decreased since water repellency was tested by Ketcheson and Price (2016), due to flushing of hydrophobic substances by percolating water, making flow more stable in sand. In order to establish whether hydrophobicity is changing over time, experiments (e.g., water drop penetration tests) should be carried out on an annual or bi-annual basis. However, regardless of whether hydrophobicity decreased over time, elongated finger-like flow patterns was shown to occur under field conditions, developing from point sources where water (or dye) breaks through into sand (Chapter 2).

Influence of rainfall depth and antecedent sand moisture on percolation patterns in flow tank tests

Despite the lack of expected finger-like flow, the lab flow tests still gave insight into how variations in topography, initial moisture conditions, and precipitation can influence wetting patterns in the Nikanotee Fen upland. The usefulness of these experiments, even though they could not replicate finger-like flow, serves as justification for using Hydrus-2D (which cannot simulate finger flow) to evaluate the effects of furrow spacing, initial moisture conditions, and runoff fraction on flow patterns and recharge. In the lab experiments, Tests B and C indicated that furrows capture runoff and are responsible for the majority of flow through sand under moderate initial moisture conditions. As was shown in Test A, periods of high infiltration arising from high-volume rainfall events (or snowmelt) are capable of wetting the LFH under both ridges and furrows, because more infiltration occurs under the ridge and because the accumulation of water in furrows

creates higher local pressures that produce lateral spreading from furrows towards ridges (Figure 3.6b). As a result, a substantial amount of water is transmitted into sand throughout most of the upland area during large events, whereas smaller events (Tests B and C) transmit little flow to the sand under ridges. The higher transfer of water into sand under ridges would hold even if finger-like flow occurred, since higher moisture (and pressure) in the LFH under the ridges from high amounts of infiltration would increase the number of capillary barrier breakthrough points and flow fingers in sand under ridges. Higher flux through a given finger is also known to increase finger width (Parlange & Hill, 1976; Glass *et al*., 1989a, 1989b), which would further increase the wetted area in sand.

Test C showed that percolation depth decreased when initial sand θ was decreased to 5%, with no substantial effect on final wetted area compared to sand having an initial θ of 8% in Test B (Figure 3.4); however, the effects of tailings sand moisture on percolation patterns are not fully understood since drier conditions produce more hydrophobic conditions (Dekker & Ritsema, 1994; Ketcheson & Price, 2016), which is a driver for finger flow (Hendrickx *et al*., 1993; Ritsema & Dekker, 1994) and can decrease finger size (Diment & Watson, 1983, 1985; Parlange & Hill, 1976). More research is needed to determine the effect of initial moisture on finger flow under field conditions in the Nikanotee Fen upland, where tailings sand had previously been shown to be slightly hydrophobic for θ less than 9.5% (Ketcheson & Price, 2016).

Na^+ flushing and redistribution

Both the flow tank and modelling tests indicated that furrows focused a large volume of flow beneath them under moderate rainfall, with much less flow occurring under ridges. Even without

preferential flow, higher amounts of residual Na^+ in unsaturated tailings sand would be expected to be flushed under furrows, though macropore flow and finger-like flow would magnify differential flushing between ridges and furrows by focusing even more flow under furrows. Nonetheless, as was demonstrated in Chapter 2, Na^+ concentrations in the vadose zone were observed to consistently decrease across the entire upland. High volume wetting events, where the wetting front occupies a greater proportion of the tailings sand area, would contribute to driving Na^+ downward through the sand and into the saturated zone under both ridges and furrows. Additionally, some water may spread laterally in sand from high flow areas under furrows into ridges (Figure 3.6a; Glass *et al*., 1988, 1989c), raising moisture content under ridges and eventually flushing a portion of the residual Na^+. Together, these processes could help explain the site-wide decrease in residual Na^+ concentrations in the Nikanotee upland tailings sand (Chapter 2). Increasing the spacing between furrows would prolong Na^+ persistence in the tailings sand by decreasing the number of high-flushing zones (under furrows) and by creating drier conditions under ridges due to the removal of interactions between furrows that can occur through lateral spreading of moisture (as indicated by Figure 3.9), which would decrease the amount of flushing under ridges. Further modelling incorporating Na^+ adsorption and advection-dispersion mechanics is necessary to confirm this hypothesis and to quantify the impacts of furrow spacing on Na^+ fate in reclaimed fen systems.

Additional recharge from furrows

Model simulations showed that the amount of additional recharge from rainfall depended heavily on furrow spacing and on runoff fraction (Figure 3.8). Compared to the flat case (no furrow), which assumes 0% runoff, the 83 cm as-built furrow spacing in the upland produced more

recharge when runoff from the ridges exceeded 25%. At lower runoff fractions, the flat case provided more recharge; this is believed to have been a result of the lower position of the furrows compared to the adjacent ridges, which would have exposed deeper layers to more drying than the flat case, as shown by the dry conditions near the end of the simulations that incorporated furrows (Figure 3.9). Ultimately, drying of deeper soil layers during and after the simulated rainfall event appears to have reduced recharge, outweighing potential increases in recharge from accumulation of water in furrows at runoff fractions under 25%. However, if runoff losses in the flat case had been considered, the amount of recharge from furrows would have been higher relative to the flat domain.

Differences in recharge from furrow spacing are related to the amount of water received by the furrows and ridges. Spacing furrows farther apart increases the contributing ridge area and supplies more water to furrows, where matric pressure becomes elevated and localized high recharge zones develop. However, spacing furrows at 150 or 200 cm apart removes interactions between furrows, leading to very dry conditions under ridges near the LFH-sand interface (Figure 3.9), thus restricting percolation of water into sand. At runoff fractions that are >30% for 200 cm spacing and >50% for 150 cm spacing, very dry conditions severely restrict deep percolation under the ridges, such that additional water inputs from the furrows are outweighed by losses in recharge from infiltrated water under ridges.

Depressional storage capacity provided by furrows is lower when they are placed farther apart, because the number of furrows in the upland decreases. For example, if furrow spacing were increased from the as-built spacing of 83 cm to 150 cm, the storage capacity provided by furrows would decrease by nearly half. Consequently, spacing furrows farther apart increases the risk of furrow flooding, potentially causing much more water to exit the upland as runoff during large

rainfall events (or snowmelt). This would be amplified by more rapid sedimentation rates in furrows spaced farther apart, associated with higher volumes of captured runoff. As such, despite the apparent increases in recharge from furrows spaced 150 cm apart when runoff fractions were small (<50%), as suggested by Figure 3.8, recharge may instead be highest when furrows are spaced closer together in the absence of larger upland features (e.g., hummocks and recharge basins) capable of retaining runoff when furrows become flooded.

The modelling simulations conducted in this study used parameters representing a completely weathered LFH profile. Within the first few years post-reclamation, the lower portions of the LFH layer remain largely unweathered, thus increasing water retention of the LFH, and suggesting that furrows are more important for conducting flow across the capillary barrier than in later years. Even after the entire LFH profile becomes weathered, furrows may still be responsible for more recharge than was found from the modelling tests due to a higher likelihood of macropore flow along root channels under furrows, considering that vegetation is denser in furrows. In fact, plant cover measurements taken in 2016 showed the mean ridge cover fraction of 16% to be significantly different than the mean furrow cover of 55% (Asten, unpublished data). The finger-like flow patterns observed in Chapter 2 would also contribute to recharge by rapidly driving moisture deep into the sand and reducing losses to ET, whereas the modelling tests did not simulate finger flow and instead showed a gradual redistribution of water in sand, with θ remaining well under the near-saturation "spikes" in sand moisture observed by Sutton & Price (2020); this was expected, as Richards' equation lacks the physical mechanics for simulating finger flow (Eliassi & Glass, 2001). However, root water uptake and interception were not considered in the model, which would create drier conditions and reduce percolation into sand.

Impacts of future upland evolution on recharge and Na^+ flushing

As evolution of the LFH progresses in the upland, competing processes will have a net effect on recharge that is difficult to predict. On the one hand, root networks will continue to develop in the LFH as more vegetation establishes, thus providing more flow conduits that allow water to rapidly traverse the LFH and percolate into the underlying tailings sand, and higher litter cover will limit evaporation from the soil surface. Furthermore, the degree of LFH weathering could increase over time, which would increase infiltration and decrease water retention in the LFH, thus increasing recharge and flushing of Na^+ from ridges.

On the other hand, the continued development of roots will transfer ET processes deeper into the LFH, which will reduce moisture content at depth and could reduce the amount of water that percolates into the sand. If the degree of LFH weathering increases, it would increase infiltration in the ridges and reduce the amount of runoff transferred into furrows, which would reduce matric pressure under the furrows. Erosion of ridges will progressively fill in the furrows with sediment, making them less effective at capturing runoff and decreasing the vertical pressure gradients attained under furrows, although erosion rates would be reduced by higher vegetation density in later years (Saynor *et al.*, 2018). Relatively high pressures are needed to overcome the capillary barrier at the LFH-sand interface, and as such, less water may percolate into the sand aquifer. In addition, macropore flow is most significant at higher pressures (Cey & Rudolph, 2009), and therefore macropore flow that bypasses the LFH soil matrix under the furrows could be reduced if less runoff were diverted into the furrows. Lastly, as a result of increased interception from vegetation growth and of increased runoff out of the upland from furrow sedimentation, the amount of infiltration in the upland is expected to decrease. The combined effect of these processes could

decrease recharge and Na^+ flushing. Further monitoring of the system is required to determine how recharge and Na^+ concentrations in tailings sand evolve over time.

Limitations

Differences in soil hydraulic conductivity between water and the Brilliant Blue FCF dye solution were either not statistically significant (for sand) or were small enough that they would have little effect on flow (for LFH). This implies that moisture migration is mostly unaffected by the addition of dye to the infiltrating solution, although some additional ponding is believed to have occurred when dye was applied during Event 4 in Test A of the series of flow tank experiments. While moisture migration would not be greatly affected by the addition of dye, the dye compound itself has been shown to be retarded compared to pure water by a range of factors. For example, retardation factors of 1.2 (Flury & Flühler, 1995) and 1.5 (Öhrström *et al*., 2004) have been found, but they vary inversely with the concentration of the dye solution (Kasteel *et al*., 2002). Retardation would be much higher in the LFH (6% clay content on average) compared to sand (<1% clay; Ketcheson, 2015) since Brilliant Blue FCF has been shown to adsorb predominantly to clay particles (Ketelsen & Meyer-Windel, 1999), though high ionic strength associated with high concentrations of leachable ions including Na^+, Ca^{2+}, Mg^{2+}, and SO_4^{2-} in tailings sand (Simhayov *et al*., 2017) could increase dye adsorption (Germán-Heins & Flury, 2000). During the tank experiments, this may have slightly impacted flow path visualization in sand, as the dye likely advanced more slowly than the wetting front. Nonetheless, the shape of the flow patterns in sand are not believed to have been greatly impacted, and the results presented for moisture redistribution in tailings sand are thought to be reasonably accurate.

The homogenization of lab soils used in the tank experiments removed many macropores and heterogeneities that would have otherwise been present in the LFH and sand. As such, preferential flow occurring along macropores or in areas of high saturated hydraulic conductivity were largely absent in the repacked soils, despite being drivers of rapid flow through soil, as was suggested by in-situ dye tracer tests (Chapter 2). In addition, the careful packing procedure used in the lab (manual packing in ~2.5 cm lifts) could have made the soils more homogenous compared to the in-situ field soils that were placed in 50 cm lifts and compacted with a dozer.

During the tank tests, very little evaporation would have occurred, since the experiments were carried out indoors and the top of the tank was usually covered. By extension, root water uptake by transpiring plants present in the field did not occur during the lab tests. ET processes would have created drier soil conditions and would likely have reduced the amount of water that percolated into sand, especially under the furrow since roots networks are believed to be denser in furrows, as previously discussed.

3.6 Conclusions and recommendations

Significant amounts of runoff were shown to collect and infiltrate in furrows. This reduces water losses by runoff, and creates higher-pressure areas under furrows that promote transmission of water across the capillary barrier between the LFH and the underlying sand. As such, furrows were shown to increase the amount of recharge supplied to the upland aquifer and therefore increase flushing of Na^+ from unsaturated tailings sand. This will reduce the period over which Na^+ is present at elevated concentrations in groundwater supplied to the fen, but in the shorter-term could also increase peak Na^+ concentrations in groundwater; this could be detrimental to fen

plant health. Furrows are most important for supplying recharge in early years when substantial soil evolution is still ongoing. During these early years, recharge is especially restricted because a strong capillary barrier remains between the LFH and the sand, and because a larger proportion of rainfall is converted to runoff.

Under realistic runoff fractions (<50%), modelling showed that furrows spaced 150 cm apart produced the greatest amount of recharge, although they would be less effective at retaining runoff during periods of heavy rainfall or snowmelt and would become filled with sediment more rapidly. The accelerated sedimentation would make the furrows even more vulnerable to flooding and would reduce the time over which they can effectively capture runoff, although this would be of lesser concern in later years when infiltration capacity has been greatly increased by soil evolution. If additional recharge is desired in future reclaimed fen watershed designs compared to the Nikanotee Fen watershed design, then furrows spaced at 150 cm could be used in conjunction with larger depressions and hummocks designed to capture runoff, in the event that the furrows become flooded. Otherwise, applying the Nikanotee upland as-built furrow spacing of ~83 cm to future reclaimed uplands would be preferred, to deter flooding of furrows and reduce the furrow sedimentation rate. Larger upland features (e.g. basins and hummocks) could also be used if furrows were spaced at ~83 cm intervals to capture runoff in later years when the furrow-ridge relief disappears due to sedimentation, but would be less crucial in early years than if furrows were spaced 150 cm apart.

As furrows become filled in with sediment, LFH weathering progresses, and vegetation continues to establish, infiltration patterns are hypothesized to become more uniform. These evolving conditions are expected to induce a more uniform flushing of Na^+ from the tailings sand, but the net rate of flushing remains uncertain because it is unclear whether the amount of recharge

(and percolation through sand) will increase or decrease. Continued monitoring and analysis of water levels, water chemistry, and Na^+ concentrations in unsaturated tailings sand is necessary to better predict how the system performs as the LFH evolves. Monitoring may be combined with projective modelling that incorporates root water uptake, interception, runoff, and 2D Na^+ transport in the vadose zone.

Chapter 4: Conclusions and recommendations

Furrows were shown to accumulate runoff from adjacent ridges, creating localized areas where higher rates and volumes of infiltration occur (Chapter 2). High vertical pressure gradients, accompanied by the presence of macropores in the LFH, encouraged percolation of water through the LFH profile and into the underlying tailings sand. Finger-like flow was also observed in sand, which further contributed to deep percolation of water and restricted lateral spreading, wetting only a small fraction of the cross-sectional area under the LFH. Thus, furrows can promote recharge by increasing infiltration and promoting deep percolation of precipitation, particularly during large precipitation events when runoff is high.

Despite the heterogeneous wetting patterns observed in unsaturated tailings sand, residual Na^+ concentrations in sand declined site-wide, with an estimated ~90% of Na^+ being flushed by 2019, including under ridges (Chapter 2). It is believed that furrows were responsible for a large proportion of Na^+ that was flushed during this period, but that lateral spreading of water from sand under furrows into adjacent ridges and occasional downward breakthrough of moisture into sand under ridges contributed to the site-wide decrease in residual Na^+ concentrations.

The hydrology and Na^+ distribution of the reclaimed system is influenced not only by the presence of furrows, but also by the spacing between them. Modelling showed that furrows placed closer together decreases the amount of runoff received by a given furrow, which reduces matric pressures attained under furrows and reduces the amount of water that can break through the capillary barrier (Chapter 3). Placing furrows closer together would create a more uniform flushing of Na^+ across the upland. The net effect on Na^+ flushing is uncertain, since the flux of water through sand would be lower when furrows are closer together, but a greater proportion of sand would experience frequent flushing. Meanwhile, furrows spaced farther apart were shown to

potentially increase recharge, although they would have a higher risk of flooding and some runoff may not be retained during large wetting events such as snowmelt or heavy rainfall. Flooding would be amplified by accelerated sedimentation rates due to increased amounts of runoff received by furrows spaced farther apart.

It is recommended that furrows be incorporated in future upland designs to ensure adequate recharge, as well as to reduce erosion (Saynor *et al*., 2018). They would be especially important within the first few years post-reclamation, when only a fraction of the LFH profile has been weathered. During this period, the fraction of runoff from precipitation events is highest, which reduces the amount of infiltration in the absence of furrows. A capillary barrier between the LFH and sand also severely limits recharge in early years, but more water is progressively able to pass into sand from successive freeze-thaw cycles that increase the hydraulic conductivity of the LFH (Sutton & Price, 2020), allowing more water to reach the interface of the LFH-sand layer and eventually break through into the sand. By capturing runoff, furrows create localized high vertical pressure gradients, thus promoting percolation across the capillary barrier and helping wet-up the newly formed aquifer. Furthermore, vegetation is poorly established within the first few years after watershed construction, making the upland more vulnerable to erosion, which would be reduced by incorporating furrows (Saynor *et al*., 2018).

The as-built upland design incorporates furrows spaced 83 cm apart, on average, which provides a good compromise between the amount of depressional storage and recharge contributions. As such, it is recommended that furrows be spaced at a distance similar to this as-built configuration. Alternatively, furrows may be placed farther apart if additional recharge in early years is desired, up to a distance of 150 cm, beyond which recharge contributions decrease and furrows are easily flooded (Chapter 3). If furrows are spaced at a distance greater than as-built

conditions, the upland design should include larger landforms, such as the recharge basins and the mounded LFH "hummocks" incorporated in the Nikanotee upland, to compensate for the restricted capacity of furrows to detain overland flow. Larger landforms could also be used to capture runoff in upland designs where furrows are placed closer together, since furrows are expected to eventually become filled with sediment regardless of spacing distance, but would be less crucial in early years than if furrows were spaced 150 cm apart. However, the effects of increased furrow spacing and of larger landforms on Na^+ flushing from unsaturated sand and on near-surface Na^+ concentrations in peat should receive further study when designing future reclaimed peatland watersheds. Future models predicting the trajectory of reclaimed watersheds should therefore simulate runoff from ridges into furrows and the associated small-scale unsaturated flow and solute transport. These models could be calibrated and verified with, for example, a grid of soil moisture probes placed under adjacent furrows and ridges, along with rigorous sampling of residual Na^+ concentrations in sand over several years. If modelling indicates that, for a given spacing between furrows, the persistence of elevated Na^+ concentrations in groundwater near the fen surface is substantially prolonged compared to other furrow spacings, then it should be avoided in future upland designs.

References

Alberta Environment and Parks. (2017). *Oil sands mine reclamation and disturbance tracking by year* [Data set]. Retrieved from http://osip.alberta.ca/library/Dataset/Details/27#

Arbel, Y., Yair, A., & Oz, S. (2005). Effect of topography and water repellent layer on the non-uniform development of planted trees in a sandy arid area. *Journal of Arid Environments, 60*(1), 67-81.

Baker, R. S., & Hillel, D. (1990). Laboratory tests of a theory of fingering during infiltration into layered soils. *Soil Science Society of America Journal, 54*(1), 20-30.

Belfort, B., Weill, S., & Lehmann, F. (2017). Image analysis method for the measurement of water saturation in a two-dimensional experimental flow tank. *Journal of Hydrology, 550*, 343-354.

Beven, K., & Germann, P. (1982). Macropores and water flow in soils. *Water Resources Research, 18*(5), 1311-1325.

Bouma, J., & De Laat, P. J. M. (1981). Estimation of the moisture supply capacity of some swelling clay soils in The Netherlands. *Journal of Hydrology, 49*(3-4), 247-259.

Cey, E. E., & Rudolph, D. L. (2009). Field study of macropore flow processes using tension infiltration of a dye tracer in partially saturated soils. *Hydrological Processes, 23*(12), 1768-1779.

Daly, C., Price, J. S., Rezanezhad, F., Pouliot, R., Rochefort, L., & Graf, M. D. (2012). Initiatives in oil sand reclamation: Considerations for building a fen peatland in a post-mined oil sands landscape. In D. Vitt, & J. Bhatti (Eds.), *Restoration and Reclamation of Boreal Ecosystems* (pp. 179-201). Cambridge University Press.

de Rooij, G. H. (2000). Modeling fingered flow of water in soils owing to wetting front instability: A review. *Journal of Hydrology, 231-232*, 277-294.

Dekker, L. W., & Ritsema, C. J. (1994). How water moves in a water repellent sandy soil: 1. Potential and actual water repellency. *Water Resources Research, 30*(9), 2507-2517.

Diment, G. A., & Watson, K. K. (1983). Stability analysis of water movement in unsaturated porous materials: 2. Numerical studies. *Water Resources Research, 19*(4), 1002-1010.

Diment, G. A., & Watson, K. K. (1985). Stability analysis of water movement in unsaturated porous materials: 3. Experimental studies. *Water Resources Research, 21*(7), 979-984.

Eliassi, M., & Glass, R. J. (2001). On the continuum-scale modeling of gravity-driven fingers in unsaturated porous media: The inadequacy of the Richards Equation with standard monotonic constitutive relations and hysteretic equations of state. *Water Resources Research, 37*(8), 2019-2035.

Eliassi, M., & Glass, R. J. (2003). On the porous continuum-scale modeling of gravity-driven fingers in unsaturated materials: Numerical solution of a hypodiffusive governing equation that incorporates a hold-back-pile-up effect. *Water Resources Research, 39*(6).

Elshorbagy, A., Jutla, A., Barbour, L., & Kells, J. (2005). System dynamics approach to assess the sustainability of reclamation of disturbed watersheds. *Canadian Journal of Civil Engineering, 32*(1), 144-158.

Flury, M., & Flühler, H. (1995). Tracer characteristics of Brilliant Blue FCF. *Soil Science Society of America Journal, 59*(1), 22-27.

Flury, M., Flühler, H., Jury, W. A., & Leuenberger, J. (1994). Susceptibility of soils to preferential flow of water: A field study. *Water Resources Research, 30*(7), 1945-1954.

Gammoh, I. A. (2011). Double furrow with raised bed–A new improved mechanized water-harvesting technique for large-scale rehabilitation of arid rain-fed areas. *Soil & Tillage Research, 113*(1), 61-69.

Germán-Heins, J., & Flury, M. (2000). Sorption of Brilliant Blue FCF in soils as affected by pH and ionic strength. *Geoderma, 97*(1-2), 87-101.

Ghodrati, M., & Jury, W. A. (1990). A field study using dyes to characterize preferential flow of water. *Soil Science Society of America Journal, 54*(6), 1558-1563.

Glass, R. J., & Nicholl, M. J. (1996). Physics of gravity fingering of immiscible fluids within porous media: An overview of current understanding and selected complicating factors. *Geoderma, 70*(2-4), 133-163.

Glass, R. J., Steenhuis, T. S., & Parlange, J.-Y. (1988). Wetting front instability as a rapid and far-reaching hydrologic process in the vadose zone. *Journal of Contaminant Hydrology, 3*(2-4), 207-226.

Glass, R. J., Steenhuis, T. S., & Parlange, J.-Y. (1989b). Wetting front instability: 2. Experimental determination of relationships between system parameters and two-dimensional unstable flow field behavior in initially dry porous media. *Water Resources Research, 25*(6), 1195-1207.

Glass, R. J., Steenhuis, T. S., & Parlange, J.-Y. (1989c). Mechanism for finger persistence in homogeneous, unsaturated, porous media: Theory and verification. *Soil Science, 148*(1), 60-70.

Glass, R., Parlange, J.-Y., & Steenhuis, T. (1989a). Wetting front instability: 1. Theoretical discussion and dimensional analysis. *Water Resources Research, 25*(6), 1187-1194.

Government of Alberta. (2015). *Coal and oil sands exploration reclamation requirements.* Retrieved from https://open.alberta.ca/publications/9781460126530

Hardie, M., Deurer, M., Doyle, R. B., Lisson, S., Cotching, W. E., & Mattern, K. (2012). Development of unstable flow and reduced hydraulic conductivity due to water repellence and restricted drainage. *Vadose Zone Journal, 11*(4).

Hendrickx, J. M. H., Dekker, L. W., & Boersma, O. H. (1993). Unstable wetting fronts in water-repellent field soils. *Journal of Environmental Quality, 22*(1), 109-118.

Hill, D. E., & Parlange, J.-Y. (1972). Wetting front instability in layered soils. *Soil Science Society of America Journal, 36*(5), 697-702.

Hillel, D., & Baker, R. S. (1988). A descriptive theory of fingering during infiltration into layered soils. *Soil Science, 146*(1), 51-56.

Irvine, S. (2018). *Dissolved organic carbon production and transport in a constructed watershed in the Athabasca Oil Sands Region, Alberta* (Master's thesis). UWSpace.

Jury, W. A., Wang, Z., & Tuli, A. (2003). A conceptual model of unstable flow in unsaturated soil during redistribution. *Vadose Zone Journal, 2*(1), 61-67.

Kasteel, R., Vogel, H.-J., & Roth, K. (2002). Effect of non-linear adsorption on the transport behaviour of Brilliant Blue in a field soil. *European Journal of Soil Science, 53*(2), 231-240.

Kessel, E. D., Ketcheson, S. J., & Price, J. S. (2018). The distribution and migration of sodium from a reclaimed upland to a constructed fen peatland in a post-mined oil sands landscape. *Science of the Total Environment, 630*, 1553-1564.

Ketcheson, S. J. (2015). *Hydrology of a constructed fen watershed in a post-mined landscape in the Athabasca Oil Sands Region, Alberta, Canada* (Doctoral dissertation). UWSpace.

Ketcheson, S. J., & Price, J. S. (2016). Hydrophysical properties of mine reclamation materials (LFH, tailings sand, petroleum coke and organic peat soils) in a constructed watershed (Submitted).

Ketcheson, S. J., Price, J. S., Sutton, O. F., Sutherland, G., Kessel, E. D., & Petrone, R. M. (2017). The hydrological functioning of a constructed fen wetland watershed. *Science of the Total Environment, 603-604*, 593-605.

Ketelsen, H., & Meyer-Windel, S. (1999). Adsorption of Brilliant Blue FCF by soils. *Geoderma, 90*(1-2), 131-145.

Kung, K.-J. S. (1990). Preferential flow in a sandy vadose zone: 1. Field observation. *Geoderma, 46*(1-3), 51-58.

Larsson, M. H., Jarvis, N. J., Torstensson, G., & Kasteel, R. (1999). Quantifying the impact of preferential flow on solute transport to tile drains in a sandy field soil. *Journal of Hydrology, 215*(1-4), 116-134.

Liu, Y., Steenhuis, T. S., & Parlange, J.-Y. (1994). Formation and persistence of fingered flow fields in coarse grained soils under different moisture contents. *Journal of Hydrology, 159*(1-4), 187-195.

MacKinnon, M. D., Matthews, J. G., Shaw, W. H., & Cuddy, R. G. (2001). Water quality issues associated with composite tailings (CT) technology for managing oil sands tailings. *International Journal of Surface Mining, Reclamation and Environment, 15*(4), 235-256.

Naeth, M. A., Chanasyk, D. S., & Burgers, T. D. (2011). Vegetation and soil water interactions on a tailings sand storage facility in the Athabasca Oil Sands region of Alberta Canada. *Physics and Chemistry of the Earth, 36*(1-4), 19-30.

Naeth, M. A., Wilkinson, S. R., Mackenzie, D. D., Archibald, H. A., & Powter, C. B. (2013). *Potential of LFH mineral soil mixes for land reclamation in Alberta.* Oil Sands Research and Information Network, University of Alberta, School of Energy and the Environment.

Nguyen, H. V., Nieber, J. L., Ritsema, C. J., Dekker, L. W., & Steenhuis, T. S. (1999). Modeling gravity driven unstable flow in a water repellent soil. *Journal of Hydrology, 215*(1-4), 202-214.

Nieber, J. L. (1996). Modeling finger development and persistence in initially dry porous media. *Geoderma, 70*(2-4), 207-229.

Nwaishi, F., Petrone, R. M., Price, J. S., Ketcheson, S. J., Slawson, R., & Andersen, R. (2015). Impacts of donor-peat management practices on the functional characteristics of a constructed fen. *Ecological Engineering, 81*, 471-480.

Öhrström, P., Hamed, Y., Persson, M., & Berndtsson, R. (2004). Characterizing unsaturated solute transport by simultaneous use of dye and bromide. *Journal of Hydrology, 289*(1-4), 23-35.

Parlange, J.-Y., & Hill, D. E. (1976). Theoretical analysis of wetting front instability in soils. *Soil Science, 122*(4), 236-239.

Penman, H. L. (1948). Natural evaporation from open water, bare soil and grass. *Proceedings of the Royal Society of London, 193*(1032), 120-145.

Philip, J. R. (1968). Steady infiltration from buried point sources and spherical cavities. *Water Resources Research, 4*(5), 1039-1047.

Philip, J. R. (1975). Stability analysis of infiltration. *Soil Science Society of America Journal, 39*(6), 1042-1049.

Pouliot, R., Rochefort, L., & Graf, M. D. (2012). Impacts of oil sands process water on fen plants: Implications for plant selection in required reclamation projects. *Environmental Pollution, 167*, 132-137.

Price, J. S., McLaren, R. G., & Rudolph, D. L. (2010). Landscape restoration after oil sands mining: Conceptual design and hydrological modelling for fen reconstruction. *International Journal of Mining, Reclamation and Environment, 24*(2), 109-123.

Raats, P. A. C. (1973). Unstable wetting fronts in uniform and nonuniform soils. *Soil Science Society of America Journal, 37*(5), 681-685.

Rezanezhad, F., Andersen, R., Pouliot, R., Price, J. S., Rochefort, L., & Graf, M. D. (2012). How fen vegetation structure affects the transport of oil sands process-affected waters. *Wetlands, 32*, 557-570.

Ritsema, C. J., & Dekker, L. W. (1994). How water moves in a water repellent sandy soil: 2. Dynamics of fingered flow. *Water Resources Research, 30*(9), 2519-2531.

Ritsema, C. J., Dekker, L. W., Nieber, J. L., & Steenhuis, T. S. (1998). Modeling and field evidence of finger formation and finger recurrence in a water repellent sandy soil. *Water Resources Research, 34*(4), 555-567.

Saffman, P. G., & Taylor, G. I. (1958). The penetration of a fluid into a porous medium or Hele-Shaw cell containing a more viscous liquid. *Proceedings of the Royal Society of London, 245*(1242), 312-329.

Saynor, M. J., Lowry, J. B., & Boyden, J. M. (2018). Assessment of rip lines using CAESAR-Lisflood on a trial landform at the Ranger Uranium Mine. *Land Degradation & Development, 30*(5), 504-514.

Scott, A. C., Mackinnon, M. D., & Fedorak, P. M. (2005). Naphthenic acids in Athabasca Oil Sands tailings waters are less biodegradable than commercial naphthenic acids. *Environmental Science & Technology, 39*(21), 8388-8394.

Šejna, M., Šimůnek, J., & van Genuchten, M. Th. (2014). *The HYDRUS software package for simulating the two- and three-dimensional movement of water, heat, and multiple solutes in variably-saturated porous media: User manual* (ver. 2.04). Prague, Czech Republic: PC-Progress.

Selker, J. S., Steenhuis, T. S., & Parlange, J.-Y. (1996). An engineering approach to fingered vadose pollutant transport. *Geoderma, 70*(2-4), 197-206.

Sheng, F., Wang, K., Zhang, R., & Liu, H. (2009). Characterizing soil preferential flow using iodine-starch staining experiments and the active region model. *Journal of Hydrology, 367*(1-2), 115-124.

Sililo, O. T. N., & Tellam, J. H. (2000). Fingering in unsaturated zone flow: A qualitative review with laboratory experiments on heterogeneous systems. *Groundwater, 38*(6), 864-871.

Simhayov, R. B., Price, J. S., Smeaton, C. M., Parsons, C., Rezanezhad, F., & Van Cappellen, P. (2017). Solute pools in Nikanotee Fen watershed in the Athabasca oil sands region. *Environmental Pollution, 225*, 150-162.

Soil Classification Working Group. (1998). *Canadian System of Soil Classification* (3rd ed.). Ottawa, ON: National Research Council of Canada.

Stormont, J. C., & Anderson, C. E. (1999). Capillary barrier effect from underlying coarser soil layer. *Journal of Geotechnical and Geoenvironmental Engineering, 125*(8), 641-648.

Sutton, O. F., & Price, J. S. (2020). Soil moisture dynamics modelling of a reclaimed upland in the early post-construction period. *Science of the Total Environment, 718*.

van Genuchten, M. Th. (1980). A closed-form equation for predicting the hydraulic conductivity of unsaturated soils. *Soil Science Society of America Journal, 44*(5), 892-898.

Vitt, D. H., Halsey, L. A., Thormann, M. N., & Martin, T. (1996). *Peatland inventory of Alberta. Phase I: Overview of peatland resources in the natural regions and subregions of the province.* Edmonton, AB: University of Alberta.

Wallach, R., & Jortzick, C. (2008). Unstable finger-like flow in water-repellent soils during wetting and redistribution – The case of a point water source. *Journal of Hydrology, 351*(1-2), 26-41.

Wallach, R., Margolis, M., & Graber, E. R. (2013). The role of contact angle on unstable flow formation during infiltration and drainage in wettable porous media. *Water Resources Research, 49*(10), 6508-6521.

Wang, Y., Li, Y., Wang, X., & Chau, H. W. (2018). Finger flow development in layered water-repellent soils. *Vadose Zone Journal, 17*(1), 1-11.

Wang, Z., Feyen, J., & Elrick, D. E. (1998). Prediction of fingering in porous media. *Water Resources Research, 34*(9), 2183-2190.

Wang, Z., Tuli, A., & Jury, W. A. (2003). Unstable flow during redistribution in homogeneous soil. *Vadose Zone Journal, 2*(1), 52-60.

Wessolek, G., Stoffregen, H., & Täumer, K. (2009). Persistency of flow patterns in a water repellent sandy soil – Conclusions of TDR readings and a time-delayed double tracer experiment. *Journal of Hydrology, 375*(3-4), 524-535.

White, I., Colombera, P. M., & Philip, J. R. (1976). Experimental study of wetting front instability induced by sudden change of pressure gradient. *Soil Science Society of America Journal, 40*(6), 824-829.

WorleyParsons. (2014). *Construction completions report: Fen wetland.* Calgary, AB: WorleyParsons Canada.

Yang, B., Blackwell, P. S., & Nicholson, D. F. (1996). A numerical model of heat and water movement in furrow-sown water repellent sandy soils. *Water Resources Research, 32*(10), 3051-3061.

Appendices

Appendix A: Additional processed images from Dye Test 1 (Chapter 2)

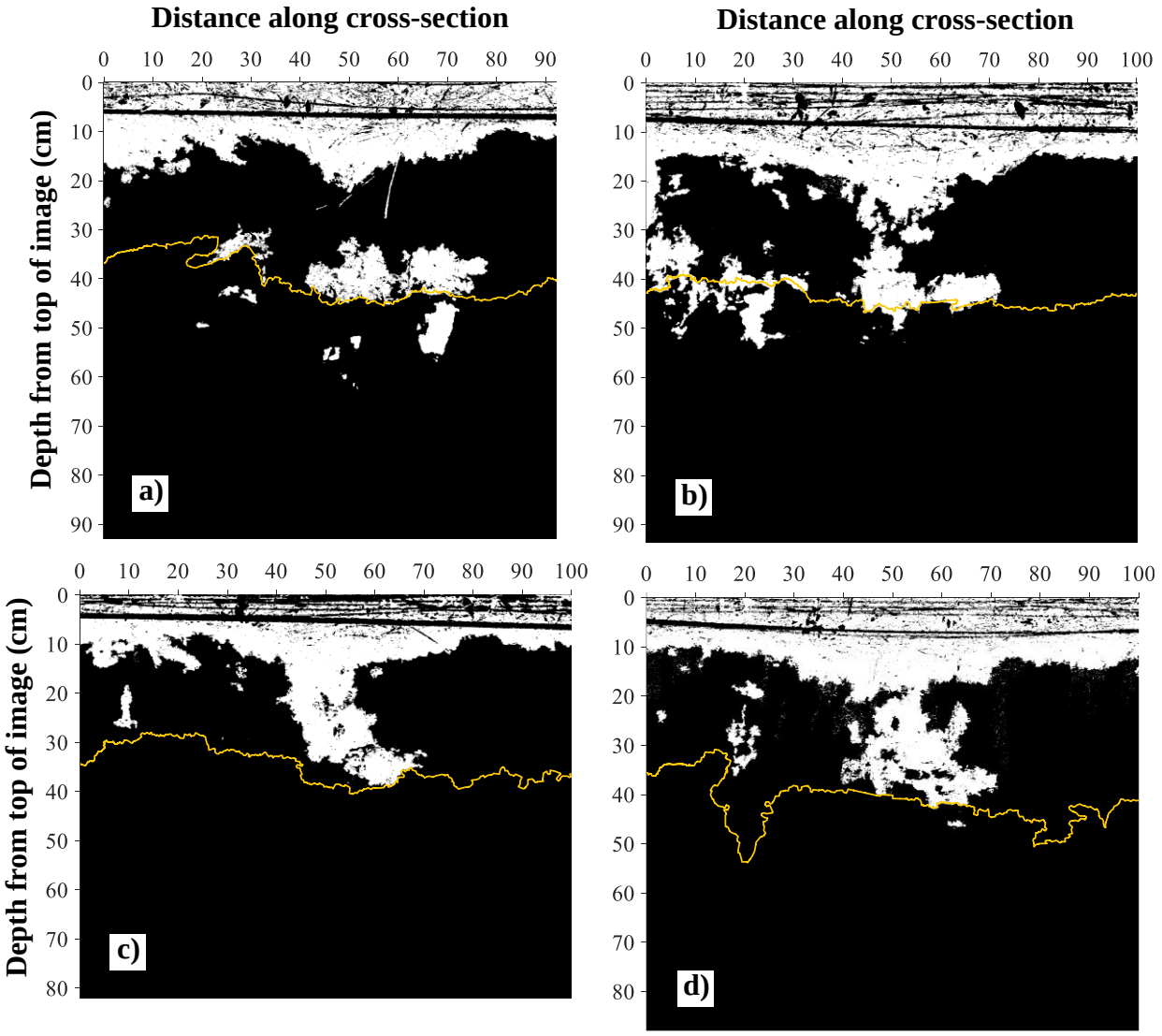

Figure A.1: Final processed black-and-white images of cross-sections exposed during excavation in Test 1, located a) 30 cm, b) 40 cm, c) 50 cm, d) 60 cm, e) 70 cm, f) 80 cm, g) 90 cm, h) 100 cm, i) 110 cm, j) 120 cm, and k) 130 cm from the west edge of the plot. Only cross-sections between 30 cm and 130 cm from the west edge were processed, in order to exclude most edge flow. White pixels correspond to areas stained by dye. The interface between LFH and sand was traced in yellow.

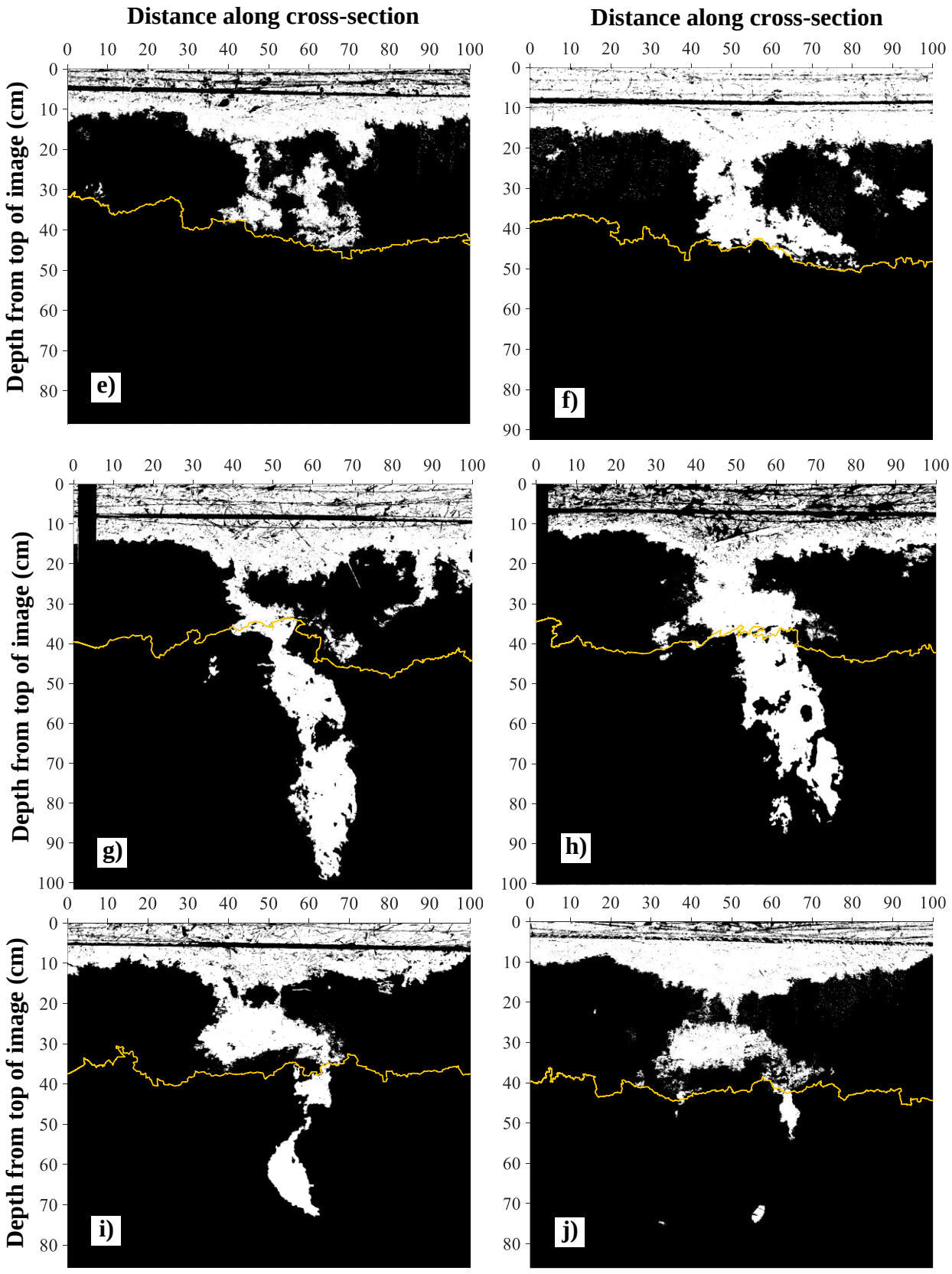

Figure A.1 (continued)

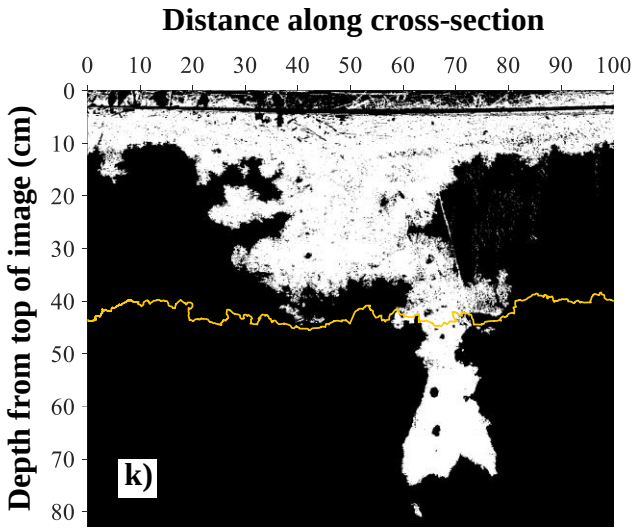

Figure A.1 (continued)

Appendix B: Additional images from the flow tank experiments (Chapter 3)

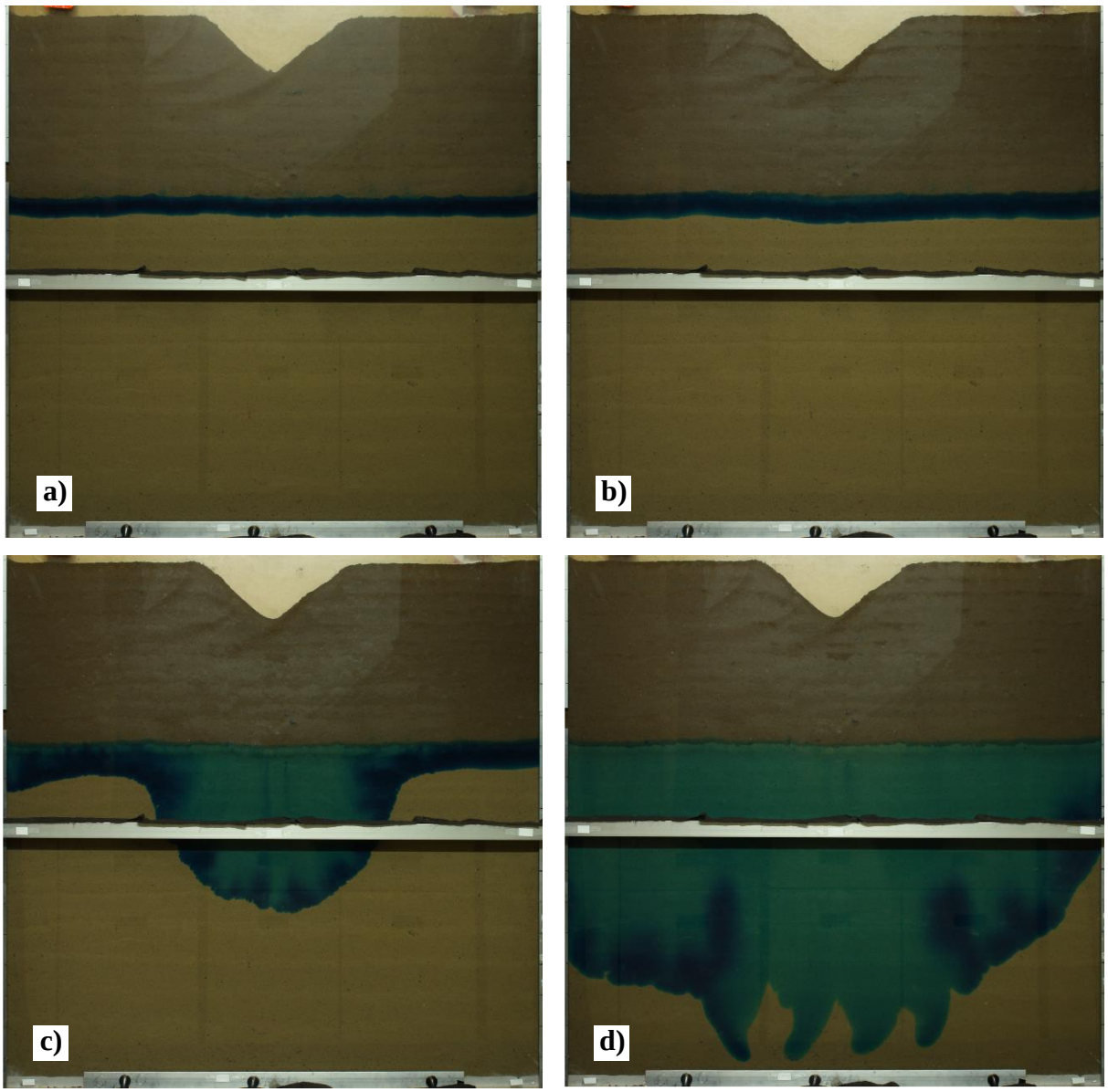

Figure B.1: Images of the flow tank taken during Test A, immediately prior to a) the start of the experiment, b) Event 2 (t=72.0 hrs), c) Event 3 (t=96.0 hrs), d) Event 4 (t=288.2 hrs), and e) the end of the experiment (t=405.9 hrs).

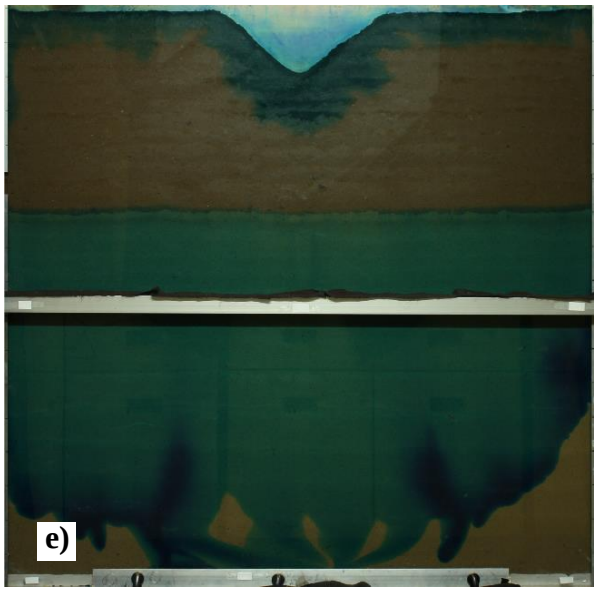

Figure B.1 (continued)

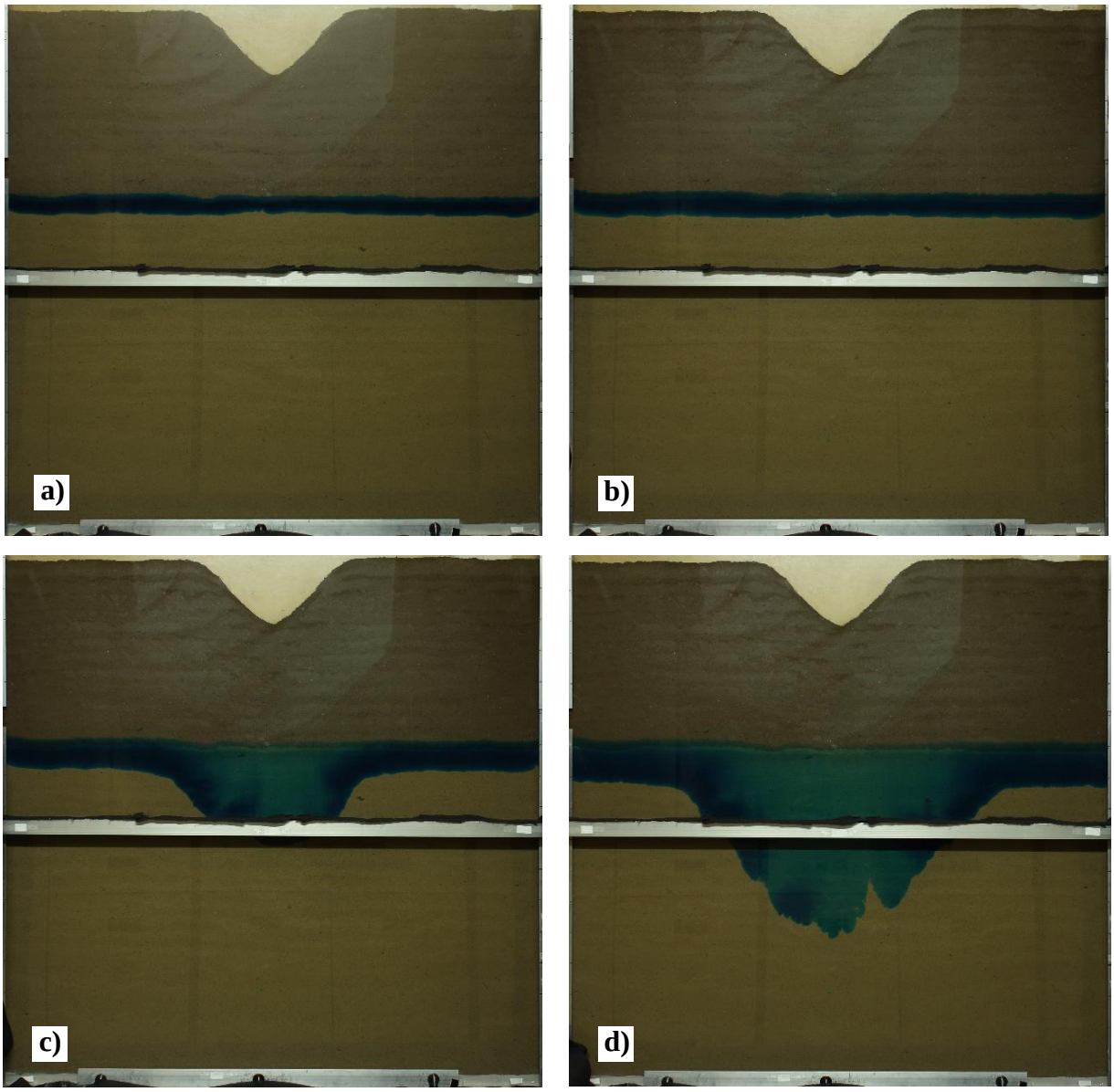

Figure B.2: Images of the flow tank taken during Test B, prior to a) the start of the experiment, b) Event 2 (t=54.9 hrs), c) Event 3 (t=144.1 hrs), and d) the end of the experiment (t=240.6 hrs).

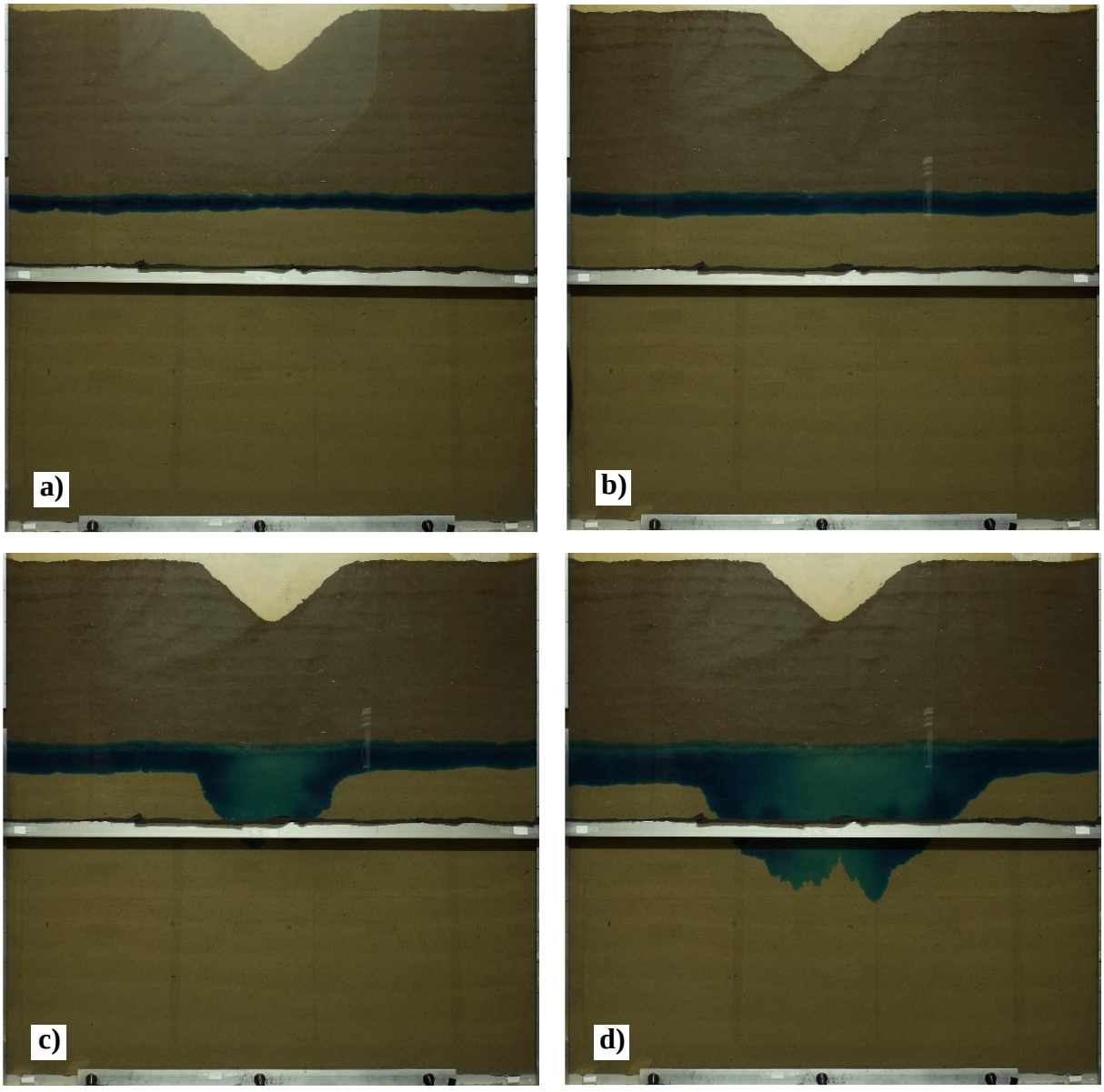

Figure B.3: Images of the flow tank taken during Test C, immediately prior to a) the start of the experiment, b) Event 2 (t=72.1 hrs), c) Event 3 (t=145.0 hrs), and d) the end of the experiment (t=240.2 hrs).

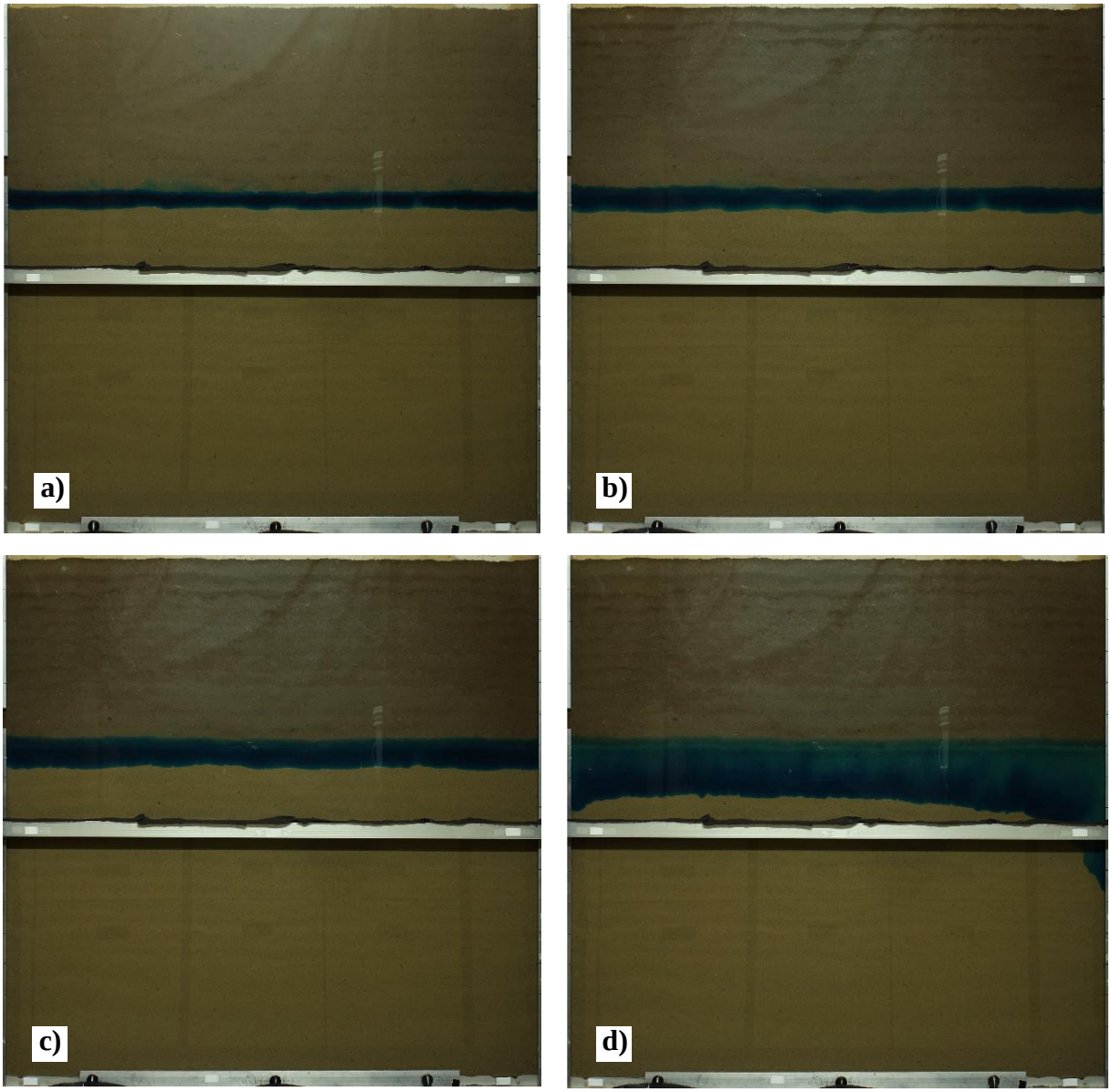

Figure B.4: Images of the flow tank taken during Test D, immediately prior to a) the start of the experiment, b) Event 2 (t=72.0 hrs), c) Event 3 (t=144.0 hrs), and d) the end of the experiment (t=240.1 hrs).